

**NASA TECHNICAL
MEMORANDUM**

NASA TM X-71611

NASA TM X-71611

8-CM MERCURY ION THRUSTER SYSTEM TECHNOLOGY

Lewis Research Center
Cleveland, Ohio 44135

TECHNICAL PAPER to be presented at the
AIAA/SAE Tenth Propulsion Conference,
San Diego, California, October 21-23, 1974



(NASA-TM-X-71611) EIGHT-cm MERCURY ION
THRUSTER SYSTEM TECHNOLOGY (NASA) 121 p
HC \$4.50 CSCL 21C

N74-35200

Unclas
G3/28 51094

TABLE OF CONTENTS

	Page
<u>ABSTRACT</u>	1
<u>INTRODUCTION</u> - B. A. Banks	1
<u>THRUSTER COMPONENT TECHNOLOGY</u>	2
<u>THRUSTER COMPONENT RESEARCH AND DEVELOPMENT TESTS</u>	2
Neutralizer Tip Erosion Studies - A. J. Weigand	2
Impregnated and Rolled Foil Insert Comparison Test - W. R. Hudson	3
High Voltage Pulse Ignition of Hollow Cathodes - E. G. Wintucky	4
Cathode Insert Contamination Tests - A. J. Weigand	5
Thrust Vectoring Systems - W. R. Hudson, R. J. Zavesky, and J. Hyman, Jr.*	6
<u>THRUSTER COMPONENT ENDURANCE TESTS</u>	8
SIT-5 Cathode Endurance Test - E. G. Wintucky	8
Impregnated Insert Cathode - W. R. Hudson	8
Cyclic Life Test of Impregnated Insert - A. J. Weigand	9
10 000 High Voltage Ignition Cycles of a Cathode - E. G. Wintucky	9
Isolator Endurance Tests - S. Nakanishi	9
Expulsion System Endurance Test - S. Nakanishi	11
<u>THRUSTER TECHNOLOGY</u>	12
<u>THRUSTER RESEARCH AND DEVELOPMENT TESTS</u>	12
Sputter Erosion and Deposition in the Discharge Chamber - J. L. Power	12
Neutralizer Position Studies - S. Nakanishi	19
Ion Beam Profile Measurements - S. Nakanishi	21
Thruster Efflux Measurements - A. J. Weigand	24
Ion Machined Accelerator Grid Tests - W. R. Hudson and B. A. Banks	24
SIT-8 Thruster - J. Hyman, Jr.* and W. R. Hudson	29
<u>THRUSTER ENDURANCE TESTS</u>	31
8-Cm Thruster Cycling Endurance Test - S. Nakanishi	31
Accelerated Thruster Cycling Rate High Voltage Pulse Ignition Tests - E. G. Wintucky	35
<u>POWER PROCESSOR TECHNOLOGY</u>	36
Laboratory Thruster Test Consoles - R. R. Robson	36
Main Vaporizer Control Loop Techniques - J. L. Power	38
Thermal Vacuum Breadboard Power Processor - W. Herron* and N. L. Milder	39
<u>APPLICATIONS</u> - B. A. Banks	41
<u>REFERENCES</u>	47

* Hughes Research Laboratory, Malibu, Calif.

8-CM MERCURY ION THRUSTER SYSTEM TECHNOLOGY
National Aeronautics and Space Administration
Lewis Research Center
Cleveland, Ohio

ABSTRACT

The technology status of 8-cm diameter electron bombardment ion thrusters is presented. Much of the technology resulting from the 5-cm diameter thruster has been adapted and improved upon to increase the reliability, durability, and efficiency of the 8-cm thruster. Technology discussed includes: dependence of neutralizer tip erosion upon neutralizer flow rate; impregnated and rolled-foil insert cathode performance and life testing; neutralizer position studies; thruster ion beam profile measurements; high voltage pulse ignition; high utilization ion machined accelerator grids; deposition internal and external to the thruster; thruster vectoring systems; thruster cycling life testing and thruster system weights for typical mission applications.

INTRODUCTION

B.A. Banks

Over the past decade auxiliary propulsion requirements for geosynchronous spacecraft have resulted in a need for lightweight, high specific impulse, and highly reliable thruster systems. Typical missions have become long, and an ever-increasing fraction of the spacecraft mass must be devoted to auxiliary propulsion propellants (ref. 1). The high specific impulse of electric propulsion devices has increased their attractiveness to potential users because of their small propellant requirements. Communication satellites are being planned in three-axis stable platform configurations with large solar arrays which allow more power to be allocated to auxiliary electric propulsion. Although auxiliary electric propulsion can provide an enormous user benefit compared to hydrazine systems, reliability and durability must be demonstrated to potential users. The Lewis Research Center has made considerable progress in demonstrating the flight readiness of the electron bombardment ion thruster.

The mercury electron bombardment ion thruster was successfully first tested in space on July 20, 1964 (ref. 2). This test, Space Electric Rocket Test I or SERT I, demonstrated that ion beam neutralization in space occurs as predicted in agreement with vacuum tank tests. SERT I shown in figure 1 was launched into a 51 minute ballistic trajectory during which the spin rate of the spacecraft was changed by thrust from the 10 cm diameter electron bombardment ion thruster.

Mercury ion thruster durability was demonstrated in space as a result of SERT II, shown in figure 2, which was launched Feb. 3, 1970

(ref. 3). During this test two 15 cm diameter mercury ion thrusters were tested resulting in durability tests of 2011 and 3781 hours. At the conclusion of these tests, the thruster systems were shut down for 15 months after which a series of 188 cathode start up cycles were performed by Kerslake (ref. 4). This demonstrated that the ion thruster system could be stored for long periods in space and then started with no change in cathode performance or starting time.

The Lewis Research Center has a strong program in both in-house research and development and contractual activities to produce a mercury ion thruster specifically designed for auxiliary propulsion. The first generation result of this effort shown in figure 3 was a Structurally Integrated Thruster 5 cm diameter (SIT-5). Durability tests of this 1.78 mN (0.4 mlb) ion thruster performed by Nakanishi (refs. 5, 6, and 7) demonstrated 9715 hours thruster life. At the conclusion of this test a program was created to determine the wear out modes of the SIT-5 thruster and how a longer lifetime thruster could be designed. A 4.45 mN (1 mlb) 8 cm diameter thruster was then chosen as the next generation auxiliary propulsion mercury ion thruster because of better suitability for projected spacecraft and mission lifetimes (ref. 8). Much of the SIT-5 thruster technology has been incorporated in the 8 cm thruster development. This paper presents the technology status of the 8 cm thruster system program.

THRUSTER COMPONENT TECHNOLOGY

THRUSTER COMPONENT RESEARCH AND DEVELOPMENT TESTS

At the conclusion of the SIT-5 thruster program, several research and development areas appeared fruitful to provide information for the design of a 4.45 mN (1 mlb) thruster with the required reliability and durability for 5 to 10 year missions. As a result, cathode evaluations were performed in the areas of neutralizer tip erosion, insert construction, high voltage pulse ignition, and starting degradation due to contaminants. Another area addressed was the thrust vectoring system. Both contractual and in-house efforts were pursued to design grid misalignment and gimbal vectoring systems. These systems were investigated to replace the electrostatic SIT-5 thruster system. This replacement was needed because of longer life and higher thrust requirements of near term missions.

Neutralizer Tip Erosion Studies A. J. Weigand

The 5 cm thruster has been life tested for as long as 9715 hours. During the duration of the test, the neutralizer operating conditions degraded. The amount of tip power required during steady state operations increased from 0 to 10 W. Examination of the neutralizer tip orifice revealed an increase in orifice diameter from 0.25 to 0.55 mm. Although the neutralizer did not cause the test to terminate, the effects

of the tip erosion were apparent.

A study was undertaken to investigate possible causes for neutralizer tip erosion. In order to get reliable results in a relatively short time (hundreds of hours) experimental LeRC neutralizers were tested in a bell jar. The neutralizers were run with very thin (0.025 mm thick) tantalum tips and a nominal 0.25 mm orifice diameter. The neutralizers were operated at 5 cm thruster conditions (the collector simulated a beam current of 25 mA) and at 8 cm thruster conditions (72 mA collector simulated beam current). Tests with rolled foil inserts, cylindrical impregnated inserts, and no inserts were investigated at both thruster conditions. Tip erosion rates were determined by making microscopic photographs of the orifice diameters. The photographs were used to measure the change in orifice diameter, and thus the loss of volume was calculated. The erosion rate in cm^3/hr was determined by dividing the volume lost by the total time of the test. If the flow rate is maintained at about 6 mA equivalent neutral flow for both the 5 and 8 cm thruster conditions (23 and 72 mA emission current, respectively) the erosion rate is reduced by a factor of 10 as compared to the lower flow rates. This should more than allow for a 20 000 hour mission. A life test using a flight type neutralizer operating a flow rate of 6 mA is being conducted to verify these results.

During the neutralizer tip erosion studies there was no attempt to maintain a constant tip temperature. The tip temperatures ranged from 800° to 1150° C, but no correlation of erosion rate with tip temperature was observed. Therefore, the authors believe that the effects of tip temperature were negligible on the erosion rate.

The results of the test indicate that the tip erosion was dependent on the neutral Hg flow rate (fig. 4). The graph is a plot of Hg flow rate (equivalent mA) against tip erosion (cm^3/hr). The neutralizers with rolled foil inserts operated at 5-cm thruster conditions showed no erosion even at a flow rate of 2.6 mA. However, when the neutralizers had no inserts, they showed an erosion rate that increased as the neutral flow rate decreased. From these data, it can be postulated that the neutralizer from the 9715 hour life test had a degraded insert which led to an increased neutralizer tip erosion.

The neutralizers operating at 8 cm thruster conditions did not show an erosion rate dependence of whether an insert was present or not and only exhibited a flow rate dependence on erosion.

Impregnated and Rolled Foil Insert Comparison Test W. R. Hudson

A series of tests is being performed to compare impregnated and rolled foil inserts in hollow cathodes and neutralizers. The commercial preparation of impregnated inserts is described in reference 9. The rolled foil inserts are the SERT II geometry with 1/2 mil tantalum foil

rolled into a tight coil and dipped into a Ba/SrCO₃ (R-500) emissive mix. Five rolled foil inserts and five impregnated inserts were tested as cathodes for SIT 8 thrusters. Measurements were taken of initial starting temperature, typical starting power, keeper voltage and current, and cathode tip power for running and lowest starting power. These numbers are summarized in table I.

There appears to be very little difference between the two kinds of inserts, when tested in main cathodes. Measurements of collector voltage at various mercury flow rates were made for four keeper currents for each of the ten main cathodes. Again there was no clear cut performance difference. One interesting and perhaps important point that was observed is that with both insert types, transition between the plume and spot mode can occur at mercury flow rates around 100 mA. This could cause potential problems in thruster operation, if the cathode operating conditions were near the transition point. Both types of inserts have been operated successfully in cathodes on thruster tests as reported in 8 Cm Thruster Cycling Endurance Tests section.

Preliminary tests indicate that a much greater performance difference occurs for mercury flow levels below 10 mA where neutralizers operate. At the lower flow rate the impregnated insert requires substantially more tip heater power to run stably.

High Voltage Pulse Ignition of Hollow Cathodes E. G. Wintucky

A high voltage pulse technique has been demonstrated capable of rapid and reliable ignition of the hollow cathode discharges (refs. 10 and 11) for both open and enclosed keeper cathodes. The high voltage pulse is generated by discharging a capacitor across the primary winding of a step-up transformer (ref. 10). The pulse is then applied to either an auxiliary electrode or directly to the keeper.

Tables II and III show some of the cathode conditions required for pulse starting of 3.2-mm diameter enclosed keeper hollow cathodes with both rolled foil and alkaline-earth oxide impregnated inserts. The auxiliary electrode consisted of a 0.75-mm diameter W-3% Rh wire positioned parallel to and 0.5 mm from the face of the keeper cap. When applied to the auxiliary electrode, the high voltage pulses were initially negative with respect to cathode ground. In general, breakdown voltage decreased with increasing cathode tip temperature and mercury flow rate, indicating that lower breakdown voltages may be possible. The high voltage pulse technique provides rapid and reliable cathode starting with moderate tip temperature and mercury flow rates at keeper voltages below around 35 V.

Cathode Insert Contamination Tests A. J. Weigand

During ground tests, the neutralizer and main hollow cathodes of the electron bombardment ion thruster are occasionally exposed to atmospheric conditions and foreign substances. These materials may have a detrimental effect on the inserts and cause the cathodes to operate poorly or not start at all. An investigation of the effects of various materials and conditions on the starting conditions of hollow cathodes was conducted.

These tests were conducted in a bell jar using LeRC experimental cathodes. Both rolled foil inserts and cylindrical impregnated inserts were studied. The cathode starting technique is shown in figure 5. The igniter voltage (1000 V) was applied to the keeper. If the cathode would not start at a tip temperature of 1200° C, the insert was considered permanently contaminated. A new insert would then be put in the cathode. Numerous substances and conditions were investigated to determine the effect on cathode inserts. These substances were used because they may be encountered while the hollow cathodes are at atmospheric conditions.

When the cathode started three successive times on the first ignition pulse, it was determined to be operating normally. The cathode was then exposed to a potential contaminant. In the case of a vapor contaminant, a beaker of the liquid form of the material was placed within 7.5 cm of the cathode tip. The beakers were heated to increase vaporization and allow the cathode to be exposed to the vapor at 1 atmosphere of pressure. The beakers were then removed and the bell jar was evacuated for cathode testing. The effects of enclosing the cathode in polyethylene bags with and without a desiccant (silica gel) were also studied. The procedure for this test included carefully removing the cathode from the bell jar and placing it in the desired polyethylene bag. The bag was then sealed. The cathode was left in this environment between 24 and 72 hours after which it was put back into the bell jar. After exposure to each substance and condition the bell jar pressure was allowed to reach 5×10^{-6} torr before the cathode was started.

Table IV shows the results of the contamination tests with rolled foil inserts and impregnated inserts. For each test except the ones for argon and argon with a hot cathode tip, the cathode was initially exposed to air. Since air has caused a slight degradation of the cathode insert, the effect of the materials shown was a measure of further degradation. No degradation indicates that the substance had no effect on the starting characteristics and the cathode started on the initial ignitor pulse after exposure. A substance or condition has a slight effect if the cathode does not start on the initial ignitor pulse after exposure. Subsequent starts may or may not start at the same cathode conditions. In some cases a higher tip temperature was needed for startups. A substance which showed a major degradation is one in which the cathode would not start even at a 1200° C tip temperature. A major degradation for the rolled foil insert was exposure to argon of a hot tip. Other substances

that should be guarded against are NA500 vapor, acetone vapor, polyethylene bag with dryrite, alcohol vapor, breath, and a hot tip exposed to air. Air, polyethylene bag with dryrite, diffusion pump oil, and a hot tip exposed to air cause major degradation for the impregnated inserts. In addition to the tests listed in table IV other substances and conditions were investigated. These included nitrogen gas, cigarette smoke, solder smoke, salt water vapor, argon gas, paint fumes, and saliva. None of these materials affected the operation of the cathode.

The number of tests conducted for each substance is statistically insufficient. There are usually less than ten tests for each substance. However, the results do indicate that certain substances have a strong effect on cathode inserts and the damage is not reversible by using the starting technique described in figure 5.

Thrust Vectoring Systems

W. R. Hudson, R. J. Zavesky and J. Hyman, Jr.

It is desirable to control the precise direction of the thrust vector to compensate for initial misalignment of the thruster, to allow changes in the thrust orientation during the mission, and to control the attitude of the satellite. It is also possible to reduce the number of thrusters required to perform attitude control of a satellite by using the vectoring capability to obtain east-west station keeping. All of the vectoring systems currently being considered are designed to be capable of $\pm 10^\circ$ of thrust vectoring in two orthogonal directions.

Several alternative thrust vectoring schemes have been investigated including three dished grid translational systems and three thruster gimbal systems. Two of the dished grid translational systems have been designed at LeRC and the third has been designed and built under contract by the Hughes Research Laboratories (HRL). Dished grid translation systems allow thrust vectoring without movement of the thruster and are in general lighter weight than thruster gimbal systems. HRL has also been contracted with to design and fabricate a thruster gimbal system. Two LeRC thruster gimbal systems have been designed, one of which presently seems to be the primary candidate for flight qualification on the SIT 8 thruster.

A rotary solenoid dished grid displacement system is shown in figure 6. The accelerator grid is supported by four flexural columns. The columns are oriented so that they are colinear with radii of curvature of the dished grid. This orientation minimizes the changes in the grid spacing with grid deflection and also provides a restoring force to return the system to its equilibrium position. Grid displacement is achieved by a rotary solenoid driven, cam actuator system. The rotary solenoid is mounted on a bracket from the screen mounting ring. A precisely machined cam is mounted touching a flat on the accelerator grid support. The rotary solenoid turns a drive arm through 45 degree rotation which results in a thrust deflection of 10° . The cam is machined to

provide thrust vector steps of angles 0° , $+10^{\circ}$, 0° , and -10° . The design also includes provisions for a return spring to hold the accelerator grid firmly against the cam drive mechanism. The second dished grid displacement system designed by LeRC is shown in figure 7. It uses the same flexural column mount ring assembly as does the rotary solenoid cam system. The grid displacement is achieved using a differential screw driven by a stepping motor. The stepping motor is mounted on the screen grid mount ring. It in turn drives a differential screw by means of a gear transmission system. The output side of the differential screw drives the grid mount ring. The differential screw system provides continuous thrust vector displacement. The exact grid position can be determined knowing the initial position and counting pulses to the stepping motor. The dished grid displacement system (fig. 8) designed by HRL also uses a flexural column support system. A remote stepping motor drives a cam enclosed in a protective bellows. The cam deflects the top of the bellows which in turn is fastened to the accelerator grid.

A thruster gimbaling system based on the SERT II gimbaling system is shown in figure 9. In this design there are two concentric rings with mutually perpendicular pivot points. The inner ring mounts onto the thruster as previously described. The outer ring mounts to the spacecraft structure. Jackscrews are used to achieve two degrees of orthogonal motion, one jackscrew mounted to each ring.

A gimbaling system designed by HRL under contract to LeRC utilizes a linear actuator of the jackscrew type. This type actuator was used on Intelsat IV to move the antenna, and has operated very successfully. The concentric ring design with mutually perpendicular pivots has been used here also. The complete system is shown in figure 10.

The gimbaling system currently favored by the Lewis designers is shown in figure 11. The gimbal mounts onto a cylindrical support tube that connects to the thruster backplate. The gimbal mounting has a combination hinge and pivot support, which allows the required two degrees of freedom. The mount ring can rotate about a diameter and simultaneously tilt on end. Opposite to the hinge-pivot point is a dynamic support which prevents excessive amplitude vibration during a launch environment. The mount ring is displaced by two jackscrew linear actuators. The jackscrews are driven by variable reluctance stepping motor and gear system. The primary reason for favoring this gimbal design over other gimbal designs is that it has greater structural strength in the launch environment. Originally the dished grid vector systems were favored over gimbaling systems on the expectation that they would be much lighter than gimbaling systems. Recent gimbaling systems have design weights of 0.57 kg which is only slightly greater than that expected for dished grid displacement system. Recent substantial thruster performance improvements resulting from the use of small hole accelerator grids preclude the use of misalignment vectoring. This, combined with the greater ability to withstand the launch environment and elimination of a high voltage insulation requirement, has directed the LeRC program towards a thruster gimbaling system as the primary approach to thrust vectoring.

THRUSTER COMPONENT ENDURANCE TESTS

Potentially attractive new component technology requires endurance testing under realistic environmental conditions to access reliability and durability. Significant component endurance tests are discussed in this section.

SIT-5 Cathode Endurance Test
E. G. Wintucky

A cathode-isolator-vaporizer assembly (CIV) designed for use in a 5-centimeter diameter ion thruster has completed over 19 000 hours of operation in an ongoing cathode endurance test. The first 9715 hours of operation were as the main cathode in a SIT-5 thruster. For the remaining time the CIV was operated in a vacuum bell jar where the ambient pressure was in the 10^{-6} torr range. Table V gives the cathode conditions for the period of operation in the thruster and the period of operation in the bell jar. Other details of operation in the thruster are found in references 5 to 7. The cathode was a 3.2 mm diameter tantalum tube with an enclosed keeper and an alkaline-earth oxide coated rolled tantalum foil insert. Other construction details are given in reference 12.

During operation in the thruster and for the first 647 hours in a bell jar the cathode was started by heating the cathode tip to a temperature sufficiently high for spontaneous ignition of the keeper discharge. The cathode starting conditions for the conventional starts are presented in table VI.

After a total of 10 362 hours of operation the cathode shut down during a facility failure and then would not restart with the conventional method. The maximum tip heater power applied was 25 W.

Restarting of the cathode was finally accomplished by applying a high voltage pulse to the keeper, using a high voltage pulse starting technique previously described. Subsequently the cathode has been restarted 19 times with a high voltage pulse to the keeper, following outages resulting from facility failures or power interruptions. The cathode conditions for the 20 high voltage pulse starts are summarized in table IV. Breakdown voltages ranged up to 7 kV.

Impregnated Insert Cathode
W. R. Hudson

A hollow cathode with an impregnated insert has operated over 16 000 hours. The cathode has a right circular cylinder impregnated porous tungsten insert. The operating conditions are consistent with the main cathode of the SIT-5 thruster. Complete details of geometry and operating conditions are given in reference 9.

Cyclic Life Test of Impregnated Insert A. J. Weigand

A test of an impregnated insert main cathode operated at 8 cm thruster conditions was conducted to ensure long life combined with many cyclic restarts. An experimental cathode with a cylindrical impregnated insert was tested. The cathode was operated at conditions of 0.25 A keeper current, 0.5 A emission current, and 85 mA equivalent flow rate.

The test was terminated after 1173 cycles and 1460 hours of operation. The cause of the termination was the ceramic keeper enclosure which developed a crack and fell apart. There was local heating at the crack which melted a portion of the ceramic. When the test was terminated, the cathode was still starting within fifteen minutes after the tip and vaporizer heaters were turned on. The tip temperature was 1050° C at ignition and during the entire test. The steady state parameters did not change significantly. Although the cathode tip face was pitted, the orifice diameter (0.50 mm) did not change. The results of this test are also reported in reference 9.

10 000 High Voltage Ignition Cycles of a Cathode E. G. Wintucky

A 3.2 mm diameter enclosed keeper cathode with a coated rolled foil insert has been started over 10 000 times by a high voltage pulse applied to an auxiliary electrode (ref. 10). No degradation in starting capability occurred, demonstrating the durability of the electrode and cathode under high voltage breakdown conditions.

The pulses were initially positive with ignitor gap breakdowns occurring at 10 to 13 kV. Up to four times as many breakdowns occurred at 4 to 7 kV on the negative part of the pulse (ref. 10). Cathode starting conditions were a tip heater power of 9.5 W (tip temperature <800° C), an equivalent Hg^+ flow of 15 to 17 mA and a keeper voltage of 100 V.

The auxiliary electrode was identical in material, position and geometry to that described in the "High Voltage Pulse Ignition of Cathodes and Neutralizer" section of this paper. After more than 10 500 pulse starts the point on the originally wedge-shaped tip was observed to have only slightly eroded (to a depth of 0.25 mm); however, no impairment of starting capability resulted.

Isolator Endurance Tests S. Nakanishi

The advantages of an electrically isolated propellant feed system for mercury bombardment ion thrusters have encouraged the development of the mercury vapor isolator (refs. 13 to 15). Early isolator tests at conditions of an operating 5 cm thruster have been reported in refer-

ence 16. A SIT-5 isolator (ref. 12) operated for 5400 hours at 1300 V potential difference with no increase in leakage current. The test was terminated to run an upgraded 8-segment isolator at 1600 V. More recently, an isolator of identical design is being tested (6235 hr to date) in a cyclic-endurance 8 cm thruster test at 1250 V.

The purpose of this section is to present the results of various isolator endurance tests. For clarity, the tests are designated as follows:

- Test A. Initial 1600 V test
- Test B. Continued 1600 V test with redesigned sputter shield
- Test C. On-going 8 cm thruster isolator test at 1250 V

A schematic drawing of the thruster simulation in a vacuum bell jar is shown in figure 12. Details of this setup are given in reference 16.

Test A was conducted on a second generation design of the SIT-5 isolator described in reference 12. The external sputter shield around the isolator body was a single layer of thin sheet stainless steel spotwelded to the isolator flange.

Test B was initiated after contamination of the external surface of the isolator from Test A required a shutdown and cleanup. The isolator cleanup was performed by wrapping all metallic parts with polyethylene plastic and sandblasting the ceramic surface. As an added precaution, the sputter shield was redesigned. Instead of spotwelding a cover around the isolator, the support cone normally used in a thruster installation was made to serve as an outer shield. The open end of the support cone was closed off with overlapping disks which were closely separated to provide an effective barrier to contaminants. The end of Test B resulted from repeated malfunctioning of the bell jar pumping system, causing diffusion pump oil to backstream into the test environment necessitating a shutdown and cleanup.

A composite history of Tests A and B is shown in figure 13. Plotted against time in hours are the vaporizer temperature and the leakage current across the isolator. The 340° C vaporizer temperature corresponded to a propellant flow rate of approximately 30.4 mA, which was the nominal cathode flow rate of the 5 cm thruster. After about 750 hours of Test A, the leakage current began to rise at a slowly increasing rate. By 3220 hours, the leakage current had increased to 6.6 μ A with no indication of leveling off. The test was terminated for cleanup and shield replacement.

For convenience of logging, the total hours on the isolator and its cathode are shown in figure 13. As a precaution, the vaporizer was started at somewhat reduced temperatures and increased to 340° C at about 5300 hours. This temperature level was held for about 1000 hours before increasing it to 350° C. After about 6300 hours (or 3080 hours into Test B) a series of facility malfunctions occurred. The subsequent rise

in leakage current may be due partly to the resulting contamination and partly to the higher vaporizer temperature.

During the final hours of this test, the vaporizer temperature was successively reduced which appeared to cause a temporary drop in leakage current. Continued operation at even the lower temperature, however, resulted in a gradual rise of leakage current. The test was terminated at 8400 hours after no indicated leveling off of the rise rate of leakage current.

The Test C isolator is being tested in an 8 cm thruster cycling endurance test. The isolator in that test has logged over 6235 hours with no progressive increase in leakage current. The careful shielding of the isolator external surfaces and environmental operating pressure maintained in the low 10^{-6} torr range have contributed to trouble-free operation.

Expulsion System Endurance Test S. Nakanishi

A mercury propellant feed system for flight application must fulfill numerous requirements such as positive and near complete propellant expulsion under weightlessness, varying thermal environment, long-term material compatibility, structural integrity, and some provision for monitoring propellant inventory. Tests were conducted on a flight prototype expulsion system to determine the long-term retention capability of the reservoir pressurizing gas and vaporizer flow control.

The reservoir test was run in conjunction with the isolator tests discussed elsewhere previously. Presented in this section are the time-pressure-vaporizer temperature history of the various tests and the conclusions drawn therefrom.

Description of the test setup for the propellant reservoir, cathode-isolator-vaporizer and simulated thruster has been given in reference 16 and in the Isolator Endurance Test section (fig. 12). Details of the SIT-5 reservoir design may be found in reference 12. Briefly, the design embodies a hemispherical rubber bladder separating the pressurizing nitrogen gas and the liquid mercury. Positive seal fill valves were used for the gas and mercury compartments. A pressure transducer senses the gas pressure indicating propellant remaining. A heater coil and thermocouple were attached to the outer wall of the mercury reservoir. Several improvements were included in a second generation design of the expulsion system and are described in reference 17.

The first of two expulsion system tests described herein was conducted on the first generation design or SIT-5I reservoir. A history of the test is shown in figure 14. As discussed in reference 16, the volume change of the pressurizing gas under isothermal conditions, and hence the loss in mercury volume, can be related to the ratio of initial to final

resistances of the reservoir pressure transducer. This parameter is shown plotted in figure 14. A variation linear with time indicates a constant flow rate as would be expected for a constant vaporizer temperature. This linearity has been reported in reference 16 with an inferred flow rate of 0.228 gm/hr or 30.4 mA equivalent Hg^+ for the period up to 5400 hours at which time the CIV assembly was changed. From 5400 to 8600 hours the new vaporizer was operated at 340°C and the plot of resistance ratio with time showed a similar linear relation. The discontinuous jog in the resistance ratio at 5400 hours is a drop in reservoir mercury volume as the new CIV assembly was fitted.

The remainder of the test covered a number of vaporizer temperatures, none of which was held sufficiently long to infer an accurate and constant flow rate. During this portion of the test, greater emphasis was placed on evaluating the isolator durability at the expense of a rigorous test on the expulsion system.

The test on the second generation design propellant reservoir is still in progress. Sufficient test time has not been accumulated to give definitive results. The gradual change in the gas pressure transducer reading indicates that the propellant flow rate is normal.

THRUSTER TECHNOLOGY

This section of the paper describes tests performed with auxiliary propulsion ion thrusters to document and/or improve thruster reliability, durability, and spacecraft compatibility.

THRUSTER RESEARCH AND DEVELOPMENT TESTS

Sputter Erosion and Deposition in the Discharge Chamber J. L. Power

A series of three ~400 hour operational tests were performed with the SIT-5 thruster to investigate the effect of the discharge potential (ΔV_I) on the sputter erosion and deposition rates in the discharge chamber. These studies have been reported (ref. 18). The thruster (fig. 15) was essentially identical to that endurance-tested for 9715 hours (ref. 7) and employed an electrostatic vector grid system. In this thruster all the discharge chamber components remain at the cathode tip potential during operation except for the cathode keeper and the anode. Constant discharge potentials of 36.6, 39.6, and 42.6 V, respectively, were maintained during the three tests by a feedback control loop which automatically adjusted the main cathode flow rate to achieve the set ΔV_I . The other thruster operating parameters were controlled or maintained at values, shown in table VII, which had previously been optimized for the thruster.

It was found (ref. 18) from these tests that the sputter erosion

rates of most of the exposed discharge chamber components were in the approximate ratio of 1:3:5 for the tests arranged according to increasing ΔV_I , as seen in figure 16. The components most heavily eroded on a weight basis were the cathode pole piece, the thruster endplate, the anode pole piece insert, the baffle assembly, and the upstream side of the screen grid.

The anode was found to gain weight in each of the erosion tests, and these weight gains were also in the ratio of 1:3:5, as seen in figure 16. For each of the tests, the anode weight gain nearly equaled the sum of the measured and estimated component weight losses for the test. Spectrographic analysis of the coating deposited on the anode confirmed the conclusion that essentially all of the material eroded from the discharge chamber components deposited on the anode. Only a negligible amount of it was lost through the grids.

Additional conclusions were drawn from the weight gains and losses of the discharge chamber components, the spectrographic analyses, and scanning electron microscope examination and X-ray fluorescence characterization of the anode coatings. One of these conclusions was that little material sputtered from the accelerator grid system could have passed through the grid system and deposited in the discharge chamber. Furthermore, material sputtered from components near the downstream end of the discharge chamber, i.e., from the screen grid and the anode pole piece insert, was found to have deposited predominantly at the downstream end of the anode, whereas material sputtered from upstream components was quite uniformly deposited over all portions of the anode.

Spalled anode coating flakes 3 to 5 μm thick were collected from the discharge chamber after completion of the erosion tests. Examination and comparison of these flakes relative to anode coating specimens from the 9715 hour SIT-5 endurance test, however, revealed no simple correlation between the tendency of the anode coating to spall off in flakes and such characteristics as the thickness and composition of the coating, its surface characteristics, or its location on the anode.

Finally, it was found that the relative sputtering rates observed in the three erosion tests could be well correlated with a semitheoretical curve (fig. 17), representing the variation in the doubly charged mercury ion (Hg^{+2}) production expected over the range of ΔV_I investigated. This correlation took into account sputter yield changes over the same ΔV_I range and also the reduced energy of the primary electrons from that given by ΔV_I , a reduction given approximately by the relation

$$V_P = \Delta V_I - V_{CK}$$

in which V_P is the primary electron energy in eV and V_{CK} is the cathode keeper potential in volts. The good correlation of the relative sputtering rates found with the relative Hg^{+2} production rates, as well

as the lack of any such correlation with the relative Hg^+ ion densities present, strongly supports the conclusion that Hg^{+2} ions are the species predominantly responsible for the observed sputter erosion of discharge chamber components in thrusters operated at ΔV_I 's near 40 V.

Spalled anode coating flakes were principally responsible (ref. 7) for the termination of the 9715 hour endurance test. Examination and X-ray analysis of these flakes and other samples of the anode coating using the scanning electron microscope revealed several interesting features. The endurance test anode flakes were 10 to 30 μm thick, indicating substantially higher average erosion and deposition rates during the endurance test than predicted from its nominal ΔV_I of 38 V on the basis of the ΔV_I -erosion test results. The flakes also showed a layered structure, as seen in figure 18, evidently reflecting rapid and substantial changes in the sputter deposition rate and deposited material composition during the course of the test. X-ray analyses of accessible flake layers and surfaces confirmed that periods occurred during the test in each of which a single component was intensely sputtered and produced most, in some cases nearly all, of the material deposited during that period. This sputtering behavior, which was not observed in the SIT-5 400-hour erosion tests described above, was at least partly responsible for the higher than predicted average erosion and deposition rates during the test.

Because of its indicated sputter resistance and other favorable characteristics, graphite is an attractive material for use in constructing ion thruster discharge chamber components subject to intense sputtering. To test this idea, thick and thin baffles for the SIT-5 thruster have been fabricated both from anisotropic pyrolytic graphite and from high purity isotropic (nonpyrolytic) graphite. In addition, pyrolytic graphite covers for the interior surface of the thruster endplate have been made. In all cases the pyrolytic graphite parts have been constructed so that the graphite molecular layers were parallel to the exposed flat surfaces of the finished pieces. Pyrolytic graphite baffles have been fabricated both by machining solid pieces and by pyrolytically depositing (ref. 19) the graphite at high temperature on graphite and tantalum substrates.

Operational tests of the SIT-5 thruster have been performed with the above-described graphite baffles (though not as yet with the pyrolytic graphite-coated baffles) and with a pyrolytic graphite endplate cover (0.53 mm thick). To install the baffles, the SIT-5 baffle mount system was substantially modified, eliminating the long screw which projected a substantial distance into the main volume of the discharge chamber (see fig. 15). The thick pyrolytic graphite baffle assembly (2.8 mm thick) is shown in figure 19 before running. Figure 20 similarly shows the thin isotropic graphite baffle (0.63 mm thick) assembled for running. It is held in place by a specially fabricated, thin head tantalum screw.

The operational tests with the graphite thruster parts, in particular

one 400 hour test with the thick pyrolytic graphite baffle assembly and the pyrolytic graphite endplate cover, demonstrated a substantial reduction in the erosion rates of these parts as compared with the standard mild steel and tantalum SIT-5 components run under comparable conditions in the erosion tests described above. Quantitative weight loss comparisons were made difficult by the pronounced tendency of the graphite to sorb and retain substantial amounts of mercury. Because of this, the pyrolytic graphite baffle assembly actually showed a net weight gain during the 400 hour test. Furthermore, the strong possibility exists that the apparently superior sputtering resistance of graphite to mercury ions, as seen in the tests, is at least partly due to this property of sorbing the neutral mercury vapor. The sorbed mercury could produce a self-renewing surface layer protecting the substrate graphite from much of the sputtering damage it otherwise would suffer.

The thick pyrolytic graphite baffle assembly used in the 400 hour test showed numerous cracks and incipient splits between graphite layers following the test, as seen in figure 21. This problem of between-layer splitting also occurred near the beginning of the cycling endurance test of an 8-cm thruster and is believed due to the anisotropic thermal expansion properties of pyrolytic graphite. No splitting or separation of the pyrolytic graphite endplate cover has been observed in any of the tests, however, nor has any structural problem been encountered in tests employing the thin, isotropic graphite baffles.

As elsewhere reported in this paper, an 8-cm thruster employing a thin isotropic graphite baffle (0.63 mm thick) and a pyrolytic graphite endplate cover has already been operated over 7400 hours and restarted over 220 times in a continuing endurance test. No structural problems of the graphite components and no effects on the thruster performance due to their erosion have so far been observed.

Another coordinated approach is being evaluated to cope with the sputter erosion of discharge chamber components and the deposition of sputtered material on the anode. One part of this approach is to assure that the exposed surfaces of all the discharge chamber components subject to sputtering are fabricated of a single material of good sputter resistance and good fabrication properties. Tantalum was the material chosen to meet these criteria.

The SIT-5 thruster was modified so that, except for the molybdenum grid system, all the exposed surfaces of the discharge chamber components subject to sputtering were either constructed of, coated with, or covered by tantalum. A diagram of the resulting thruster is shown in figure 22, which may be compared with the SIT-5 thruster diagram in figure 15 to identify the changes made. Tantalum foil covers were installed over the exposed mild steel surfaces of the cathode pole piece and a tantalum baffle and baffle hold-down screw, seen in figure 23, were employed in a baffle assembly exactly like that shown in figure 20. The assembled cathode pole piece and baffle structure is shown in figure 24. A tantalum endplate cover was installed, and the nickel-plated surfaces of the

anode pole piece insert were plasma spray-coated with a 0.08 to 0.10 mm thick coating of tantalum, resulting in the rough, granular surface appearance seen in figure 25.

The SIT-5 thruster with the above alterations (and with anode modifications subsequently described) was operated continuously for 200 hours at a discharge voltage of 64.6 V and otherwise standard SIT-5 operating conditions, as tabulated in table VIII. A preliminary report (ref. 20) describing the test and its results is in preparation. The high ΔV_I was employed in an attempt to achieve accelerated life testing of the discharge chamber components with regard to their sputter erosion, as suggested by the results of the SIT-5 erosion tests described previously. The test was also designed to investigate the adherence of this sputtered material to the anode. A ΔV_I of 64.6 V was chosen because this value was found in preliminary experiments to be essentially the maximum ΔV_I at which the thruster could be stably operated over an extended period of time with the available power processing unit.

The discharge chamber components most severely sputter eroded on a weight basis in the accelerated life test were the screen grid upstream surface (as estimated), the tantalum foil cover over the cathode pole piece tip, and the baffle. These and the other major component weight losses found are given in table IX. Figure 26 shows the severe sputter erosion evident on the exposed downstream surface of the baffle.

The only individual discharge chamber components used without modification in both the previous SIT-5 erosion tests and the accelerated life test were the baffle and the screen grid. A comparison may be made between the sputter erosion rates measured or estimated for these two components in the accelerated life test at $\Delta V_I = 64.6$ V and in the SIT-5 erosion test at the normal ΔV_I of 39.6 V. (All erosion of the screen grid in both tests is presumed to have been on the discharge chamber side, in accordance with observation.)

For both components such a comparison indicates that the erosion rates at the higher ΔV_I were ~75 times greater than those at the normal ΔV_I . Thus the equivalent operating time at $\Delta V_I = 40$ V indicated for the 200 hour accelerated life test, as regards the sputtering of the discharge chamber components, is approximately 15 000 hours. The very large acceleration factor found in the sputtering rates cannot be accounted for solely by the Hg^{+2} ion sputtering theory which the SIT-5 erosion test results support. This theory would predict an acceleration factor of only ~24 in the sputtering rates. The accelerated life test results suggest that sputtering by Hg^{+3} ions becomes important when the discharge potential is raised to the neighborhood of 65 V.

None of the discharge chamber components was sputter eroded in the accelerated life test to such an extent that its structural integrity or further serviceability was at all threatened. In fact, no component appeared in danger of such deterioration for at least several times the 15 000 hour equivalent operating duration of the accelerated life test.

The most heavily eroded component in the test, relative to its size, was the baffle, which lost 10 percent of its weight, 13 percent of its outer edge thickness, and 1.3 percent of its outside diameter during the test.

Despite some differences, the qualitative sputter erosion pattern and characteristics observed in the accelerated life test were quite similar to those seen in the SIT-5 erosion tests. Furthermore, it was again found in the accelerated life test that the weight gain of the anode (including material spalled from it) essentially accounted for all the weight lost by the other discharge chamber components. These observations support the validity of conducting an accelerated life test at an elevated ΔV_I to reproduce, at a much accelerated rate, the general features of the discharge chamber sputtering and sputter deposition occurring during normal, uncycled thruster operation.

The second part of the coordinated approach under investigation as a solution to the problems of sputtering and sputter deposition in mercury ion engines is to drastically alter the surface character of the anode. The aim of this innovation, which was also evaluated in the accelerated life test, is to prevent the spalling of dangerously large flakes of the sputter-deposited anode coating, either by greatly improving the adhesion of the sputtered coating to the anode or by ensuring that any flakes that spall off are so small as to pose no threat to the thruster operation.

To test the possibilities of improving the adhesion of the sputtered coating to the anode, smooth and coarsely grit-blasted anode surfaces of both stainless steel and tantalum were exposed in the accelerated life test. The complete anode assembly employed in this test is shown in figure 27. The tantalum surfaces comprised a tantalum foil insert attached to the interior of the anode while the stainless steel surfaces were exposed portions of the anode itself. The roughened sections of both materials were prepared by a standard grit-blasting procedure using a 50 μm -size silicon carbide abrasive powder in a micro-sandblasting apparatus. The roughened stainless steel anode surface is shown before the test in figure 28. An electron micrograph of this surface at 2000 times magnification is seen in figure 29 and shows its extreme, small scale angularity and roughness.

To test the possibilities of limiting the size of spalled flakes of the sputtered anode coating, a tightly woven stainless steel wire cloth insert was also installed on the interior surface of the anode for the accelerated life test. Figure 30 shows an enlarged view of the wire cloth used. The superficial mesh openings of the cloth measured 0.40 by 0.50 mm, and the question of interest in testing the insert was whether any coating flakes which spalled from it would be limited to these dimensions. Thus the complete anode assembly (fig. 27) employed in the accelerated life test consisted of two inserts and five different exposed surfaces, as described above.

Examination of the anode assembly following the accelerated life test revealed that the anode coating adhesion was immensely improved by

grit-blasting the substrate surface, indeed that this had an overriding effect on the coating adhesion. The sputtered coating adhered completely, without cracks, flaws, or spalling, to both the grit-blasted stainless and the grit-blasted tantalum surfaces. The lower portion of figure 31 shows the coated, grit-blasted tantalum surface as it appeared following the test. Even on severely stressing these coated grit-blasted surfaces by cutting out pieces of them, no cracking or spalling of the coating occurred.

Both the smooth stainless and the smooth tantalum surfaces, on the other hand, showed extensive spalling of their sputtered coatings, as seen in figure 32. The coating on well over half the area of both these surfaces had spalled off completely when examined following the test, and on stressing the smooth surface of the tantalum insert by cutting out samples from it much of the remaining coating separated from it. A portion of the copious amount of anode coating flakes found in the thruster following the test is shown in figure 33. These flakes clearly originated from spalling of the sputtered coating off of the smooth anode surfaces. Many of the flakes were over 1.0 mm long, much longer than necessary to short out the grid system or cause other serious problems.

The overriding importance that grit-blasting of the substrate surface has on the adhesion of the sputtered anode coating is well demonstrated in figure 31. This figure shows that the boundary between the completely spalled and the completely unspalled coating regions on the tantalum anode insert exactly coincides with the boundary between the smooth and the grit-blasted areas of the insert.

The stainless wire cloth anode insert initially showed fairly good adhesion of its sputtered coating following the accelerated life test. However, on microscopic examination many cracks in the coating could be seen along the exposed wire crests. And with time, much of the coating on the exposed wire surfaces spalled off, leaving coating fragments on the individual wires of the insert which appeared as shown in figure 34 when viewed with the scanning electron microscope. On extensive examination of the spalled coating areas of the wire cloth insert, no evidence could be found for the spalling of flakes larger than a fraction of the superficial mesh opening dimensions of the cloth; indeed, no cases could be found in which a continuous coating extended from one wire of the cloth to an adjacent or crossing wire. Hence the results of the experiment indicate that the size of spalled anode coating flakes can indeed be limited as required by employing a tightly woven wire cloth anode surface of appropriately small mesh size.

The results of the accelerated life test strongly support the effectiveness of the coordinated design approach described above in solving the twin problems of component sputter erosion and sputtered deposit spalling from the anode. The solution consists of fabricating from tantalum all the discharge chamber component surfaces subject to sputtering by the main discharge (apart from the molybdenum screen grid) and employing

either grit-blasted or fine mesh wire cloth anode surfaces.

The attractive possibility also exists, and is presently being investigated, of utilizing a combined grit-blasted and fine mesh wire cloth anode surface. Such a surface will presumably combine the advantages both of superior anode coating adhesion and of mesh dimension-limited flake size should any spalling of the coating occur. An electron micrograph of a grit-blasted fine mesh stainless wire cloth which will be tested as an anode surface is shown in figure 35. The gross difference in surface character between the grit-blasted portion of the screen at the bottom of the figure and the non grit-blasted portion at the top is evident.

Neutralizer Position Studies S. Nakanishi

Some requirements for a hollow cathode plasma bridge neutralizer to be used on long duration space missions are:

- (1) Good coupling and hence lower power loss neutralization of the thruster ion beam
- (2) Minimum erosion of the neutralizer due to ion beam impingement or plasma discharge sputtering
- (3) Minimum neutralizer caused erosion of the accelerator grid from fall-back of low energy neutralizer ions

It is believed that these requirements can be fulfilled by proper geometrical design and positioning of the neutralizer. To this end, a series of systematic tests have been conducted to determine the effects of neutralizer position and keeper hole size on beam neutralization.

The 8-cm thruster was operated at a constant ion beam current of 72 mA while the neutralizer was moved axially and radially. A range of keeper hole sizes from 0.132 to 0.178 cm was tested. All tests were conducted in a 1.5 by 4.9 m vacuum facility at operating pressures of 3×10^{-6} torr or less.

A photograph of the movable neutralizer thruster installation is shown in figure 36. Horizontally translatable tracks were used to project the thruster past a close-off gate valve and into the 1.5-m diameter section of the vacuum facility. Any possible wall effects upon beam neutralization were thereby minimized.

The 8-cm diameter thruster was essentially identical to the one used in the thruster cycling-endurance test except no auxiliary electrode was used. The accelerator grid had an active area 8 cm in diameter.

The neutralizer vaporizer assembly was also obtained from the 5-cm

thruster program, using an insert of the rolled foil type. An auxiliary electrode was mounted on the neutralizer to permit auxiliary electrode pulse ignition. Two-directional movement of the neutralizer was accomplished by a carriage assembly mounted on a push-pull tube. A sealed shaft inside the tube was fitted with a pinion gear which engaged a rack on the neutralizer carriage. The axial position of the neutralizer could be varied 6.3 cm by sliding the tube in or out parallel to the thruster axis. The radial movement of 3.1 cm was accomplished by rotating the shaft through an angle of 360 degrees.

Following preheat of the neutralizer, the cathode, and their vaporizers, the neutralizer was pulse-ignited. The cathode usually ignited by application of a 400 V d.c. keeper voltage. The thruster was then operated at constant conditions for at least 4 hours to bring the long propellant feed coil line to equilibrium temperatures before taking flow measurements.

The effects of neutralizer position on ion beam neutralization were determined by holding a constant neutralizer flow rate and neutralizer keeper current with the thruster beam current held at 72 mA; then at a given axial location, the neutralizer was moved radially from 2.75 to 5.85 cm measured between the neutralizer keeper hole and the outermost active acceleration grid beamlet hole. Axial positions of the keeper hole varied from 2.5 to 8.9 cm downstream of the accelerator. The neutralizer floating potential was used as an indicator of coupling with the ion beam.

Because it was desirable to use the same neutralizer keeper throughout the test, the smallest keeper hole was tested first. The keeper hole was progressively enlarged, obtaining position effect data at each hole size.

The nominal operating conditions of the thruster used throughout the test are shown in table X. The cathode flow was automatically controlled to hold a discharge voltage of 40 V. Propellant utilization efficiency in the ion chamber averaged about 76 percent. It was considered more significant to hold a constant ion beam current rather than the utilization for ion beam coupling purposes.

The typical effects of neutralizer keeper current on keeper voltage and floating potential are shown in figure 37A. The keeper hole size was 0.159 cm. The neutralizer to keeper gap was 0.108 cm. The axial and radial distances were 5.0 and 2.75 cm, respectively. Data are shown for flow rates of 4.5 and 7.7 mA.

Over the range of keeper current varied, the keeper voltage was not greatly affected at either flow rate. Decreasing the flow rate from 7.7 to 4.5 mA increased the keeper voltage about 1 V regardless of the keeper current.

Neutralizer floating potential, however, was significantly affected

by keeper current particularly at the lower flow rate. As keeper current was reduced below 0.40 A, the floating potential increased rapidly. The rate of increase was more rapid for the lower flow rate below a keeper current of 0.35 A. From these data, the selection of 0.45 A keeper current during neutralizer position changes appear logical.

The effects of radial-position at various axial distances upon floating potential are shown in figure 37B. The keeper hole and gap were 0.159 and 0.108 cm, respectively. The flow rate was 7.7 mA at a keeper current of 0.45 A. As would be expected, the floating potential increased as the neutralizer moved farther away from the ion beam. A later section on beam profile measurements will discuss the ion beam divergence. The data of figure 37B indicate that at the 8.9 cm axial position, the neutralizer was immersed in the ion beam for radial positions of 5 cm and less.

These distances infer a beam boundary divergence of approximately 29 degrees with respect to the thruster axis. It is also interesting to note that at a radial distance of 2.75 cm, the initial 1.3 cm of axial movement from 2.5 to 3.8 cm resulted in over 10 V reduction in floating potential. Further axial movement of the neutralizer had increasingly lesser effect upon the floating potential.

The effects of changes in keeper hole size upon floating potential are shown in figure 38. The axial position selected was 5 cm which made the neutralizer lie on a 28 degree line at a radial position of 2.75 cm. Larger radial distances would, of course, take the neutralizer outside of the 28 degree line. The data are for keeper hole sizes from 0.132 to 0.178 cm. Inasmuch as each hole size change involved a shutdown and a restart with the necessary temperature stabilization period, the quoted flow rate is based on an earlier temperature calibration.

With the 0.132 keeper hole, the floating potential was about 60 V, increasing to over 100 V as the neutralizer was moved radially outward. Larger keeper holes reduced the floating potential until with the 0.178 cm hole, the floating potential was about 10 V regardless of radial position. Further tests are planned to determine if further reduction or a reversal in trend might occur at larger hole sizes. The data obtained thus far tend to indicate that when beam coupling is good, neutralizer position has a broad latitude and that other considerations such as sputter erosion of the neutralizer, structural integrity, and thermal characteristics may be more significant.

Ion Beam Profile Measurements S. Nakanishi

As an aid to determining the proximity limit of neutralizer position relative to the ion beam, current density profiles have been obtained. Two types of current measurement devices were used. One type was a single molybdenum planar probe 0.64 cm in diameter. The probe was mounted on

one leg of a U-shaped tube such that the probe axis lay parallel to the thruster axis for a distance of 18.4 cm before making a 90° bend. The other leg was of sufficient length to serve as a feed-through and actuator from outside the vacuum port cover flange. The circular planar probe was thus perpendicular to the thruster axis and moved in an 11 cm radius arc across the accelerator as the actuator leg was rotated. The actuator leg could move axially to locate the probe from zero to 12.7 cm downstream of the accelerator.

The second type of current measurement device was a horizontal rake with 47 Faraday cups spaced 1.27 cm on centers. The Faraday cups were 0.48 cm in diameter and covered by a faceplate having 0.159 cm apertures. The faceplate was attached to the rake body giving a projected frontal dimension of 1.27 cm height and 61 cm width. The Faraday cups and the faceplate could be independently biased with respect to facility ground. The rake was mounted on a motorized actuator so that the rake could be moved vertically over a distance of 90 cm.

The beam profile measurements were made in conjunction with the neutralizer position studies using the same 8-cm diameter thruster and the vacuum facility. With the thruster extended fully forward, the Faraday cup rake was 30 cm downstream of the accelerator. This distance could be increased by retracting the thruster as desired.

In both the planar probe and the Faraday cups, current was determined by measuring the potential difference across precision resistors of suitable values. Voltage readings from the planar probe were recorded manually. The rake readings were recorded automatically on the central Automatic Digital Data Encoder (CADDE) system of the Lewis Research Center.

A typical current density profile taken with the planar probe is shown in figure 39. Because the probe moved in an arc passing through the center of the accelerator rather than along a diameter, each probe position was corrected and plotted as radial distance. If axial symmetry is assumed for the beam profile, the resulting plot would thus be representative of the profile along a diameter.

Profiles for three axial locations are shown as a fraction of the maximum observed value. As expected, the beam was highly peaked near the axis for all three axial locations. The current density showed a maximum at 5 cm rather than at the closer location of 1.27 cm. The latter peak was in turn lower than the peak farthest downstream at 12.7 cm. The peak of the profile coincided with the thruster centerline only for the 5 cm location. It is believed that in spite of an attempt to achieve geometrical alinement the axis of the ion beam was not consistently colinear with the probe axis. This condition could be caused by inadvertent beam deflection or misalinement of the thruster assembly which was cantilevered on long movable tracks. This line of reasoning is supported by the fact that the peak at 1.27 cm occurred to the left of center and to the right of center at 12.7 cm. Any traverse, however misaligned,

would still display the characteristic bell-shaped curve because the traverse cut across a current distribution which resembles a paraboloid of revolution.

The current density distribution taken with the Faraday cup rake is shown in figure 40. A bias voltage of -15 V was applied to the cups for these measurements. The complete profile is presented in two parts. Figure 40(a) shows profiles taken from the upper half of the beam down to the vertical position where the beam appeared to have a maximum density. Figure 40(b) shows profiles for the lower half of the beam starting with the maximum position.

The values of measured current are presented as fractions of the observed maximum value. As previously shown by the planar probe measurements, the beam was highly peaked. The profiles are labeled with numbers denoting the vertical distance in centimeters off the maximum profile which is labeled zero. At large distances from the zero position, the profile lost symmetry. An apparent axis of symmetry passed through each profile showed that the beam might be misaligned from the geometrical axis of the thruster as also indicated by the planar probe measurements.

If the ion thruster is assumed to be a point ion source 30 cm upstream of the probe rake, the resulting thrust loss due to ion beam divergence is 2.16 percent. Obviously this thrust loss is dependent upon the particular grid system used and may not be identical to that of a small accelerator hole or compensated accelerator grid system.

In the section on Neutralizer Position Studies, sputter erosion was discussed as a factor limiting proximity of the neutralizer to the ion beam. An effort was made to determine an inferred beam boundary wherein the current density would be below some limiting value. The molybdenum planar probe was used for this purpose. Figure 41 shows the current density measured by the planar probe at three axial locations. At each location, the probe was moved toward the thruster centerline from a large radial distance where the probe current was imperceptible.

At an axial position of 1.27 cm from the accelerator the current density rose sharply as the beam was approached radially. At larger axial distances, the beam boundary became more diffuse as indicated by the more gradual rise in current density as the beam was approached.

An apparent beam envelope or beam diversion angle can be deduced from the data. Selecting an arbitrary value of 0.01 mA/cm^2 , the radial distance at which this current density is reached for each axial location can be determined. These values are shown plotted in figure 42. A line faired through the points and directed toward the radial distance of the outermost active beam hole in the accelerator plane subtends an angle of 24 degrees with respect to the thruster axis. The actual beam boundary probably is neither sharp nor linear. For neutralizer positioning purposes near the accelerator, an apparent angle is a convenient design criteria. Also, beam focusing and ion trajectories are strongly in-

fluenced by accelerator optics. The beam angle should therefore be determined for each optic design.

Thruster Efflux Measurements A. J. Weigand

The use of electron bombardment ion thrusters on communication satellites, scientific satellites, and other spacecraft will require that all avenues of interaction between other components of the spacecraft and the thrusters be investigated. One area of interest is the amount and distribution of sputtered material from the thruster, in particular, the grids. Although the amount of sputter efflux resulting from charge exchange sputter erosion can be reduced by increasing the thruster utilization, knowledge of where the sputtered material goes and its rate of deposition is important to spacecraft designers.

A method of employing glass samples and change in transmittance as a means of mapping the sputter efflux was first reported in reference 21. This technique together with the use of quartz crystal microbalances (QCM) to measure the rate of deposition is presently being used on an 8-cm cyclic endurance test. A QCM and glass sample are mounted on a rod that is parallel to other thruster axis and located 13 cm from the center of the thruster. A plot of the rate of sputter deposition as a function of distance from the ground screen plane is shown in figure 43. The curve indicates that the greatest rate is at the ground screen plane. At about 4 cm downstream of the ground screen plane the QCM is in the ion beam to the extent that the deposition is sputtered off as fast as it arrives. The glass samples show this same trend and spectrographic analysis of the films indicate that the deposition is mostly molybdenum. (The grids are made of molybdenum.)

Figure 43 also shows deposition occurring upstream of the ground screen plane. This is probably due to accelerator grid material passing through the perforations in the ground screen. Analysis of the coating also indicates the deposit is molybdenum. Tests were performed with samples at the ground screen plane but oriented and shielded so that only sputtered material traveling upstream could be detected. The low molybdenum sputter deposition rate observed (probably from resputtering of molybdenum of the frozen mercury target) tends to support the theory that all the molybdenum sputter efflux resulting from thruster operation comes in a line of sight fashion from the accelerator grid system. The engineering model SIT-8 thruster will have a nonperforated ground screen thus preventing any upstream flow of sputtered molybdenum.

Ion Machined Accelerator Grid Tests W. R. Hudson and B. A. Banks

Introduction. - A dished two-grid ion extraction system is presently employed on an 8-cm thruster. It consists of two dished grids with

matched hexagonal arrays of holes. The grids are fabricated from arc cast molybdenum sheet by photochemical etching and hydroforming (refs. 22 and 23).

Described herein is an alternative grid fabrication technique which resulted in a substantial thruster performance improvement. The screen and accelerator grid are simultaneously hydroformed as before, but only the screen grid hole array is etched. The accelerator grid is initially unperforated. The grid set is then mounted on a thruster in the usual manner. The screen electrode focuses individual ion beamlets onto the blank accelerator grid, selectively sputtering a matching array of holes in the accelerator grid. The resulting accelerator grid holes are sized, shaped, and aligned with respect to their corresponding screen holes. The resulting accelerator holes are much smaller than previously used accelerator grid holes, reducing the neutral mercury loss, which in turn enhances propellant utilization and reduces charge exchange erosion. (This result is consistent with trends documented by Rawlins (refs. 24 and 25).) As a result, the reduced charge exchange sputtering should greatly reduce sputtered material efflux from the thruster.

A thruster with an ion machined grid has been tested for 1006 hours at an ion chamber propellant utilization of 91.9 percent and at discharge losses of less than 350 eV/ion. This represents a substantial increase in propellant utilization (previously ≈ 70 percent) over thrusters operated previously with larger hole diameter accelerator grids.

Apparatus and procedure. - The 0.38 mm thick screen grid used had a hexagonal array of 1.97 mm diameter holes on 2.21 mm center to center spacings (72.5 percent open area). The 0.38 mm thick accelerator dished sheet was spaced 0.76 mm from the screen grid.

The electrical circuit shown in figure 44 was used to operate the thruster during ion machining and normal thruster operation. The anode was held at the net accelerating voltage, V_I . The cathode was negatively biased by the discharge chamber supply and the neutralizer floating potential was measured between the neutralizer tip and facility ground. There are only two differences between the power supplies and circuit used in this experiment and the normal thruster electrical circuit: a 4 μ f capacitor was connected in parallel between the accelerator grid and the cathode common, and an accelerator supply was used that had a current capability of one hundred milliamps. The purpose of the capacitor was to prevent flakes of sputtered material from permanently shorting the grids together. When a flake shorted the grids, the capacitor discharged through the flake thereby vaporizing it. Grid shorts occurred at the rate of a few per minute during the first 20 hours of the machining process. The extra current capacity of the accelerator supply was necessary because in the initial stages of the machining operation the accelerator supply must carry the full beam current.

At the start of the ion machining process it was necessary to throttle the mercury flow back to a few equivalent milliamps because the

unperforated accelerator grid prevented normal ion and neutral mercury propellant flow from the discharge chamber. The mercury flow was regulated such that the discharge voltage was above 30 V. Later as the ion beamlets sputtered through the accelerator grid, the mercury flow rate was gradually increased to the normal levels.

Because the thruster ion beam current, J_B , was measured as the current drawn by the neutralizer circuit (fig. 44), it read zero as long as there were no holes sputtered through the accelerator grid. The V_I (net accelerating potential) supply current, J_B' , is equal to the sum of the beam current, J_B , and the accelerator current, J_A . Initially because J_B equals zero, J_B' equals J_A . These three currents served as convenient parameters for monitoring the machining process. As the holes begin to sputter through the accelerator grid, J_B starts increasing and J_A starts decreasing. The relative magnitudes of J_B and J_A are sensitive indicators of the progress of the ion machining. Starting with a blank accelerator grid J_B increases from zero to the full beam current (72 mA) equilibrium level.

After two hours of operation of the ion beam current holes began to sputter through the 0.38 mm thick accelerator grid. As might be expected, the first breakthrough occurred in the center of the accelerator grid. The time of breakthrough was denoted by an increase in J_B and a decrease in J_A . Figure 45 is a plot of both normalized accelerator current J_A/J_B' and normalized beam current J_B/J_B' . Figure 46 is a plot of the accelerator current over a 1000 hour test interval.

Photographs of the upstream and downstream faces of the grid assembly are shown in figure 47. Measurements of the accelerator grid hole diameters were made from photomicrographs of several positions on both sides of the grid. Accelerator grid hole diameter measurements at five different times and at four locations are listed in table XI.

Results and discussion. - Because of higher beam density in the center of the grid, ion machining occurred at a faster rate there. After four hours accelerator holes were sputtered through in the center, but not at the outer edges of grid. Upstream views of partially sputtered through region (after 4 hr of ion machining) of the accelerator grid are presented in figure 48. Figure 48(a) is low magnification view of a region where some of the holes are sputtered all the way through and others are only partially through the 0.38 mm thick accelerator. The accelerator and screen grid were mounted on the grid assembly during photographing and, as a consequence, the upstream photographs include the screen grid. Figure 48(b) is a high magnification photograph of one particular accelerator hole. The picture shows the upstream and downstream perimeters of a sputtered accelerator hole. The individual beamlets appear to be focusing toward a point downstream of the accelerator grid.

Near the outer edges of the accelerator grid the ion machining process was slower and complex in structure. Measurements indicated that

on the downstream side the outer edge holes increased in size throughout the test, but on the upstream side they stabilized after 462 hours. On the upstream side of the accelerator grid the holes were circular, but on the downstream side of the accelerator grid the ion machined holes more closely approximated hexagons. Figure 49 is a photomicrograph of several holes after 462 hours of ion machining. The hexagonal shape appears to be related to the screen hexagonal hole array pattern. The sides of a particular hexagon are roughly perpendicular to lines connecting the center of the hexagon to its nearest neighbors. Figure 49(b) is a higher magnification photomicrograph of an accelerator hole. Similar accelerator grid erosion results were observed and described in reference 26.

The resulting accelerator holes are optimally sized to the ion beamlets. The smaller accelerator holes result in reduced neutral mercury loss, which in turn enhances the propellant utilization. The discharge chamber propellant utilization, η_{uD} , is equal to the ratio of beam current to total discharge chamber mercury flow,

$$\eta_{uD} = \frac{J_B}{J_B + J_N} \quad (1)$$

where J_N is equal to the unionized part of the total discharge chamber mercury flow. If it is assumed that the neutral loss rate from the discharge chamber is proportional to the open area of the accelerator grid, then

$$\frac{J_{N1}}{J_{N2}} = \frac{A_1}{A_2} = \frac{D_1^2}{D_2^2} \quad (2)$$

where A_1 and A_2 are two different open areas and D_1 and D_2 are the corresponding accelerator hole diameters. Then given empirical results of a particular accelerator hole diameter a relation can be derived for the approximate propellant utilization as a function of accelerator hole diameter. For $D_1 = 1.69$ mm and $J_B = 72$ mA thrusters have operated at 70 percent propellant utilization, J_{N1} can be calculated from equation (1) to be 30.8 mA. Then using equations (1) and (2)

$$\eta_{uD2} = \frac{J_B}{J_B + J_{N1} \left(\frac{D_2^2}{D_1^2} \right)} = \frac{1}{1 + \frac{J_{N1}}{J_B} \left(\frac{D_2^2}{D_1^2} \right)}$$

Substituting

$$\eta_{uD} = \frac{1}{1 + 0.149 D^2} \quad (3)$$

Figure 50 is a plot of the discharge chamber propellant utilization as a function of accelerator hole diameter calculated from equation (3). Large increases in propellant utilization are predicted for small accelerator grid holes. The ion beamlet diameter represents a lower limit to the accelerator hole diameter. As demonstrated by the results of ion machining experiments if the accelerator holes are smaller in diameter than the beamlet diameter, they will be enlarged by sputtering. The ion machined accelerator grid geometry then results in an accelerator grid having the maximum achievable propellant utilization efficiency.

The performance of an 8-cm thruster with an ion machined accelerator grid can be compared with the predictions of figure 50. Because the hole diameter of the ion machined accelerator grid varies with respect to hole location and which side of the grid is being viewed, the conservative choice might be the accelerator grid hole diameter as measured in the center of the grid on the downstream side after 462 hours. The upper limit listed in table XI is 0.83 mm, which would predict a discharge chamber propellant utilization efficiency of approximately 90 percent. This represents a lower limit of propellant utilization because many of the accelerator holes are considerably smaller.

The discharge power losses are plotted as a function of the discharge chamber propellant utilization in figure 51 for thruster with ion machined accelerator grid at 149 and 1006 hours and the same thruster with a large hole accelerator grid. The large hole accelerator grid had hole diameters of 1.69 mm. The ion machined accelerator grid results in lower discharge chamber losses and yet much higher propellant efficiencies. During most of the ion machining experiment the thruster was run near 90 percent discharge chamber utilization and 325 eV/ion. A complete set of thruster operating parameters is shown in table XII. For comparison, the small thruster program goals and the operating parameters of large hole conventional accelerator grid thrusters are listed. The total efficiencies are very close. The goal was 57.5 percent and the ion machined accelerator grid thruster operated at 56.7 percent. The large hole accelerator grid configured thruster was tested at two operating points. The first operating point was with the same mercury flow rate and discharge power as the ion machined accelerator grid thruster. This resulted in a beam current of 59.8 mA which corresponds to a thrust of 0.94 mlb at 465 eV/ion. The second test point was with the mercury flow rate increased such that the thruster could produce a 72 mA beam current (1.14 mlb thrust). This point is listed in table XII. A mercury flow rate of 106 mA was required. Propellant utilization was below 70 percent at 381 eV/ion. The lower propellant utilization decreased the specific impulse to 2247 seconds.

The two operating points mentioned above for the large hole conventional accelerator grid thruster are plotted in figure 51.

Figure 52 exhibits the accelerator current dependence on total voltage. Values are plotted for -300 V and zero volts applied to the accelerator grid. The thruster operated satisfactorily without any applied

accelerator voltage if the net accelerating voltage increased to maintain the same total voltage. With zero accelerator voltage the accelerator current was slightly less than with -300 V applied to the accelerator grid. This result suggests the possibility of operating the thruster without an accelerator supply which would result in weight savings on a spacecraft mission. Perhaps electrically attaching the accelerator grid to the neutralizer tip potential would ensure enough of an electron backstreaming barrier even if the small accelerator holes were photo etched rather than ion machined. Certainly accelerator grid lifetime should be greatly lengthened if the grid could operate near zero volts.

SIT-8 Thruster

J. Hyman, Jr. and W. R. Hudson

The basic objective of the SIT-8 thruster program is to advance the technology of satellite control thruster systems to accommodate the demands imposed by spacecraft mission requirements projected for the next decade and beyond. Hughes Research Laboratories is involved in the development of an 8-cm Structurally Integrated Ion Thruster system (SIT-8) under NASA contract NAS3-17791, and had previously been involved in the development (under NASA contracts NAS3-14129 and NAS3-15483) of the SIT-5 system.

The primary goal of the SIT-8 thruster program is the development of a high-performance structurally and thermally qualified ion thruster system (thruster and its power processor) which operates efficiently at a true thrust level of 1 mlb, with a lifetime expectancy in excess of 20 000 hours. The thruster will be equipped with a thruster gimbal system which is capable of thrust vectoring $\pm 10^\circ$ in two orthogonal directions.

The ion-thruster design is based on the SIT-8 thruster configuration which is currently under development at Hughes. Design of this prototype thruster was based on a mechanical structure similar to that of the flight-qualified SIT-5 system. Because of this similarity, results of extensive structural and thermal analyses which were successfully implemented under the SIT-5 program are considered to be applicable to this design also. Performance goals of the prototype SIT-8 design were developed in a study by Hudson and Banks (ref. 8) and are outlined in table XIII. To achieve these goals, design innovations have been incorporated in the discharge chamber and beam-extraction system which were developed or proved under other NASA or Hughes-sponsored programs. An isometric drawing of the SIT-8 thruster is shown in figure 53. A photograph of the present SIT-8 thruster without its gimbal system and with an auxiliary electrode ignitor is shown in figure 54.

The discharge chamber of the SIT-8 thruster consists of an outer shell assembly, which is formed by rolling thin stainless steel sheet stock. Structural rigidity of this thin-walled shell is provided by circular stiffening ribs and by flanged sleeves located at the two ends.

Axial strength of the structure is provided by the rod-shaped permanent magnets mounted axially around the periphery. Magnets are mounted to the flanges on the ends of the cylinders by lugged collars which are swaged onto the ends of the magnets and spot-welded securely to the flanges. These flanges also serve as the interface between the endplate on the closed end of the discharge chamber, and the mount for the beam-extraction system on the opposite end. A cylindrical anode is supported within the shell by means of insulating support posts which are totally shielded against sputtering. As with the thruster shell, stiffening ribs are used to ensure maintenance of its circular cross section.

The Cathode-Isolator-Vaporizer (CIV) assembly located on the upstream end of the 8-cm thruster endplate is essentially the same as that employed successfully with the SIT-5 system. By choosing a vaporizer plug of slightly different shape than that employed in the SIT-5 system, a porous cylinder of the same diameter is capable of supplying the higher mercury vapor flow required for this thruster.

The Neutralizer Isolator Vaporizer (NIV) assembly follows the SIT-5 design closely, with the single modification being the inclusion of a neutralizer isolator. The neutralizer is mounted so that the cathode axis is directed parallel to the axis of the thruster. An enclosed keeper is used, which is mounted directly to the neutralizer-cathode alignment structure. This mounting structure extends the full length of the thruster ground screen and provides a support for all components of the neutralizer assembly.

A ring of terminals is provided on the ground screen endplate for the various electrical connections. Connections between these terminals and the thruster components are made using short lengths of uninsulated wire. Sputter shielding is employed at both ends of these terminals to ensure that shorting cannot occur across insulating surfaces.

The SIT-8 beam-extraction system is fabricated with a dish-contoured surface to maintain structural rigidity against deformation. This permits the use of a high-perveance grid pair, because the screen-to-accelerator separation can be set to a small value without fear of grid shorting under operating conditions where thermal gradients might otherwise cause severe deformation.

When the SIT-8 thruster was received by LeRC it was operated in its as-delivered configuration. The results are tabulated in the as-delivered column of table XIV. The neutralizer, as supplied, had a LeRC specified impregnated insert and required very high flow, 25 mA, and tip heat, 9.89 watts, to operate with a coupling voltage of -64 V. When this neutralizer was replaced by one with a rolled foil insert and a 1.52 mm diameter keeper orifice, the neutralizer performance improved. The replacement neutralizer operates with no tip heater power at mercury flow rates at and below 6 mA. The coupling voltage is -10 V.

The beam extraction system on the SIT-8 thruster was replaced by the newly developed small hole accelerator grid geometry described in the previous section. This resulted in the dramatic increase in propellant utilization shown in table XIV. Originally, the discharge propellant utilization was 65.1 percent; with the small hole accelerator grid beam extraction system it increased to 90.0 percent.

The SIT-8 thruster was further modified by reducing the magnetic field in the discharge chamber and by replacing the LeRC specified impregnated insert cathode with a rolled foil insert main cathode. The resulting thruster operating conditions are tabulated in column titled After optimization in table XIV. It now compares very favorably with the SIT-8 performance goals. The projected Engineering Model SIT-8 thruster operating conditions are listed in table XV. The thruster will use a small hole accelerator grid and a rolled foil insert cathode and neutralizer. Lifetime and reliability enhancing features such as a grit-blasted fine mesh wire cloth anode, high voltage pulse ignition via the keeper electrode, and proper neutralizer position and flow rate shall be incorporated in the Engineering Model SIT-8 thruster design. The final Engineering Model SIT-8 thruster will be dynamically, thermally, and electrically qualified in conjunction with its power processor and gimbal system as part of the LeRC program.

THRUSTER ENDURANCE TESTS

8-Cm Thruster Cycling Endurance Test S. Nakanishi

A 9700-hour durability test on a 5-cm diameter thruster (ref. 7) demonstrated its inherent capability for continuous long-term operation. Much of the technology developed under the 5-cm thruster program has been incorporated into the 8-cm thruster design. The design of the cathode-isolator-vaporizer, the cathode pole piece, enclosed keeper neutralizer, propellant feed-system, and the concept of introducing the ion chamber propellant wholly through the cathode have been equally adaptable to both thruster sizes.

Several improvements have been incorporated into the 8-cm thruster to minimize ion chamber erosion and peeling of sputtered metal observed in the 5-cm thruster life test. The present test seeks to evaluate the effectiveness of these improvements and also to determine reliability under a cyclic mode of operation.

Because of the early inception of the present test, the specific designs used are preliminary. Wear and lifetime data obtained, however, should be useful in guiding the ultimate design.

Figure 55 shows the 8-cm thruster assembly prior to the test. The mercury propellant to the cathode and the neutralizer were fed from separate capillary tubes to permit independent flow measurement. The cathode-

isolator-vaporizer and the neutralizer-vaporizer assemblies were those formerly fabricated for the 5-cm thruster. The rolled-foil inserts of the cathode and neutralizer were replaced with inserts of the barium-impregnated porous tungsten type. The thruster has a 9.4 cm diameter by 7.77 cm long anode fabricated of a coarse stainless steel wire mesh. The cathode pole piece is a conical vented design which has an exit diameter of 1.59 cm. Two cathode baffles have been used thus far in the test. The original baffle was 0.63 cm in diameter and identical to the design reported in reference 20. A second design was similar to the SIT-5 baffle but fabricated of nonisotropic graphite instead of tantalum. The thruster back plate was clad with pyrolytic graphite. An auxiliary electrode was mounted through the thruster back plate on shadow shielded insulators to allow high voltage pulse ignition of the cathode.

The ion accelerator optics were dished grids with 1.97 mm diameter screen holes on 2.21 mm centers (72.5 percent open area) and 1.69 mm diameter accelerator holes (51 percent open area). The accelerator grid was 0.52 mm thick. The minimum gap between grids near the thruster axis was 0.0507 cm.

Also visible in the photograph is the neutralizer mounted with its axis parallel to the thruster axis. The keeper aperture was positioned 3.57 cm downstream and 3.54 cm radially outward from the outermost active accelerator beam hole. The neutralizer was also equipped with an auxiliary electrode for pulse ignition. The entire thruster assembly was covered by a mask and screen enclosure floated at neutralizer potential. The rectangular box mounted on a movable rod contained glass slides to document sputter efflux.

Figure 56 shows the interior of the 1.37 by 1.83 m vacuum facility prior to the test. The 112-cm diameter stainless steel pan for the target mercury was attached to 12 radial copper struts to which copper cooling coils were brazed. A cylindrical cooling coil welded to a perforated stainless steel shell formed the cryowall which extended along the vertical wall of the tank.

The thruster was operated at a distance of 76 cm from the frozen mercury target. To prevent the backspattering of condensible conductive material upon the thruster from the sides of the vacuum facility, in addition to the frozen mercury target, a set of nonmetallic baffles was installed in line of sight of the thruster ion beam. The baffle assembly consisted of three slanted annular baffles spaced 25 cm apart with an 83.8-cm inside diameter opening. The baffles were made from 0.63 cm thick sheets of Fiberfax insulation (50 percent Al_2O_3 ; 50 percent SiO_2) fitted and supported on a frame fabricated of stainless steel sheet strips.

The 8-cm thruster durability test procedures were essentially similar to those of the 5-cm thruster test with two exceptions. Duty cycle operation was simulated by weekday runs of $22\frac{1}{2}$ hours on and $1\frac{1}{2}$ hours off.

On weekends and holidays the thruster was operated continuously. Startup followed the conventional cathode and vaporizer heating procedures, but ignition was by a high voltage pulse to the auxiliary electrode with 40 V d.c. applied to the keeper. Shutdown was accomplished by a single switch which simultaneously deenergized all power supplies.

The thruster was operated at fixed conditions with minor adjustments to maintain a beam current of 72 mA. The cathode vaporizer power was controlled by a loop which sensed the discharge voltage about a set point of 40 V. The resulting cathode flow rate was between 114 to 117 mA.

The neutralizer vaporizer temperature was manually controlled to maintain a flow rate of 6.5 to 7.5 mA. This level of flow was selected on the basis of previously discussed tests. These tests indicated less neutralizer erosion than observed in the 5-cm thruster test which used 2.2 mA neutralizer flow.

The cathode was operated without tip heat except during startups. Neutralizer tip heat was adjusted as required to assure stable operation.

The test has operated over 7400 hours and 229 startups as of October 1974. It was interrupted once at 1156 hours when the pyrolytic baffle delaminated, thus necessitating a shutdown for replacement. The thruster was disassembled for photographic documentation and reassembled with only a baffle change (a nonoriented graphite baffle was installed).

In the discussion that follows, a history of the test up to 6235 hours will be presented including various abnormal events. Performance profiles at 2057 and 5500 hours will be compared. Significant photographs taken at the 1156 hour shutdown will be shown. Finally, a brief discussion of starting characteristics will be given.

A chronological history of the test is shown in figure 57. The four parameters plotted were those most subject to change as the test progressed. Other parameters were either invariant or adjusted to hold pre-selected values. The cathode keeper current and the neutralizer keeper current were held at 0.24 and 0.45 A, respectively.

The initial 2000 hours of the test were characterized by numerous neutralizer extinctions. Accelerator drain (fig. 62) current exhibited variations from a high of 0.38 mA to a low of 0.2 mA until finally settling out to a value of about 0.2 mA. The neutralizer extinctions did not appear to be related to accelerator grid arcs and occurred during periods of high drain as well as low drain current.

The cathode keeper voltage (fig. 57) also exhibited considerable variation in the early hours of the test. After about 2500 hours into the test, the voltage stabilized to about 14 V. Major variation from this level occurred only after a high tank pressure condition occurred at 3750 hours. Temporary poisoning of the cathode insert may have caused the increase in cathode keeper voltage, but this conjecture is not sup-

ported by lack of similar changes in the neutralizer keeper voltage. The neutralizer keeper voltage, however, was sensitive to changes in neutralizer heater power (fig. 57). In an attempt to stabilize the neutralizer, different levels of neutralizer heater power were tried as indicated on figure 57. The many changes in heater power level were motivated by the necessity of avoiding neutralizer extinction on the one hand and of reducing heater power losses on the other. A general trend noticed in the 5-cm thruster test was also evident here. Decreasing the heater power increased the neutralizer keeper voltage and to some extent, the floating potential. In the present test, however, operating the neutralizer with heater power less than about 7.2 watts appeared to cause excessively high keeper voltage or eventual extinction. The neutralizer is currently operating with 7.2 watts of heater power. Periods of neutralizer extinctions still occur. Running the neutralizer for 24 hours with 14.4 watts of heater power seemed to restore stable operation again at 7.2 watts.

Thruster performance profiles taken at 2057 and 5500 hours are compared in table XVI. The early profile was taken about 900 hours after the baffle replacement. Because of adjustments to fixed point values, beam power and thrust did not change with time. A small increase in discharge current and a 10 percent increase in cathode flow rate was observed. The accuracy of recent flow values is supported by a time plot of propellant weights added to maintain the reservoir mercury level. This plot shows a flow rate of about 120 mA.

Accelerator drain current showed a slight decrease with time. This is in contradiction to trends normally found with increase in propellant flow or poorer utilization efficiency. Power dissipated in the neutralizer was due mostly to keeper discharge and heater power. The profile at 2057 hours was taken when heater power was 14.4 watts.

The neutralizer floating potential shown in figure 57 increased gradually from approximately -22 V at the start to about -35 V at 3000 hours. It was subject to variations because of frequent changes in the heater power. Even prolonged periods of constant heater power, however, showed some rise in the mean level of the floating potential. Subsequent reduction in heater power to 7.2 watts accounted for most of the change in total input power between 2057 and 5500 hours.

The baffle delamination at 1156 hours occurred too soon to permit an accurate evaluation of component weight change due to sputter erosion. Of particular interest were the cathode baffle, thruster back plate, anode accelerator, and neutralizer.

After 1156 hours of operation the fractured pieces of the baffle showed an aggregate weight increase of 0.04864 g. The graphite back plate decreased 0.10353 g. The anode increased 0.0579 g. The accelerator and its mounting ring lost 0.5558 g. The integral structure of the neutralizer did not permit its weighing. Microphotographs of the neutralizer aperture and face taken after 1156 hours are shown in figure 58. The tool marks on the face of the neutralizer are distinct to the very

edge of the aperture, indicating minimal erosion.

Before and after photographs of the cathode baffle, pole piece, and graphite backplate assembly are shown in figures 59 and 60; also visible is the auxiliary electrode used for pulse ignition of the cathode. Figure 60 shows the nature of the baffle fracture. The graphite backplate shows a glazed appearance. The surface when new was smooth in spite of the blistered appearance characteristic of pyrolytic graphite.

Because the present test was intended primarily to evaluate thruster durability and restart capability, no attempt was made to determine the minimum starting requirements at each restart. Rather, emphasis was placed on establishing those conditions which assured a quick and positive restart without overheating the cathode and neutralizer tips or their vaporizers. Application of the maximum attainable pulse voltage was avoided whenever possible so that various power supply components would not be overstressed.

Over the course of numerous restarts some statistics on starting requirements have been accumulated as shown in table XVII. The starting conditions representative at about 500 hour intervals and the corresponding start numbers are given together with the cathode and neutralizer conditions. The pulse voltage and number denote the no breakdown peak output voltage and the number of pulse discharges required before ignition.

As the data shows, there was no strong or consistent trend in either the cathode or neutralizer starting characteristics. The cathode generally started at a lower tip heater power than the neutralizer because of its higher propellant flow rate at similar starting vaporizer temperatures.

The neutralizer invariably required a tip heat of over 20 W and vaporizer temperatures approaching 400° C which corresponds to about 10 mA flow. After about 100 starts, a pulse voltage of 15 kV was routinely used. As shown by starts number 155 through 157, restarts were always possible but the starting characteristics were not consistent.

Accelerated Thruster Cycling Rate High Voltage Pulse Ignition Tests E. G. Wintucky

An 8-cm ion thruster has completed 286 cycles in an ongoing accelerated cycling rate thruster endurance test. A typical cycle consisted of (a) thruster startup in 15 minutes or less using a high voltage pulse to ignite the cathode keeper discharges, (b) one hour of operation at roughly 1.2 mlb ideal thrust, and (c) a thruster off period which varied from 0.5 hours to days.

The cathode starting sequence consisted of first turning on the tip heaters and after five minutes, the vaporizer heaters. When the vaporizer

temperatures were at or near their equilibrium operating temperatures, the keeper discharges were ignited. Starting times range from 10 to 15 minutes. The cathode starting conditions are summarized in table XVIII. Igniting the keeper discharges was accomplished by applying a high voltage pulse to an auxiliary electrode positioned 0.5 mm from the face of the keeper cap. The high voltage pulse technique is described more fully elsewhere in this paper. Breakdown voltages were generally 8 to 10 kV for the main cathode and 10 to 12 kV for the neutralizer. Usually a single pulse sufficed although occasionally more than one pulse was required to start the neutralizer, probably because of low Hg flow.

Table XIX presents the thruster operating conditions averaged over cycles 201 to 225. The ideal thrust level of 1.23 mlb should more than allow for 1 mlb thrust after losses from beam divergence and double ionization. The low efficiencies are a consequence of the thruster not being optimized with respect to grid optics, discharge chamber configuration, cathodes and thermal characteristics. The thruster was cycled manually which accounts for the wide range of thruster off times.

POWER PROCESSOR TECHNOLOGY

Thruster power processor technology discussed in this section includes both the laboratory test consoles used for research and development testing and a more flightlike configured thermal vacuum breadboard power processor. A new thruster control loop is also described because of its significant improvement over previous techniques.

Laboratory Thruster Test Consoles R. R. Robson

The laboratory thruster test console (fig. 61) is a self-contained power supply system incorporating all the power supplies, control loops, and data acquisition equipment required to run an 8-cm mercury ion thruster. It is built from off-the-shelf 60 Hz power supplies and no attempt has been made to simulate flight hardware. It is packaged in one movable rack and can be rolled from one test facility to another to operate a thruster.

A block diagram of the test console is shown in figure 62 and a tabulation of the power supply outputs in table XX.

The screen supply is a 0 to 2000 V d.c., 0 to 200 mA, voltage and current regulated supply with automatic crossover. Regulation for both voltage and current is better than 0.01 percent of full scale. The supply has approximately 4 microfarads of capacitance in its output. The accelerator supply is a 0 to 2000 V, 0 to 10 mA supply with 20 percent load regulation. It has a 5 henry choke in its output to limit surge currents during arcs.

The discharge supply is a 100 V d.c., 0 to 1.5 A supply with a 0 to 1.5 A current regulator in its output. The output of the current regulator has only stray capacitance associated with it and therefore delivers constant current to the discharge well into the kilohertz frequency range.

The keeper supplies are 34 V d.c., 0 to 0.5 A supplies with 0 to 1.0 A current regulators in their outputs. These regulators are similar to the regulator used for the discharge supply. The ignitor supplies for the keepers are either 450 or 900 V d.c. (depending on the thruster being tested). The output of these supplies are ballasted with a resistor to provide a short circuit current of ≈ 100 mA. The ignitor supplies are isolated from the keeper supplies by means of a diode and circuitry is provided to turn the ignitors off once their associated discharge is established.

The tip heater power is provided from a.c. supplies consisting of a Variac and a transformer capable of delivering 12 V at 10 A. The only regulation is provided by the line regulator for the primary power.

The cathode vaporizer supply is a voltage regulated d.c. supply capable of delivering 6 V at 10 A. The regulator can be set manually or can be switched to accept the discharge voltage as a feedback signal and maintain control around some predetermined level. This supply can be run at cathode potential, neutralizer potential, or at facility ground depending on the mercury isolator system employed on a given thruster.

The neutralizer vaporizer supply is a voltage regulated d.c. supply capable of delivering 6 V at 10 A. The regulator can be set manually or can be switched to accept the neutralizer keeper voltage as a feedback signal and control around some predetermined level. This supply can be run at neutralizer potential or at facility ground depending on the mercury isolator system employed on a given thruster.

A clamp circuit consisting of back to back gas discharge tubes is provided to maintain the neutralizer potential to within 150 V of ground potential.

A line regulator is provided to eliminate line transients from the primary power. Primary power for the supplies at cathode potential is isolated from ground by way of a Variac core with an added secondary winding insulated for 5 kV.

All voltages and currents associated with the operation of a thruster are displayed on panel meters in the rack. Direct current voltage signals proportional to these voltages and currents are also provided at ground or neutralizer potential for recording on an automatic central data collection system. Voltage and current signals floating at cathode potential are transported to ground potential by means of optical d.c. signal isolators. These isolators consist of a voltage to frequency converter,

a light emitting diode/photo diode combination, and a frequency to voltage converter. The light emitting diode/photo diode combination provides the voltage isolation for the signal.

Presently LeRC has seven laboratory test consoles, one of which has accumulated over 15 000 hours of thruster operation.

Main Vaporizer Control Loop Techniques J. L. Power

The power processor packages used to operate the 5- and 8-cm mercury ion thrusters at LeRC are equipped with an auto control circuit (fig. 63) designed to maintain a constant, preset ΔV_I during unattended thruster operation by adjustment of the main cathode mercury flow rate. At the same time an independent, constant current power supply maintains the emission current, J_E , at the level required to produce the desired beam current, J_B , under the thruster operating conditions.

The control circuit is a feedback loop which operates to maintain the desired ΔV_I by generating a proportional error signal from the difference between the sensed ΔV_I and the ΔV_I set point. Via this error signal the control circuit continuously and linearly corrects the main vaporizer current, decreasing the current when ΔV_I is too low and increasing it when ΔV_I is too high. Thus the control circuit holds the desired ΔV_I by continuously adjusting the main cathode flow rate. Since J_B nominally remains constant during this adjustment, the discharge chamber utilization varies along with the main cathode flow rate during normal operation of the control circuit.

After several thousand hours operation of the SIT-5 thruster used to conduct the discharge chamber erosion tests described earlier in this paper, it was noted that fluctuations were occurring in the main cathode keeper potential, V_{CK} , while the keeper current was held fixed, normally at 400 mA. These V_{CK} fluctuations, of undetermined origin, became more frequent and random with continued thruster operation and began to interact strongly and undesirably with the ΔV_I auto control circuit.

The V_{CK} fluctuations were generally a few seconds in duration and 1 to 3 V in magnitude, normally in the positive direction. Thus they usually caused V_{CK} to increase from its normal value of 14 to 15 V to 15 to 18 V before returning again to its normal range. Frequently, instantaneous or discontinuous small changes in V_{CK} were noted during the fluctuations. The V_{CK} fluctuations, so far as is known, are unique to the SIT-5 thruster tested and do not represent a general problem observed in long term operation of small mercury ion thrusters.

It was normally observed that whenever V_{CK} underwent one of the above-described fluctuations, ΔV_I experienced an identical and simultaneous fluctuation, so that the difference ($\Delta V_I - V_{CK}$) remained con-

stant before, during, and after the fluctuation. These ΔV_I fluctuations caused considerable difficulty in the functioning of the ΔV_I auto control circuit, when this circuit was in operation. The problem was due to the fact that the time scale and response lag of the mercury flow control changes initiated by the control circuit in response to the changes in ΔV_I were considerably longer than the duration of the ΔV_I and V_{CK} fluctuations themselves. During periods of frequent or nearly continuous V_{CK} and ΔV_I fluctuations, interaction between the fluctuations and the control circuit operation caused gross variations, often of more than 15 percent, in the main cathode flow rate. These occurred as the control circuit attempted to counteract the constantly varying ΔV_I .

The identical, coincident fluctuations noted in V_{CK} and ΔV_I indicated that the main discharge plasma in the SIT-5 thruster is normally coupled between the cathode keeper potential and the anode. Hence this plasma is characterized by the potential drop given by $(\Delta V_I - V_{CK})$. The observed V_{CK} (and ΔV_I) fluctuations evidently were fluctuations only in the potential drop across the plasma sheath at the cathode tip and were not transmitted to the main discharge.

This analysis suggested a basic improvement could be made in the ΔV_I auto-control circuit for 5- and 8-cm thrusters - a modification which would eliminate interaction of the circuit with V_{CK} (and ΔV_I) fluctuations - by rewiring the circuit to sense and control on $(\Delta V_I - V_{CK})$ instead of on just ΔV_I . This modification was made in the control circuit (see fig. 63) and the modified control loop was tested during the SIT-5 accelerated life test described previously. The revised auto control circuit performed up to full expectations during the test, maintaining the desired nominal ΔV_I of 64.6 V with a steady, stable cathode flow rate throughout the 200 hour test despite nearly continuous V_{CK} (and ΔV_I) fluctuations. The main cathode flow rate was observed to vary $< \pm 2$ percent over the course of the test.

The thruster operating conditions maintained during the accelerated life test posed more stringent performance requirements on the ΔV_I auto-control circuit than would the normal operating conditions at a ΔV_I of 40 V. Hence satisfactory performance of the revised control circuit under normal SIT-5 operating conditions is anticipated, though such performance has not yet been demonstrated in an extended test.

Thermal Vacuum Breadboard Power Processor W. Herron and N. L. Milder

For all near future missions, electric power requirements for ion propulsion systems will be derived from solar arrays. It is thus necessary to provide lightweight, efficient power conversion electronics as part of thruster subsystems. In addition to providing the d.c. voltages and currents necessary to operate the thruster, the electrical subsystem must include control electronics for sustained thruster operation, must

be capable of protecting itself and the solar array bus from high energy transients, and must be able to receive and process digital commands as well as provide appropriate telemetry outputs. In short, the thruster power processing system is to be an efficient, reliable and lightweight self-contained unit capable of providing sustained power and control to a highly dynamic load over a specified range of operating conditions.

To accomplish this task, LeRC has initiated a contractual program with Hughes Research Laboratories to design, fabricate, and test a thermal vacuum breadboard (TVBB) power processing unit capable of providing sustained operation of an 8-cm diameter thruster at a maximum thrust level of about 2 mlb (8.9 mN) and a nominal thrust level of 1 mlb (4.4 mN). Some design criteria for this unit are given in table XXI.

The functional elements of the TVBB power processor are shown in figure 64. All inverters used incorporate transistor power switching. The relay in the housekeeping supply receives simple on/off commands and applies +28 V d.c. power to the low voltage (housekeeping) inverter section, which converts the +28 V d.c. to a 16 V a.c., 10 kHz square wave. This power operates the command storage and control logic section and is also used by the other supplies in the power processor for synchronization and bias. The line regulator converts the 70 ± 20 V d.c. bus to a regulated 48 V d.c. The line filter will filter the ripple current from the line regulator, screen and discharge supplies. The a.c. distribution inverter converts the 48 V d.c. from the line regulator to 96 V a.c. for use by the magnetic amplifier regulators. These mag amp regulators convert this 96 V a.c. to the voltages and currents required by the various heaters and two keepers. The accelerator supply is a linear regulator and also uses the 96 V a.c. The screen and discharge supplies are pulse width modulated and deliver the required power to the thruster screen and main discharge, respectively. The command storage and control logic (controller) receives strobed 16-bit command words. It operates on these words to produce the setpoints and other automatic functions as required by the rest of the power processor.

The grounding system used in the TVBB magnetically isolates power processor common from the power return (S/C common). Photocouplers are used to isolate power processor common from the input command word and strobe signal return. Analog telemetry signals (0 to 5 V) from the power processor supplies are referenced to power processor common. A 50-V "clamping" or limiter circuit prevents an excessive voltage differential between the power processor common and the power return.

Figure 65 is a block diagram showing power supplies and control functions interfacing with the thruster. The main discharge, cathode keeper, vaporizer and heater supplies are all referenced to cathode common, or screen potential. Neutralizer heater, keeper and vaporizer power supplies are referenced to power processor common. Two control loops are incorporated to stabilize and sustain thruster operation at preset performance levels. One loop maintains discharge voltage constant to a se-

lected level over a range of discharge currents by controlling neutral mercury flow to the discharge chamber. The second loop controls neutralizer propellant flow by maintaining the neutralizer keeper voltage proportionally constant to a digital-to-analog reference by adjustment of neutralizer vaporizer power. The control circuitry also provides for thruster recycling following a high-voltage arc or breakdown.

Additional unique circuitry incorporated in the TVBB includes the capability of supplying short-term energy pulses in the screen supply for metal flake or chip clearing, and high-voltage (10 kV max) pulsed igniter circuits for cathode and neutralizer keeper startup.

Figure 66 shows a preliminary design of the TVBB package. The unit is separated into two modular sections. The smaller module contains interface command logic, the digital and analog control circuitry, and the housekeeping bias supplies. The larger module houses the low and high voltage power supplies, and will be additionally partitioned by a grounded barrier to separate low- and high-voltage circuitry. Each section will be vented to eliminate low pressure entrapped gas. Internally, components will be mounted on terminals swaged into metal T section to provide a conductive thermal path to the baseplate. An almost straight-through flow of power from left-to-right (fig. 66) minimizes potential EMI problems and provides a logical separation of voltage levels. Inputs for command/control and power will enter the unit by connectors. Output power will exit by means of "flying" terminal leads.

APPLICATIONS

B. A. Banks

The SIT-8 4 mN (1 mlb) mercury ion thruster is specifically designed to perform north south station keeping of geosynchronous spacecraft. In addition the SIT-8 gimbal system allows east west station keeping, momentum wheel dumping, and/or attitude control to be performed if the spacecraft is suitable configured. The north south station keeping velocity requirement greatly exceeds the other requirements and represents the most probable use of the SIT-8 thruster system. In this section system weights will be determined based on the north-south station keeping requirements for a variety of typical missions. The projected SIT-8 Engineering Model Thruster System weight breakdown is shown in table XXII. The propellant and tankage masses listed are sufficient to provide five years of north-south station keeping of a 680 kg (15 000 lb mass) spacecraft or 10 years for a 347 kg (765 lb mass) spacecraft.

Total thruster system mass, M_{TOT} , for an arbitrary duration and mass mission is given by

$$M_{TOT} = N(M_{Th} + M_G + M_{Hg} + M_{Tk} + M_{PC})$$

where

N = number of independent thruster systems

M_{Th} = mass of thruster, kg

M_G = mass of each gimbal system, kg

M_{Hg} = mass of mercury propellant for each thruster, kg

M_{Tk} = mass of propellant tankage for each thruster, kg

M_{PC} = mass of each power conditioner (including all cabling), kg

Both M_{Th} and M_G values are not mission length or spacecraft mass dependent and values from table XXII can be used. The amount of mercury propellant required, M_{Hg} , depends upon the number of thruster operating hours T and the propellant flow rate and is given by

$$M_{Hg} = \frac{(3.6)^{g/w}}{N_A e} \dot{m} T$$

where M_{Hg} is in kg and

g/w = molecular weight of mercury, 200.59 kg/k mole

N_A = Arogadro's number, 6.022169×10^{26} /k mole

e = electron charge, $1.6021917 \times 10^{-19}$ C

\dot{m} = thruster equivalent mass flow rate, mA

T = thruster total operating time, hr

Substitution of the actual constants results in

$$M_{Hg} = 7.484 \times 10^{-6} \dot{m} T$$

The thruster total operating hours required for north south station keeping consists of the total time, T_{SK} hours, that each thruster is actively station keeping by providing thrust and the total preheat and cool down time, T_{PH} hours. Assuming that a characteristic preheat and cooldown time can be determined such that the equivalent propellant flow rate, \dot{m} , during the preheat and cooldown time is characteristic of that during steady state operation, then

$$M_{Hg} = 7.484 \times 10^{-6} \dot{m} (T_{SK} + T_{PH})$$

The total hours of north south station keeping required can be com-

puted by knowing the geosynchronous satellite velocity change requirement necessary to counteract the solar and lunar gravitational disturbance forces. Those disturbing forces cause an inclination in the orbit of the satellite unless corrective thrust is applied at the points where an uncorrected inclined orbit crosses the equatorial plane (see fig. 67). The disturbance forces of the Sun and Moon cause a torque $\vec{\tau}$ to act upon the angular momentum \vec{L} of the geosynchronous satellite. The resulting effect of this is simply Newton's second law of motion applied to rotational motion. Thus

$$\frac{d\vec{L}}{dt} = \vec{\tau}$$

where t = time and

$$\int d\vec{L} = \int \vec{\tau} dt$$

$$\Delta\vec{L} = \int \vec{r} \times \vec{F} dt$$

where $\Delta\vec{L}$ is the corrective angular momentum required, \vec{r} is the geosynchronous radius vector, and \vec{F} is the thrust vector.

Since the corrective angular momentum required is usually expressed as linear velocity change, $\Delta\vec{L}$ can be written

$$\Delta L = |\Delta\vec{L}| = M_{SC} r \Delta V$$

where

M_{SC} = spacecraft mass, kg

ΔV = N-S station keeping velocity requirement in m/sec-yr = 46 m/sec-yr

If the torque integral is evaluated over one fourth of the orbit and there are N thrusters where $N = 1$ or any even number, then

$$\frac{\Delta V}{(365.25 \text{ days/yr})} = \frac{2N}{M_{SC} r} \int_0^{t_0/2} |\vec{r} \times \vec{F}| dt$$

The thrusters thus operate for t_0 seconds each. By symmetry, only the $rF \cos \theta$ torque components are additive and if the thrusters are inclined at an angle ϕ from true north or south we have

$$\frac{\Delta V}{365.25} = \frac{2N}{M_{SC}r} \int_0^{t_o/2} rF \cos \theta \cos \phi \, dt$$

If

$r = \text{constant}$

$\phi = \text{constant}$

$F = \text{constant}$

then

$$\frac{\Delta V}{365.25} = \frac{2NF}{M_{SC}} \cos \phi \int_0^{t_o/2} \cos \theta \, dt$$

Because the orbit is geosynchronous

$$\frac{\theta}{2\pi} = \frac{t}{24(60)^2}$$

or

$$\frac{\Delta V}{365.25} = \frac{2NF \cos \phi}{M_{SC}} \int_0^{t_o/2} \cos\left(\frac{\pi t}{43\,200}\right) dt$$

thus

$$\frac{\Delta V}{365.25} = \frac{2NF \cos \phi}{M_{SC}} \frac{(43\,200)}{\pi} \sin\left(\frac{\pi t_o}{86\,400}\right)$$

and

$$t_o = 2.75 \times 10^4 \arcsin \left\{ (4.58 \times 10^{-6}) \frac{M_{SC}}{NF \cos \phi} \right\}$$

for $\Delta V = 46 \text{ m/sec-yr.}$

The operating time, t , per orbit per thruster in hours is

$$t = \frac{t_o}{3600}$$

or

$$t = 7.64 \text{ arc sin} \left\{ 4.58 \times 10^{-6} \frac{M_{SC}}{NF \cos \phi} \right\}$$

For a mission of length Y years, the total north south station keeping time per thruster in hours is

$$T_{SK} = (2.79 \times 10^3) Y \text{ arc sin} \left\{ \frac{4.58 \times 10^{-6} M_{SC}}{NF \cos \phi} \right\}$$

If there are two thrusters ($N = 2$) and redundancy is required such that either thruster has sufficient lifetime and propellant to entirely accomplish the mission, then the required thrusting time per thruster is

$$T_{SK} = (2.79 \times 10^3) Y \text{ arc sin} \left(\frac{4.58 \times 10^{-6} M_{SC}}{F \cos \phi} \right)$$

The additional total time that propellant is being consumed due to preheat and cool down can be expressed in hours as

$$T_{PH} = 365.25 Y t_{PH}$$

where t_{PH} is the equivalent amount of time, in hours per orbit, that propellant is being expended during thruster preheat or cooldown. For the above, t_{PH} , the flow rate is assumed to be that of normal thruster operation.

Assuming thruster redundancy (either thruster has sufficient lifetime and propellant to entirely accomplish the mission) and using the derived expressions for T_{SK} and T_{PH} result in

$$M_{Hg} = 2.088 \times 10^{-2} Y \dot{m} \text{ arc sin} \left\{ \frac{(4.58 \times 10^{-6}) M_{SC}}{F \cos \phi} \right\} + 2.73 \times 10^{-3} Y t_{PH} \dot{m}$$

Propellant tank masses, M_{Tk} , for the small size typically required for north-south station keeping can be empirically expressed as

$$M_{Tk} = (0.123) M_{Hg} + 0.2$$

Summing all the thruster system masses for two redundant thrusters using the following projected SIT-8 engineering model thruster system values:

$$M_{Th} = 1.69 \text{ kg}$$

$$M_G = 0.68 \text{ kg}$$

$$\dot{m} = 84.4 \text{ mA}$$

$$F = 4.45 \times 10^{-3} \text{ N}$$

$$t_{PH} = 0.25 \text{ hour}$$

$$M_{PC} = 6.49 \text{ kg}$$

results in

$$M_{TOT} = 18.12 + 3.96 Y \arcsin \left\{ \frac{1.03 \times 10^{-3} M_{SC}}{\cos \phi} \right\} + 0.129 Y$$

A plot of the total thruster mass M_{TOT} using the above equation is shown in figure 68(a) and (b) for thrusters oriented at $\phi = 0^\circ$ and 45° , respectively. If there were only one thruster, then all the M_{TOT} values would be one half those shown in figures 68(a) and (b).

Because the propellant mass required is lowest at $\phi = 0$ and thruster efflux must be considered, mounting of thrusters at the ends of the solar arrays as shown in figure 69 is desirable.

REFERENCES

1. Owens, W. L., "Optimization of Ion Propulsion for North-South Station-keeping of Communications Satellites," presented at the AIAA/SAE 8th Joint Propulsion Specialist Conference, 1972, New Orleans, La.
2. Cybulski, R. J., et al., "Results from SERT I Ion Rocket Flight Test," TN D-2718, 1965, NASA.
3. Kerslake, W. R., Goldman, R. G., and Nieberding, W. C., "SERT II - Mission, Thruster Performance, and in-Flight Thrust Measurements," Journal of Spacecraft and Rockets, Vol. 8, No. 3, March 1971, pp. 213-224.
4. Kerslake, W. R., and Finke, R. C., "SERT II Hollow Cathode Multiple Restarts in Space Stationkeeping and Primary Electric Propulsion," AIAA Paper 73-1136, Lake Tahoe, Nev., 1973.
5. Nakanishi, S., and Finke, R. C., "A 2000-Hour Durability Test of a 5-Centimeter Diameter Mercury Bombardment Ion Thruster," TM X-68155, 1972, NASA.
6. Nakanishi, S., "Durability Tests of a 5-Centimeter Diameter Ion Thruster System," AIAA Paper 72-1151, New Orleans, La., 1972.
7. Nakanishi, J., and Finke, R. C., "A 9700-Hour Durability Test of a Five Centimeter Diameter Ion Thruster," AIAA Paper 73-1111, Lake Tahoe, Nev., 1973.
8. Hudson, W. R., and Banks, B. A., "An 8-Centimeter Electron Bombardment Ion Thruster For Auxiliary Propulsion," AIAA Paper 73-1131, Lake Tahoe, Nev., 1973.
9. Hudson, W. R., and Weigand, A. J., "Hollow Cathodes with BaO Impregnated Porous Tungsten Inserts and Tips," AIAA Paper 73-1142, Lake Tahoe, Nev., 1973.
10. Wintucky, E. G., "High Voltage Pulse Ignition of Mercury Discharge Hollow Cathodes," AIAA Paper 73-1140, Lake Tahoe, Nev., 1973.
11. Wilbur, P. J., "Performance of a 15-Centimeter Ion Thruster with Reliable Restart Capability," AIAA Paper 73-1139, Lake Tahoe, Nev., 1973.
12. Hyman, J., Jr., "Design and Development of a Small Structurally Integrated Ion Thruster System," 1971, Hughes Research Labs., Malibu, Calif., available as CR-120821, NASA.

13. Nakanishi, S., and Pawlik, E. V., "Preliminary Experimental Operation of High-Voltage Isolation Device for Propellant System of Ion Rocket," TM X-1026, 1964, NASA.
14. Nakanishi, S., "Experimental Investigation of a High-Voltage Isolation Device for Ion-Thruster Propellant Feed," TN D-3535, 1966, NASA.
15. Nakanishi, S., "Experimental Investigation of Mercury Propellant Feed Isolators for Kaufman Thrusters," TM X-1579, 1968, NASA.
16. Nakanishi, S., "Durability Tests of a Five-Centimeter Diameter Ion Thruster System," AIAA Paper 72-1151, New Orleans, La., 1972.
17. Hyman, J., Jr., "Performance Optimized, Small Structurally Integrated Ion Thruster System," 1973, Hughes Research Labs., Malibu, Calif., available as CR-121183, NASA.
18. Power, J. L., "Sputter Erosion and Deposition in the Discharge Chamber of a Small Mercury Ion Thruster," AIAA Paper 73-1109, Lake Tahoe, Nev., 1973.
19. Performed by Dr. A. W. Moore, Union Carbide Corp.
20. Power, J. L., "Accelerated Life Test of Sputtering and Anode Deposit Spalling in a Small Ion Thruster," Proposed NASA Technical Memorandum.
21. Weigand, A., and Mirtich, M., "Change in Transmittance of Fused Silica as a Means of Detecting Material Sputtered from Components on a 5-Centimeter Ion Thruster," TM X-68073, 1972, NASA.
22. Rawlin, V. K., Banks, B. A., and Byers, D. D., "Design, Fabrication, and Operation of Dished Accelerator Grids on a 30-Centimeter Ion Thruster," AIAA Paper 72-486, Bethesda, Md., 1972.
23. Danilowicz, R. L., Rawlin, V. K., Banks, B. A., and Wintucky, E. G., "Measurement of Beam Divergence of 30-Centimeter Dished Grids," AIAA Paper 73-1051, Lake Tahoe, Nev., 1973.
24. Rawlin, V. K., "Studies of Dished Accelerator Grids for 30-Centimeter Ion Thrusters," AIAA Paper 73-1086, Lake Tahoe, Nev., 1973.
25. Rawlin, V. K., "Performance of 30-Centimeter Ion Thrusters with Dished Accelerator Grids," AIAA Paper 73-1053, Lake Tahoe, Nev., 1973.
26. Byers, D. C., and Banks, B. A., "Beam Focusing Characteristics of Various Shaped Grid Holes," TM X-67922, 1971, NASA.

TABLE I. - CATHODE INSERT COMPARISON TABLE

Insert	Initial starting		Typical starting		Keeper		Cathode tip power		Number of starts
	Temperature, °C	Power, W	Temperature, °C	Power, W	Voltage, V	Current, A	Running, W	Lowest starting, W	
Rolled foil									
#1	1150	23.8	1100	20.8	14-16	0.2-0.4	8.1	20.4	10
#2	1140	22.6	1150	20.8	12-16	0.2-0.5	7.7	17.2	12
#3	----	21.3	----	19.8	12-14	0.2-0.4	7.7	17.5	9
#4	----	20.9	----	20.9	10-12	0.2-0.4	7.7 (auto)	20.9	3
#5	----	19.5	----	19.5	10-14	0.2-0.4	7.1 (auto)	18.1	3
Impregnated									
#1	1150	22.7	1100	20.4	13-16	0.2-0.4	7.0	23.1	10
#2	----	20.8	----	21.2	14-17	0.2-0.4	7.2 (auto)	20.0	10
#3	----								
#4	----	23.0		20.8	10-14	0.2-0.4	7.7	20.2	3
#5	----	23.0	1000	12-13	12-15	0.2-0.4	7.7	10.7	23

TABLE II. - MAIN CATHODE STARTING CONDITIONS FOR ENCLOSED
KEEPER WITH 2.54-MM DIAMETER ORIFICE

Starting technique	Tip temperature, °C	Hg flow, mA	Keeper voltage, V	Breakdown voltage, kV
(a) Rolled foil insert				
A	~800	15-50	25	6-10
B	~800	15-50	35	0.5-4
C	~825	45-50	600	-
(b) Impregnated insert				
A	~1050	43-70	30	3-4
B	~1050	43-70	40	5-7
A	~1150	15	40	3
B	~1150	15	50	3
C	~1150	50	600	-
A	~1200	15	25	2
B	~1200	15	35	0.5
C	~1200	25	600	-

A - Pulse-to-auxiliary electrode.
B - Pulse-to-keeper
C - Conventional start

TABLE III. - NEUTRALIZER CATHODE STARTING CONDITIONS FOR
ENCLOSED KEEPER WITH 1.15-MM DIAMETER ORIFICE

Starting technique	Tip temperature, °C	Hg flow, mA	Keeper voltage, V	Breakdown voltage, kV
(a) Rolled foil insert				
A	~800	5-20	25	5-7
B	~800	5-20	35	0.5-2.5
C	~800	5-20	500	No start
A	825-850	10-12	20	7
B	825-850	10-12	30	0.5-1
C	825-850	10-12	500	-
(b) Impregnated insert				
A	~925	12-22	30-35	5-8
B	~925	12-22	40-50	6-7
A	~1000	6-34	20-30	6-10
B	~1000	6-34	35-40	5-9
A	~1075	8-10	20	5-7
B	~1075	8-10	40	6
A	~1150	60-65	10	4-5
B	~1150	60-65	18	0.5-1
C	~1150	60-65	600	-

A - Pulse-to-auxiliary electrode

B - Pulse-to-keeper

C - Conventional start

TABLE IV. - EFFECTS OF VARIOUS
CATHODE CONTAMINANTS

Substance or condition	Rolled tantalum foil insert	Cylindrical impregnated insert
Initial start	Slight degradation	Slight degradation
Air	Slight degradation	Major degradation
Polyethylene bag	Slight degradation	
Acetone vapor	Slight degradation	
Polyethylene bag with silica gel	Slight degradation	
Alcohol vapor	Slight degradation	
Breath	Slight degradation	
Mechanical shaking	Slight degradation	
Diffusion pump oil vapor	Slight degradation	Major degradation
Argon vapor with cathode tip at 100° C	Major degradation	
Air with cathode tip at 100° C	Slight degradation	Major degradation

TABLE V. - CATHODE OPERATING CONDITIONS

	SIT-5 thruster (0-9715 hr)	Vacuum bell jar (9716-19 000 hr)
Keeper voltage, V	12-15	15-17
Keeper current, A	0.28-0.30	0.25-0.29
Discharge voltage, V	37-40	36-40
Discharge current, A	0.35-0.40	0.37
Equivalent Hg^+ flow, mA	32-34	50-52
Tip heater power, W	0	2.5-2.8
Vaporizer power, W	5.6	6.5-7.2

TABLE VI. - CATHODE STARTING CONDITIONS

	Tip heater power, W	Keeper voltage, V	Equivalent Hg^+ flow, mA
Conventional starting	20-25	500-800 (Open circuit)	~70
High voltage pulse- to-keeper	^a 16.0-18.5	35-37	50-52

^a A tip heater power of 20.3 W was used for one of the starts following diffusion pump oil contamination of the bell jar.

TABLE VII. - CHARACTERISTIC OPERATING CONDITIONS
DURING SIT-5 EROSION TESTS

Discharge potential (ΔV_I), V	36.6	39.6	42.6
Ion beam accelerating potential, ^a ($V_I + V_G$), V	1400	1400	1398
Accelerator potential (V_A), V	-700	-700	-700
Neutralizer coupling potential (V_G), V	-7	-7	-9
Beam current (J_B), mA	23.4	23.4	23.4
Accelerator drain current (J_A), mA	0.127	0.090	0.079
Emission current (J_E), mA	268	311	332
Cathode Hg flow rate (\dot{m}_C), equiv. mA	40.0	34.5	33.4
Neutralizer Hg flow rate (\dot{m}_N), equiv. mA	1.7	2.2	2.4
Cathode keeper potential (V_{CK}), V	14	14	14
Cathode keeper current (J_{CK}), mA	400	400	400
Cathode tip heater power, W	0	0	0
Discharge utilization, percent	58.5	67.8	70.0
Discharge losses, ^b eV/ion	419	526	604
High voltage on time, hr	409	400	407
Discharge on time, hr	416	416	416

^aEquals net accelerating potential, V_I , plus neutralizer coupling potential, V_G (<0).

^bExcluding cathode keeper losses and neglecting double ionization.

TABLE VIII. - CHARACTERISTIC OPERATING CONDITIONS
DURING ACCELERATED LIFE TEST

Discharge potential (ΔV_I), V	64.6
Ion beam accelerating potential, ^a ($V_I + V_G$), V	1393
Accelerator potential (V_A), V	-700
Neutralizer coupling potential (V_G), V	-14
Beam current (J_B), mA	23.4
Accelerator drain current (J_A), mA	0.063
Emission current (J_E), mA	372
Cathode Hg flow rate (\dot{m}_C), equiv. mA	29.9
Neutralizer Hg flow rate (\dot{m}_N), equiv. mA	^b 14.7
Cathode keeper potential (V_{CK}), V	15
Cathode keeper current (J_{CK}), mA	400
Cathode tip heater power, W	0.0
Discharge utilization, percent	78.2
Discharge losses, ^c eV/ion	1027
High voltage on time, hr	200
Discharge on time, hr	200

^aEquals net accelerating potential, V_I , plus neutralizer coupling potential, V_G (<0).

^bExcessively high neutralizer flow rate required to maintain satisfactory neutralizer coupling potential; defective neutralizer operation indicated.

^cExcluding cathode keeper losses and neglecting double ionization.

TABLE IX. - MAJOR COMPONENT WEIGHT LOSSES
IN ACCELERATED LIFE TEST

Component	Initial wt, g	Weight loss, mg
Cathode pole piece ^a	10.9	11.44
Cathode pole piece tip cover	0.182	59.48
Cathode pole piece outer flange cover	.561	14.54
Baffle	.267	25.63
Baffle screw	.110	8.77
Baffle nut and washer ^b	.159	1.43
Endplate cover	16.2	5.37
Screen grid upstream surface ^c	-----	d90.1

^aWith tantalum covers and baffle parts disassembled.

^bLocated upstream of baffle location; see fig. 22.

^cAll screen grid erosion observed to be on upstream surface.

^dEstimated from total measured grid system weight loss of 99.5 mg.

TABLE X. - TYPICAL THRUSTER OPERATING CONDITIONS

Net accelerating potential, V	1250
Accelerator potential, V	-500
Beam current, mA	72
Discharge chamber utilization efficiency, percent	76
Neutralizer Parameters	
Tip heater power, W	0
Vaporizer power, W	2.2
Flow rate, mA	7.0
Keeper voltage, V	17.0
Keeper current, A	0.45

TABLE XI. - ACCELERATOR GRID HOLE DIAMETER MEASUREMENTS AT FOUR LOCATIONS AND AT FIVE TIMES

Time, hr	Upstream surface		Downstream surface	
	Center, mm	Edge, mm	Center, mm	Edge, mm
4	0.68	Not sputtered through	0.47	Not sputtered through
20	0.84	0.72	0.61	Hexagonal ^a 0.51-0.61
149			0.83	Hexagonal ^a 0.61-0.69
462	1.04	0.86	0.83	0.66-0.76
1006	1.12	0.86	0.83	0.71-0.82

^aSmaller value is distance between opposite sides of hexagon. Larger value is distance between opposite vertices of hexagon.

TABLE XII. - 8-CM ION THRUSTER OPERATING CONDITIONS

	Program goal	Small hole accelerator grid	Large hole accelerator grid
Thrust ^a (ideal), mlb	1.14	1.15	1.15
Specific impulse, ^a sec	2804	2958	2247
Total input power, W	122.19	131.54	134.21
Total efficiency, ^a percent	57.5	56.7	42.2
Power efficiency, percent	71.3	66.4	65.3
Total utilization, ^a percent	80.6	85.4	64.6
Discharge utilization, ^a percent	86.4	91.9	68.3
Total neutral flow, mA	89.3	85.2	112.0
Power/thrust, ^a W/mlb	107	114	116.7
eV/ion excluding keeper, V	294	286	369
eV/ion including keeper, V	328	338	381
Beam current, J_B , mA	72	72.8	72.4
Net accelerating voltage, V_I , V	1220	1220	1220
Neutralizer floating potential, V_g , V	-10	-20	-10
Output beam power, W	87.12	87.36	87.60
Accelerator voltage, V_A , V	-500	-300	-300
Accelerator drain current, J_A , mA	0.23	0.25	0.35
Accelerator drain power, W	0.40	0.38	0.53
Discharge voltage, ΔV_I , V	40	38.5	40.5
Emission current, J_E , A	0.53	0.54	0.66
Discharge power, W	21.2	20.79	26.73
Cathode:			
Keeper voltage, V_{CK} , V	10.0	17.5	16.5
Keeper current, J_{CK} , A	0.240	0.22	0.05
Keeper power, W	2.4	3.85	0.83
Heater voltage, V_{CH} , V	0	0	0
Heater current, J_{CH} , A	0	0	0
Heater power, W	0	0	0
Vaporizer voltage, V_{CV} , V	4.0	2.2	2.2
Vaporizer current, J_{CV} , A	1.0	2.1	2.1
Vaporizer power, W	4.0	4.6	4.6
Flow rate, mA	83.3	79.2	106.0
Neutralizer:			
Keeper voltage, V_{NK} , V	14.1	17.8	18.0
Keeper current, J_{NK} , A	0.360	0.5	0.5
Keeper power, W	5.08	8.9	9.0
Heater voltage, V_{NH} , V	0	0	0
Heater current, J_{NH} , A	0	0	0
Heater power, W	0	0	0
Vaporizer voltage, V_{NV} , V	1.65	2.1	2.1
Vaporizer current, J_{NV} , A	.77	2.0	2.0
Vaporizer power, W	1.27	4.2	4.2
Flow rate, mA	6.0	6.0	6.0
Neutralizer coupling power, W	0.72	1.46	0.72

^aAccounting for neutralizer floating potential but neglecting beam divergence and double ionization.

TABLE XIII. - SIT-8 PERFORMANCE GOALS

Performance standards

Startup to design-performance operation within a minimum time not to exceed 30 min

Operating characteristics that permit stable closed-loop control operation

Thrust vector angle, $\pm 10^\circ$ in two orthogonal directions

Projected lifetime, 20 000 hr

Capability to undergo 100 000 vectoring cycles under space conditions

Capability to undergo 10 000 restarts under space conditions

Structurally integrated design

Thrust, 1 mlb

Performance parameters

Electrical efficiency, 0.75

Propellant utilization efficiency 0.85

Overall efficiency, 0.63

Effective specific impulse, 2944 sec

Net accelerating voltage, 1220 V

Approximate total weight, 2.1 kg (not including propellant or tankage)

TABLE XIV. - 1-MLB 8-CM ION THRUSTER OPERATING CONDITIONS

	Program goals	As delivered	After optimization
Thrust ^a (ideal), mlb	1.14	1.12	1.14
Specific impulse, ^a sec	2804	1805	2912
Total input power, W	122.19	144.99	131.66
Total efficiency, ^a percent	57.5	30.5	55.4
Power efficiency, percent	71.3	57.4	66.2
Total utilization, ^a percent	80.6	53.1	83.7
Discharge utilization, ^a percent	86.4	65.1	90.0
Total neutral flow, mA	89.3	135.6	86.0
Power/thrust, ^a W/mb	107	129.5	115.5
eV/ion excluding keeper, V	294	270	328
eV/ion including keeper, V	328	288	328
Beam current, J_B , mA	72	72	72
Net accelerating voltage, V_I , V	1220	1220	1220
Neutralizer floating potential, V_g , V	-10	-64	-10
Output beam power, W	87.12	83.23	87.12
Accelerator voltage, V_A , V	-500	-300	-300
Accelerator drain current, J_A , mA	0.23	0.195	0.320
Accelerator drain power, W	0.40	0.30	0.49
Discharge voltage, ΔV_I , V	40	38.9	39.3
Emission current, J_E , A	0.53	0.50	0.60
Discharge power, W	21.2	19.45	23.58
Cathode:			
Keeper voltage, V_{CK} , V	10.0	8.5	8
Keeper current, J_{CK} , A	0.240	0.15	0
Keeper power, W	2.4	1.28	0
Heater voltage, V_{CH} , V	0	5.5	0
Heater current, J_{CH} , A	0	3.0	0
Heater power, W		16.5	0
Vaporizer voltage, V_{CV} , V	4.0	2.3	4.3
Vaporizer current, J_{CV} , A	1.0	0.9	2.1
Vaporizer power, W	4.0	2.07	9.0
Flow rate, mA	83.3	110.6	80
Neutralizer:			
Keeper voltage, V_{NK} , V	14.1	15.0	17.5
Keeper current, J_{NK} , A	0.360	0.5	0.5
Keeper power, W	5.08	7.5	8.75
Heater voltage, V_{NH} , V	0	4.6	0
Heater current, J_{NH} , A	0	2.15	0
Heater power, W	0	9.89	0
Vaporizer voltage, V_{NV} , V	1.65	0.80	2.0
Vaporizer current, J_{NV} , A	0.77	0.20	1.0
Vaporizer power, W	1.27	0.16	2.0
Flow rate, mA	6.0	25.0	6.0
Neutralizer coupling power, W	0.72	4.61	0.72

^aAccounting for neutralizer floating potential but neglecting beam divergence and double ionization.

TABLE XV. - PROJECTED ENGINEERING MODEL SIT-8

THRUSTER OPERATING CONDITIONS

Thrust ^a (ideal), mlb	1.14	
Specific impulse, ^a sec	2955	
Total input power, W	125.4	
Total efficiency, ^a percent	58.8	
Power efficiency, percent	68.9	
Total utilization, ^a percent	85.3	
Discharge utilization, ^a percent	91.8	
Total neutral flow, mA	84.4	
Power/thrust, ^a W/mlb	110	
eV/ion excluding keeper, V	289	
eV/ion including keeper, V	339	
Beam current, J_B , mA	72	
Net accelerating voltage, V_I , V	1220	
Neutralizer floating potential, V_g , V	-20	
Output beam power, W		86.4
Accelerator voltage, V_A , V	-300	
Accelerator drain current, J_A , mA	0.23	
Accelerator drain power, W		0.4
Discharge voltage, ΔV_I , V	38.5	
Emission current, J_E , A	0.54	
Discharge power, W		20.8
Cathode:		
Keeper voltage, V_{CK} , V	14.5	
Keeper current, J_{CK} , A	0.25	
Keeper power, W		3.6
Heater voltage, V_{CH} , V	0	
Heater current, J_{CH} , A	0	
Heater power, W		0
Vaporizer voltage, V_{CV} , V	2.2	
Vaporizer current, J_{CV} , A	0.9	
Vaporizer power, W		2.0
Flow rate, mA	78.4	
Neutralizer:		
Keeper voltage, V_{NK} , V	18	
Keeper current, J_{NK} , A	0.5	
Keeper power, W		9.0
Heater voltage, V_{NH} , V	0	
Heater current, J_{NH} , A	0	
Heater power, W		0
Vaporizer voltage, V_{NV} , V	3.5	
Vaporizer current, J_{NV} , A	0.5	
Vaporizer power, W		1.8
Flow rate, mA	6.0	
Neutralizer coupling power, W		1.4

^aAccounting for neutralizer floating potential but neglecting beam divergence and double ionization.

TABLE XVI. - PERFORMANCE PROFILE

Test hours	2057	5500
Net accelerating potential, V	1218	1202
Accelerator potential, V	500	500
Beam power, W	87.9	86.5
Discharge power, W	25.5	28.0
Component power		
Accelerator drain, W	0.35	0.33
Cathode		
Heater, W	0	0
Keeper, W	3.74	3.52
Vaporizer, W	5.25	5.39
Neutralizer		
Heater, W	14.4	7.2
Keeper, W	8.0	9.35
Vaporizer, W	0.16	0.72
Total input power, W	145.3	141.0
Power efficiency, percent	60.5	61.3
Utilization efficiency, percent	64.8	59.3
Overall efficiency, percent	39.2	36.4
Thrust, mN	5.11	5.08
Specific impulse, sec	2262	2056
P/T ratio, W/mN	28.5	27.8

TABLE XVII. - 8-CM THRUSTER STARTING REQUIREMENTS

Test, hr	Start number	Cathode vaporizer temperature, °C	Cathode heater power, W	Voltage, kV, and pulse number	Neutralizer vaporizer temperature, °C	Neutralizer heater power, W	Voltage, kV, and pulse number
500	12	360	15	13.9/1	370	15	14.6/4
1000	31	330	15	13.9/1	400	21	13.9/1
1088	36	340	15	13.9/1	340	21	13.9/1
1500	54	350	14	15.0/5	350	21	15.0/1
2000	68	360	15	13.9/3	380	21	13.9/2
2500	90	360	15	11.9/1	400	20	13.9/1
3000	102	390	14.5	12.5/2	400	20	15.0/2
3500	121	370	15	13.5/5	390	21	15.0/1
3557	122	380	15	12.5/4	400	21	15.0/2
4000	134	380	15	12.5/2	390	21	15.0/2
4500	154	350	15	12.5/1	350	21	15.0/10
	155	340	15	12.5/1	380	21	15.0/8
	156	340	15	12.5/3	370	21	15.0/1
	157	340	15	12.5/5	400	21	15.0/1
5000	169	370	15	12.5/2	375	21	15.0/1

TABLE XVIII. - SUMMARY OF CATHODE STARTING CONDITIONS

	Tip heater power, W	Vaporizer power, W	Equivalent Hg ⁺ flow, mA	Keeper voltage, V	Breakdown voltage, kV
Main cathode	19-20	9.5-10	120	30-31	8-10
Neutralizer	13-14	6.5-7.0	8	34-35	10-12

TABLE XIX. - SUMMARY OF THRUSTER OPERATING CONDITIONS
AVERAGED FOR CYCLES 201-225

Thrust ^a (ideal), mlb	1.23	
Specific impulse, ^a sec	2100	
Total input power, W	145.95	
Total efficiency, ^a percent	38.7	
Power efficiency, percent	63.8	
Total utilization, ^a percent	60.6	
Discharge utilization, ^a percent	64.7	
Total neutral flow, mA	128	
Power/thrust, ^a W/mlb	119	
eV/ion excluding keeper, V	337	
eV/ion including keeper, V	348	
Beam current, J_B , mA	77.6	
Net accelerating voltage, V_I , V	1220	
Neutralizer floating potential, V_g , V	-19.4	
Output beam power, W		93.12
Accelerator voltage, V_A , V	-300	
Accelerator drain current, J_A , mA	0.48	
Accelerator drain power, W		0.73
Discharge voltage, ΔV_I , V	37.4	
Emission current, J_E , A	0.70	
Discharge power, W		26.2
Cathode:		
Keeper voltage, V_{CK} , V	15.9	
Keeper current, J_{CK} , A	0.052	
Keeper power, W		0.82
Heater voltage, V_{CH} , V	0	
Heater current, J_{CH} , A	0	
Heater power, W		0
Vaporizer voltage, V_{CV} , V	3.00	
Vaporizer current, J_{CV} , A	2.95	
Vaporizer power, W		8.86
Flow rate, mA	120	
Neutralizer:		
Keeper voltage, V_{CK} , V	17.4	
Keeper current, J_{CK} , A	0.300	
Keeper power, W		0.52
Heater voltage, V_{CH} , V	4.64	
Heater current, J_{CH} , A	1.83	
Heater power, W		8.50
Vaporizer voltage, V_{NV} , V	2.46	
Vaporizer current, J_{NV} , A	2.31	
Vaporizer power, W		5.69
Flow rate, mA	8	
Neutralizer coupling power, W		1.51

^aAccounting for neutralizer floating potential but neglecting beam divergence and double ionization.

TABLE XX. - LABORATORY THRUSTER TEST CONSOLE POWER SUPPLIES

Supply	Voltage	Current	Regulation, percent	Control
Screen	2000 V d.c.	200 mA d.c.	V or I, 0.01	Manual
Accelerator	2000 V d.c.	10 mA d.c.	V, 20	Manual
Discharge	100 V d.c.	1.5 A d.c.	I, 1	Manual
Cathode keeper	34 V d.c.	0.5 A d.c.	I, 1	Manual
Ignitor	450 or 900 V d.c.	100 mA short circuit		Manual
Neutralizer keeper	34 V d.c.	0.5 A d.c.	I, 1	Manual
Ignitor	450 or 900 V d.c.	100 mA short circuit		Manual
Cathode vaporizer	6 V d.c.	10 A d.c.	V, 3	Manual or discharge voltage
Neutralizer vaporizer	6 V d.c.	10 A d.c.	V, 3	Manual or neutralizer keeper voltages
Cathode tip	12.6 V a.c.	10 A a.c.	V, 3	Manual
Neutralizer tip	12.6 V a.c.	10 A a.c.	V, 3	Manual

TABLE XXI. - DESIGN CRITERIA

	Thrust level	
	1 mlb level	2 mlb level
Main bus voltage, V d.c.	70±20	70±20
Housekeeping bus voltage, V d.c.	28±10%	28±10%
Input power, W	120	240
Electrical efficiency	0.82	0.85
Maximum allowable input ripple, percent	1	1
Nominal operating baseplate temperature, °C	50±5	60±5
Baseplate area, cm ²	1587	1587

TABLE XXII. - SIT-8 THRUSTER SYSTEM WEIGHT BREAKDOWN

	Mass, kg	Weight, lb
Thruster	1.69	3.7
Gimbal	.68	1.5
Tankage (empty)	1.28	2.8
Power processor	6.49	14.3
Total thruster system (dry)	10.14	22.3
Propellant	8.75	19.3
Total thruster system	18.89	41.6

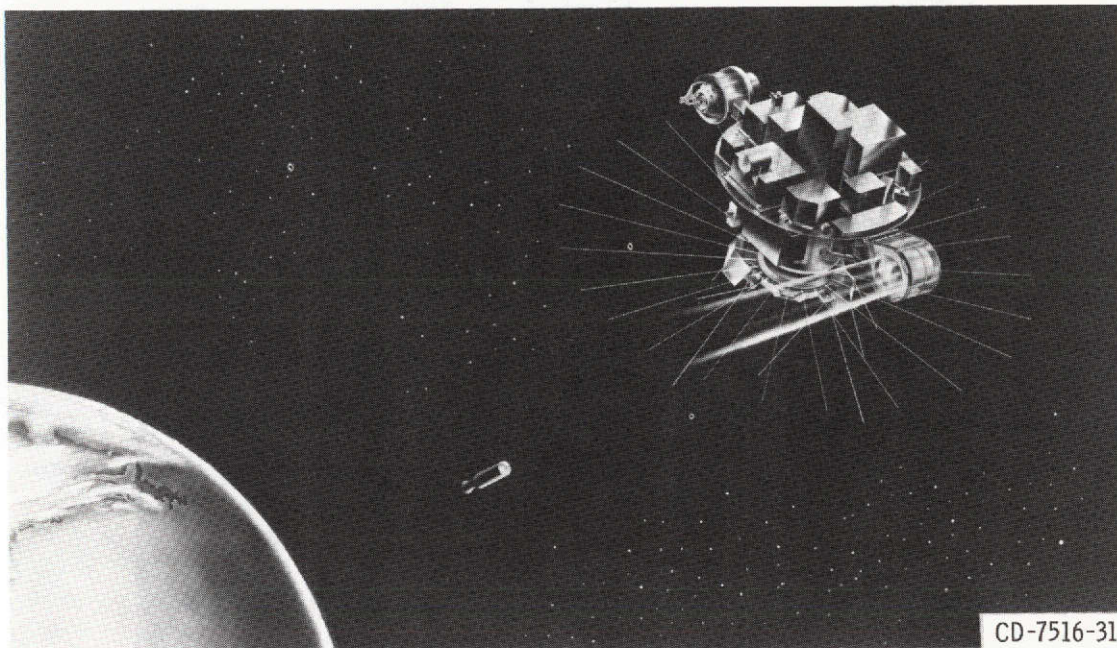
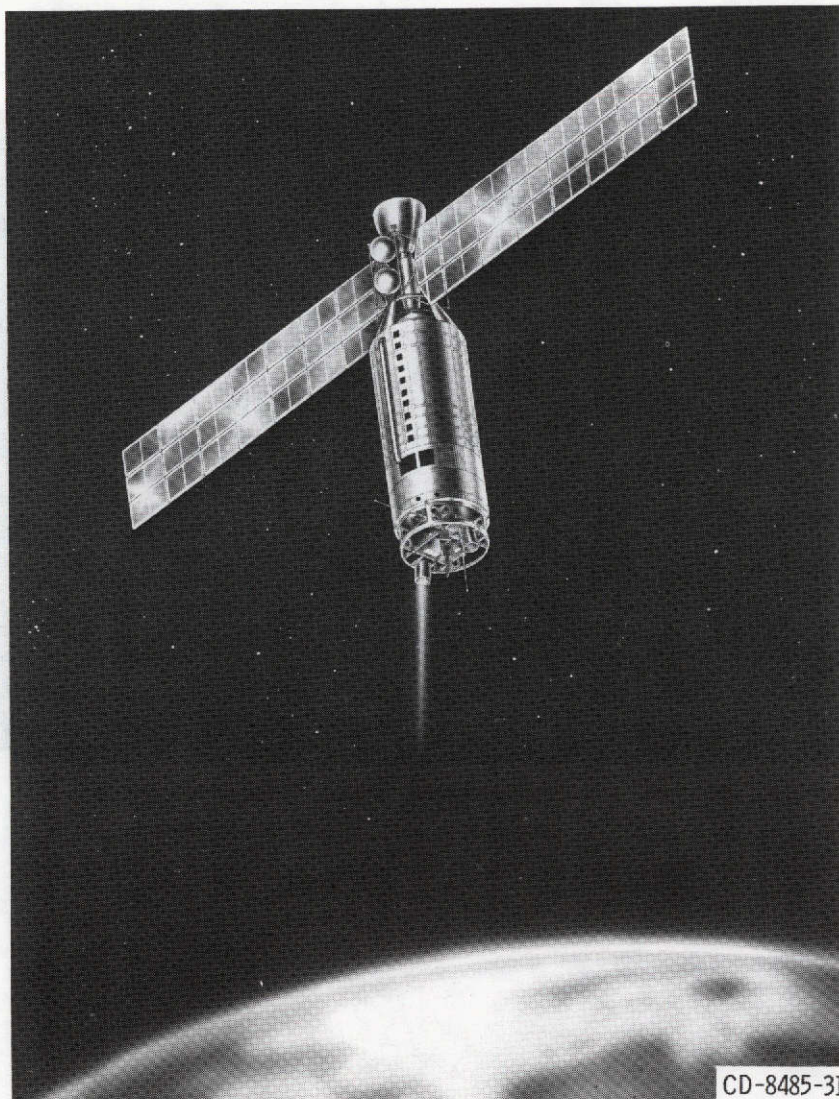


Figure 1. - SERT I.

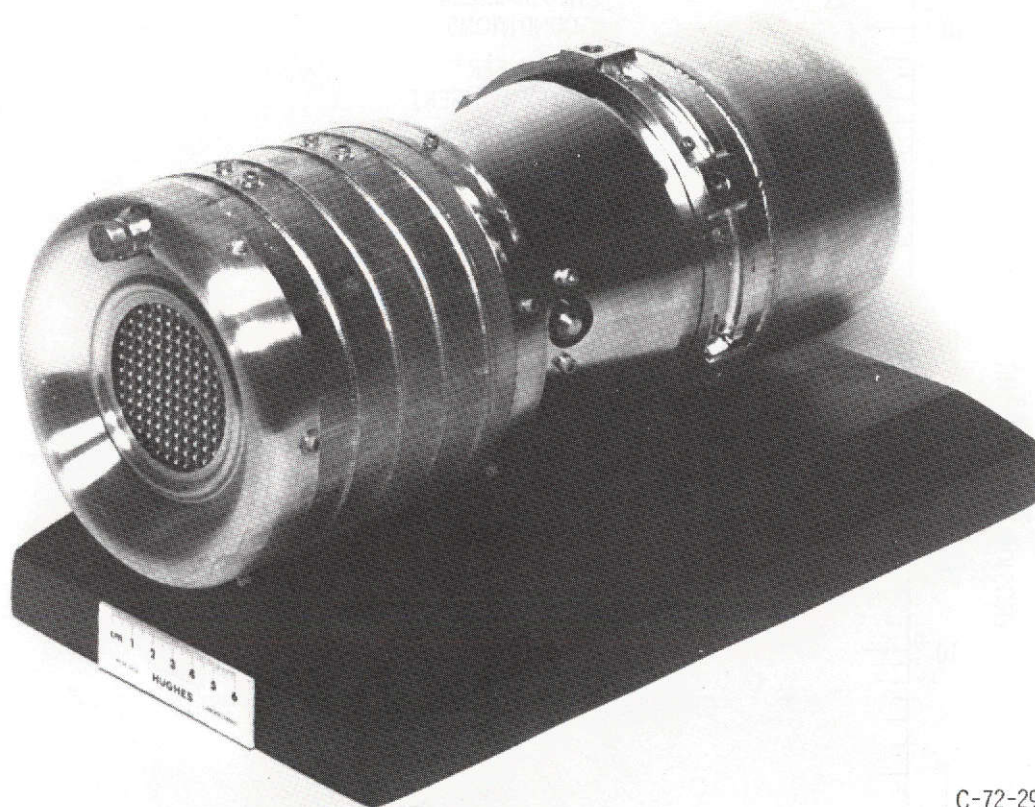
REPRODUCIBILITY OF THE
ORIGINAL PAGE IS POOR



CD-8485-31

Figure 2. - SERT II.

REPRODUCIBILITY OF THE
ORIGINAL PAGE IS POOR



C-72-2960

Figure 3. - SIT-5 thruster.

REPRODUCIBILITY OF THE
ORIGINAL PAGE IS POOR

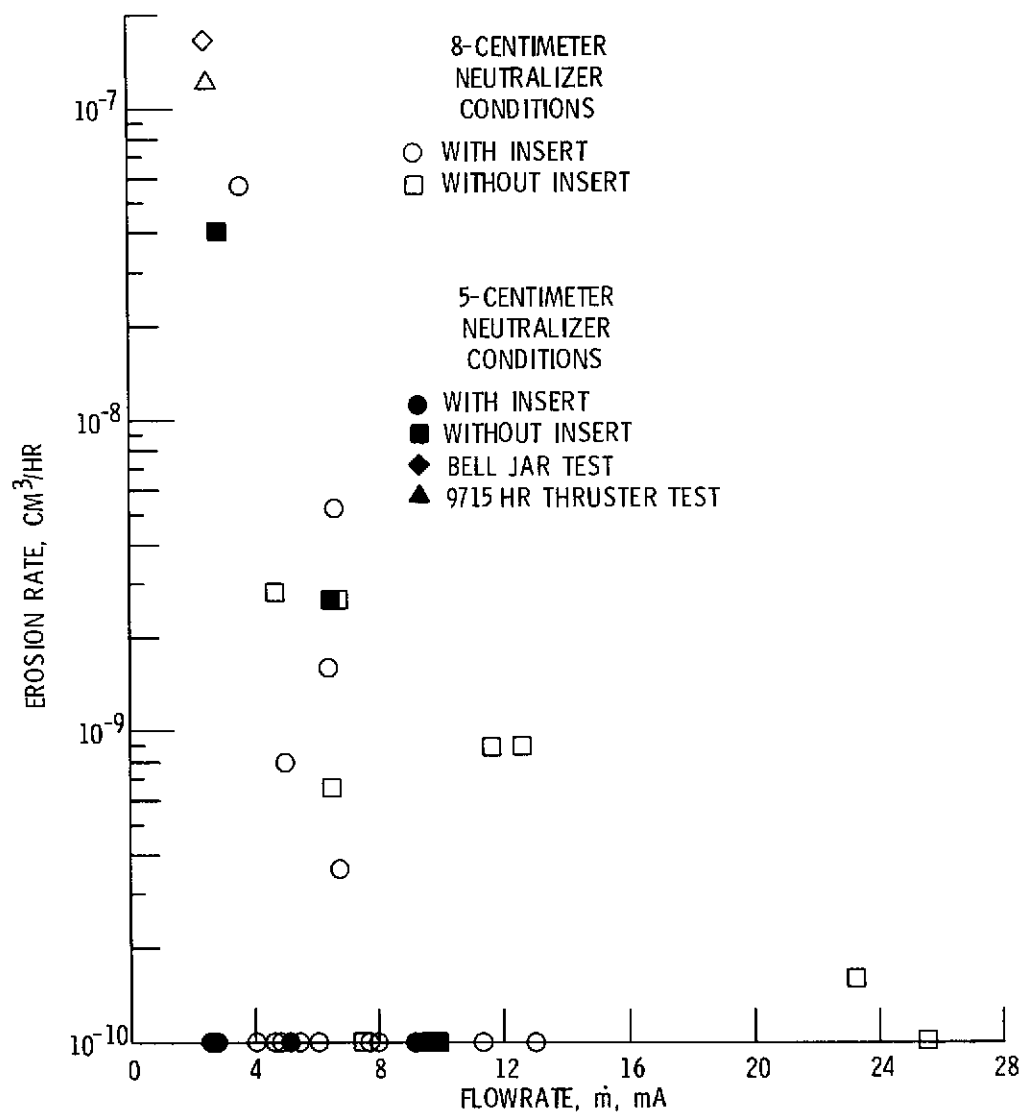


Figure 4. - Flow rate dependance of tip erosion rate.

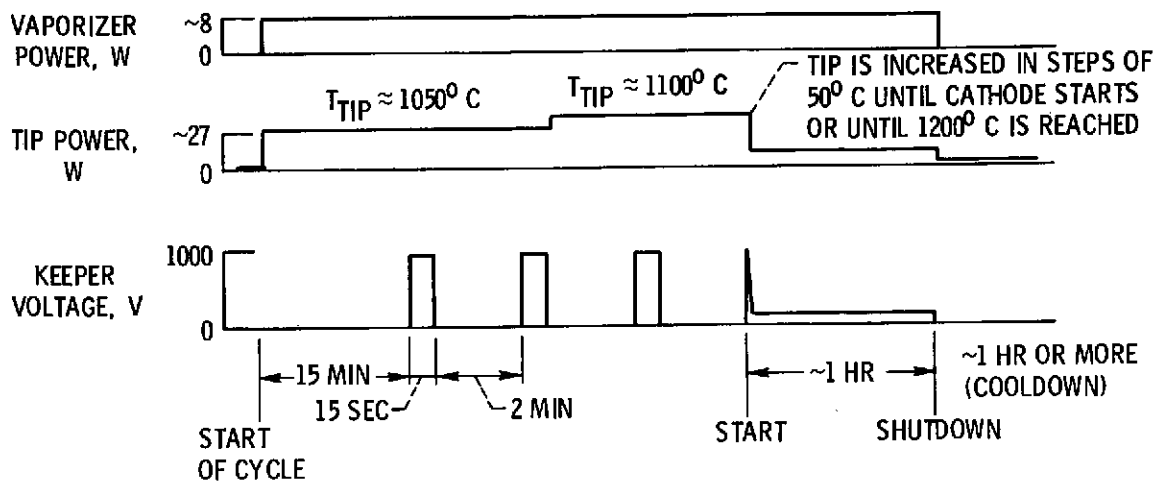
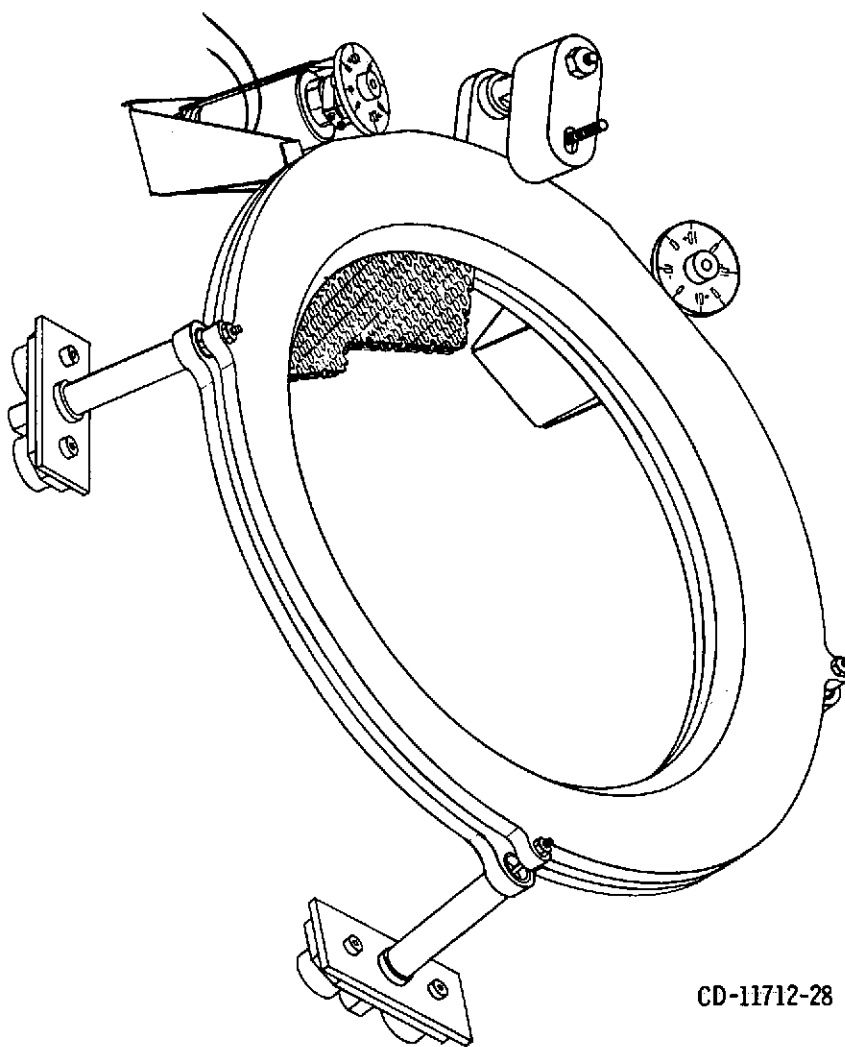


Figure 5. - Cathode starting sequence.



CD-11712-28

Figure 6. - Rotary solenoid dished grid displacement vectoring system.

REPRODUCIBILITY OF THE
ORIGINAL PAGE IS ≥ 0.5

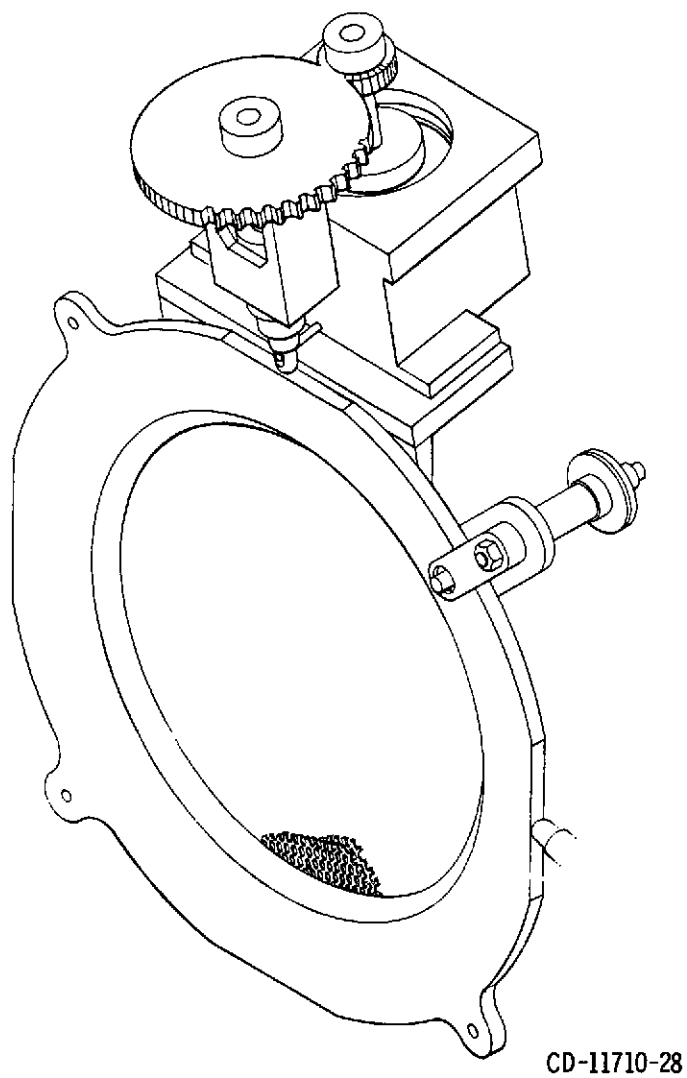


Figure 7. - Differential screw dished grid displacement vectoring system.

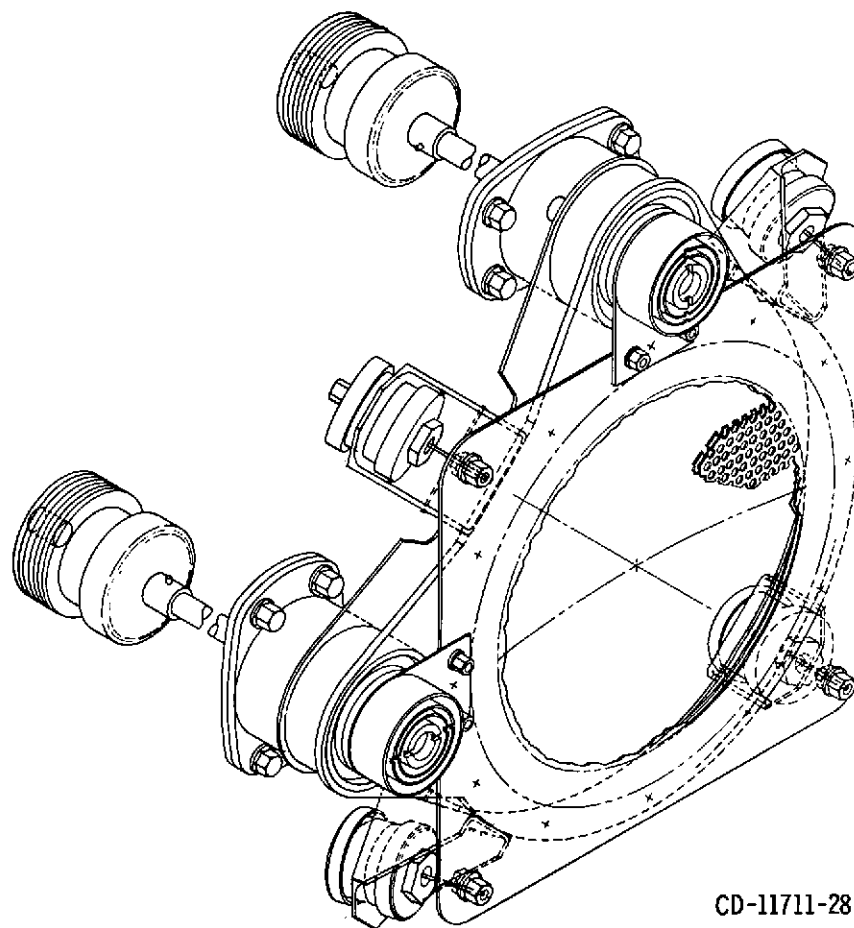
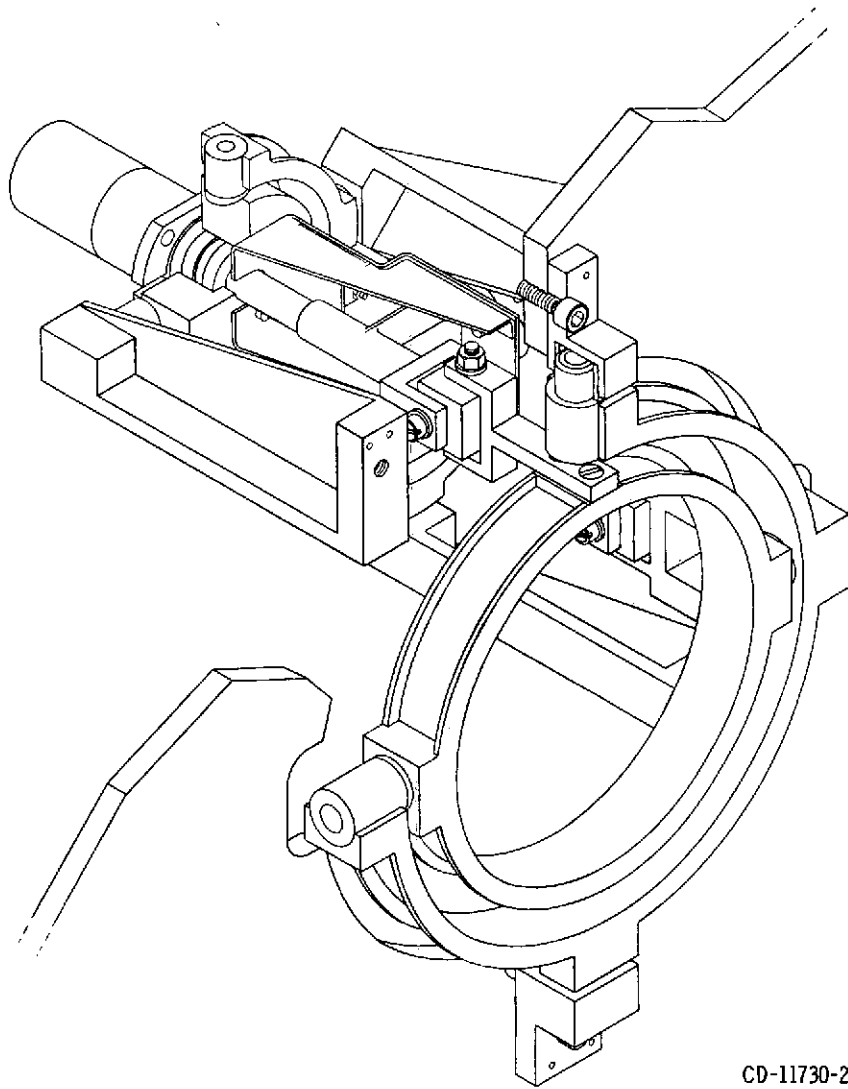
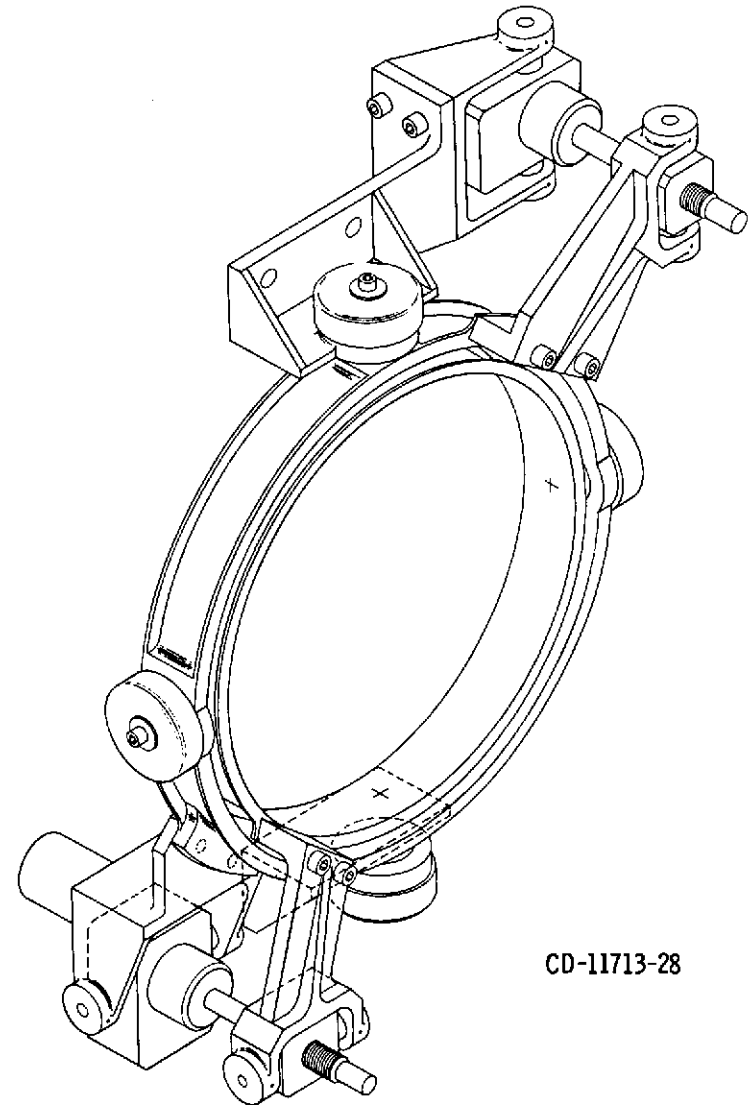


Figure 8. - Bellows enclosed cam driven grid displacement vectoring system.



CD-11730-28

Figure 9. - Double-ring gimbal system.



CD-11713-28

Figure 10. - Double ring gimbal system using an Intelsat IV type linear actuator.

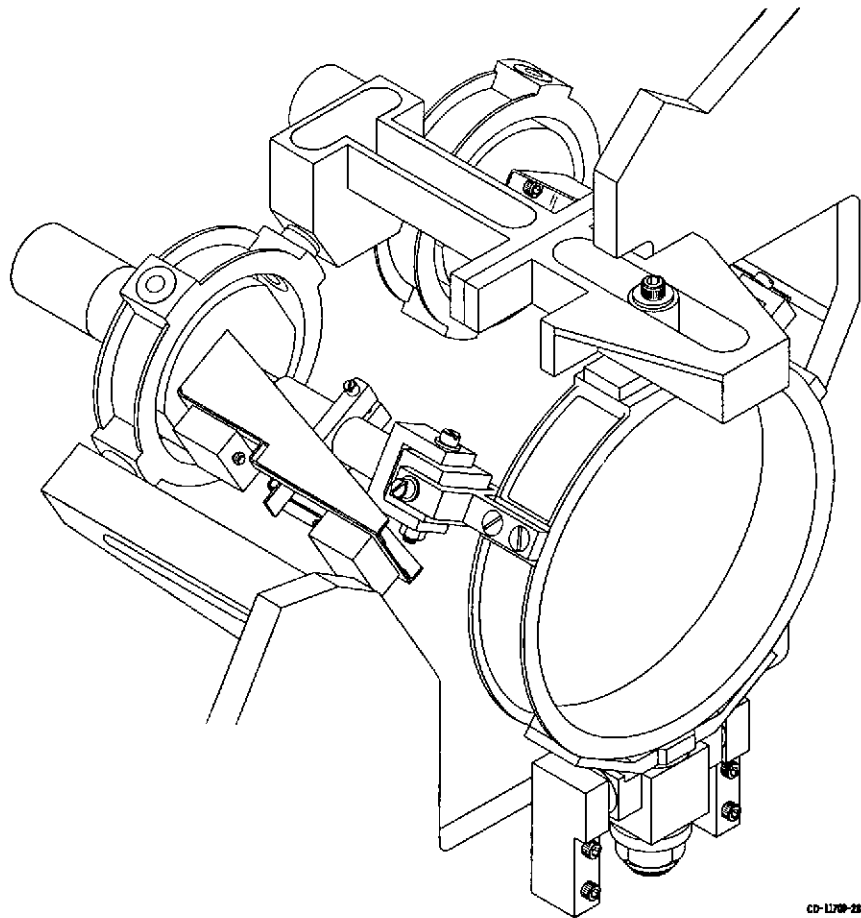


Figure 11. - Single ring gimbal with combination hinge-pivot support and jackscrew linear actuators.

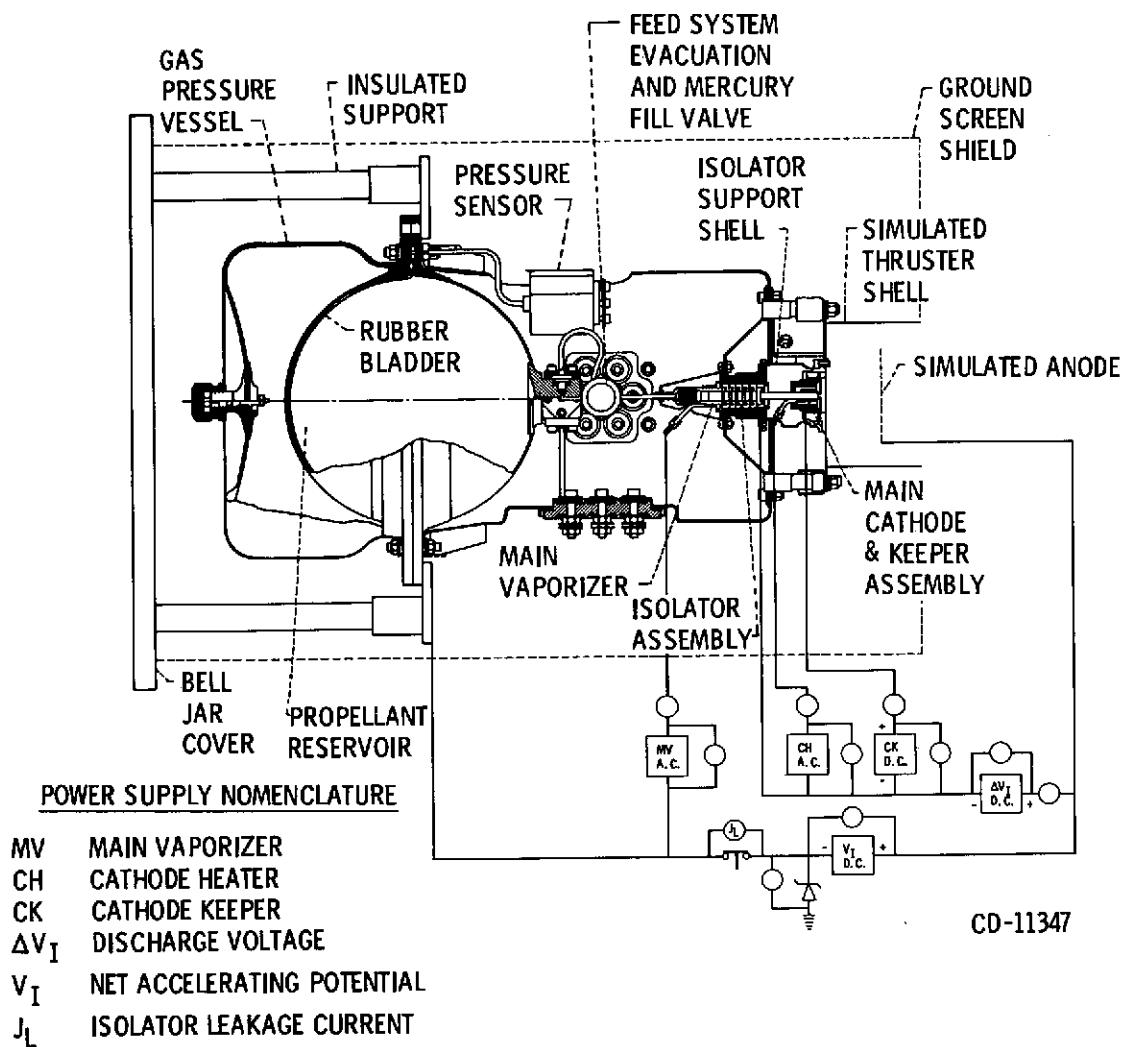


Figure 12. - Schematic of propellant feed and isolator system test installation.

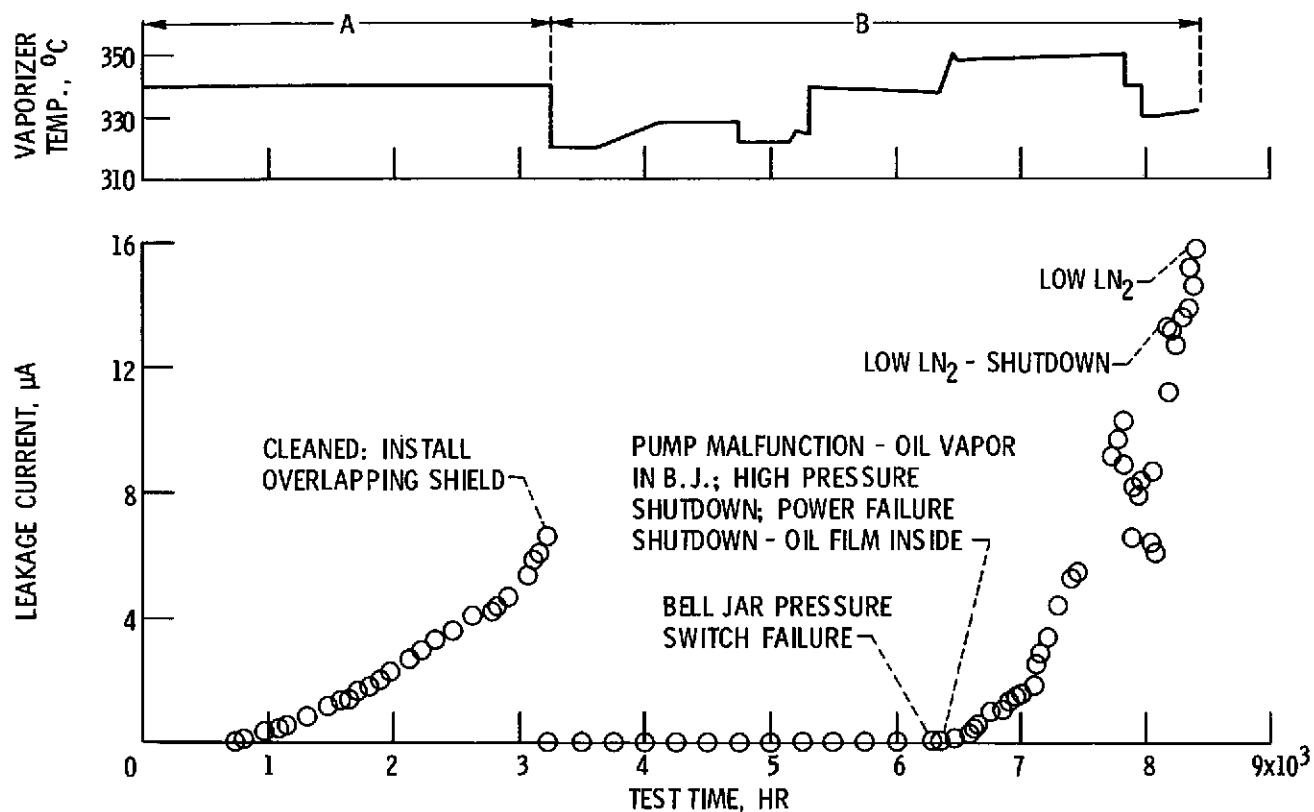


Figure 13. - History of 1600 volts isolator test.

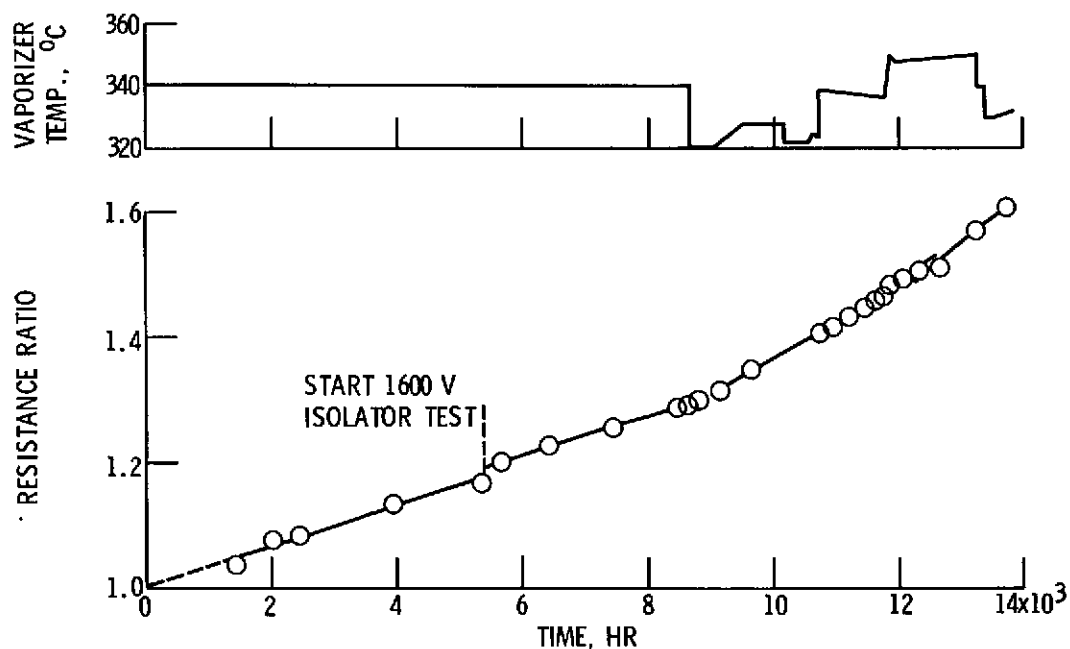


Figure 14. - History of SIT-51 mercury propellant expulsion test.

CONSTRUCTION MATERIALS:

1. 304 STAINLESS STEEL
2. 302 STAINLESS STEEL
3. 1010 MILD STEEL
4. 1010 MILD STEEL-NI PLATED
5. MOLYBDENUM
6. TANTALUM

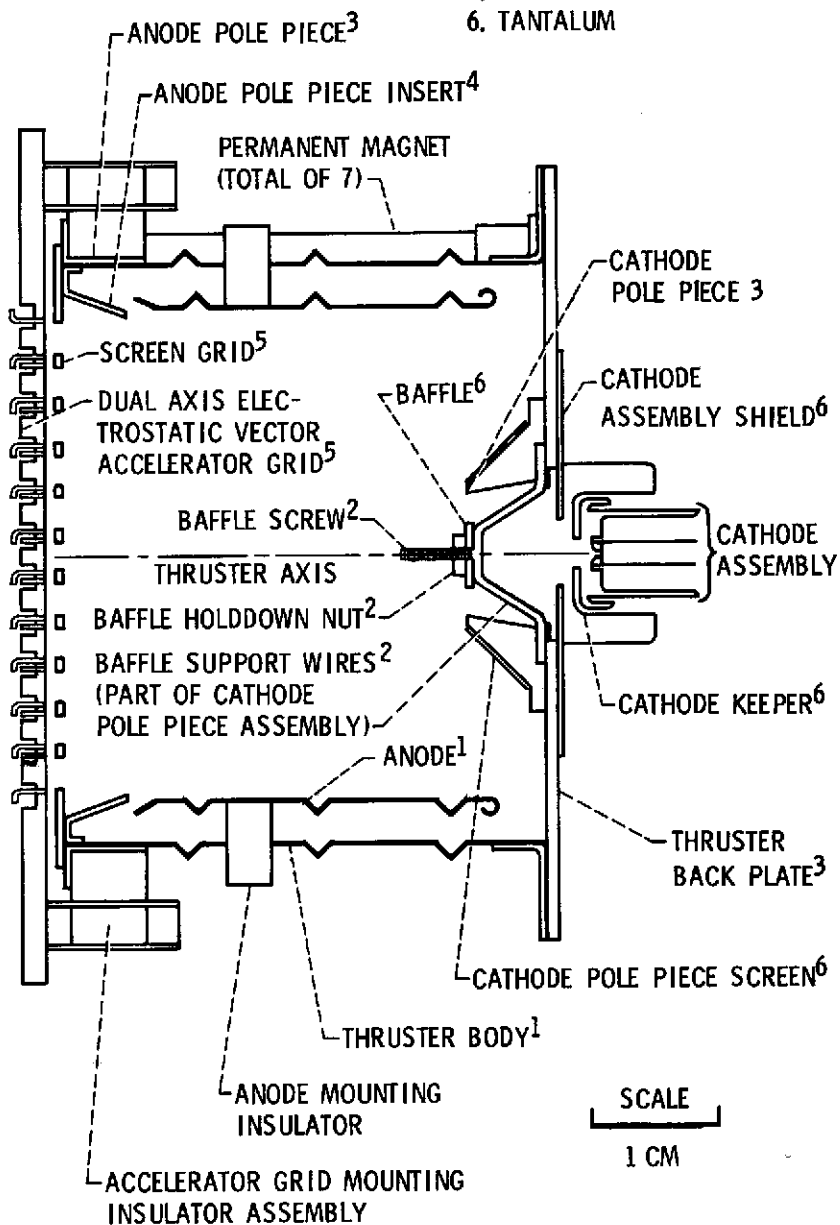


Figure 15. - 5-cm Thruster sectional view. (Neutralizer and ground screen not shown.)

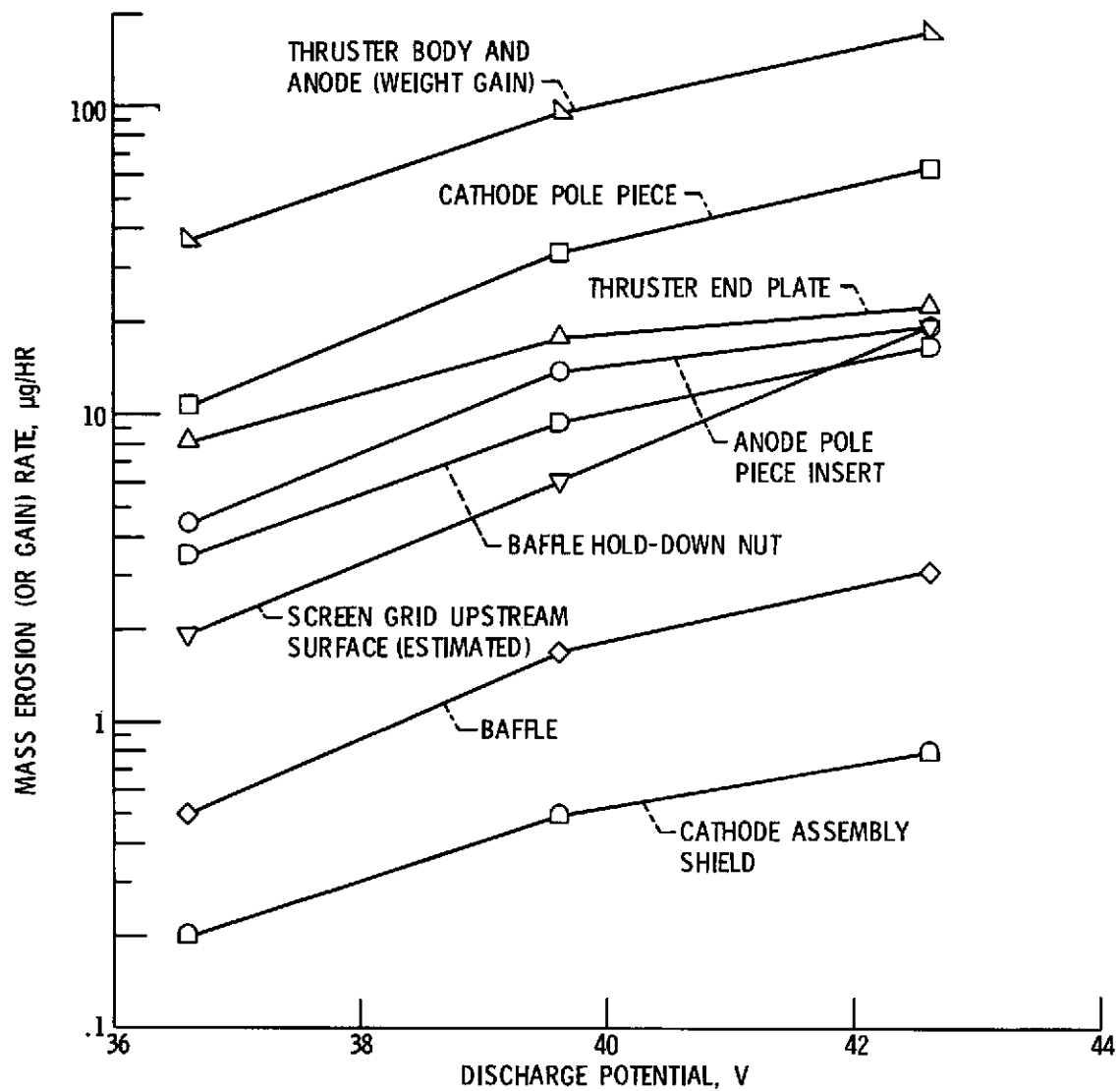


Figure 16. - Weight erosion (or gain) rate of discharge chamber components versus discharge potential.

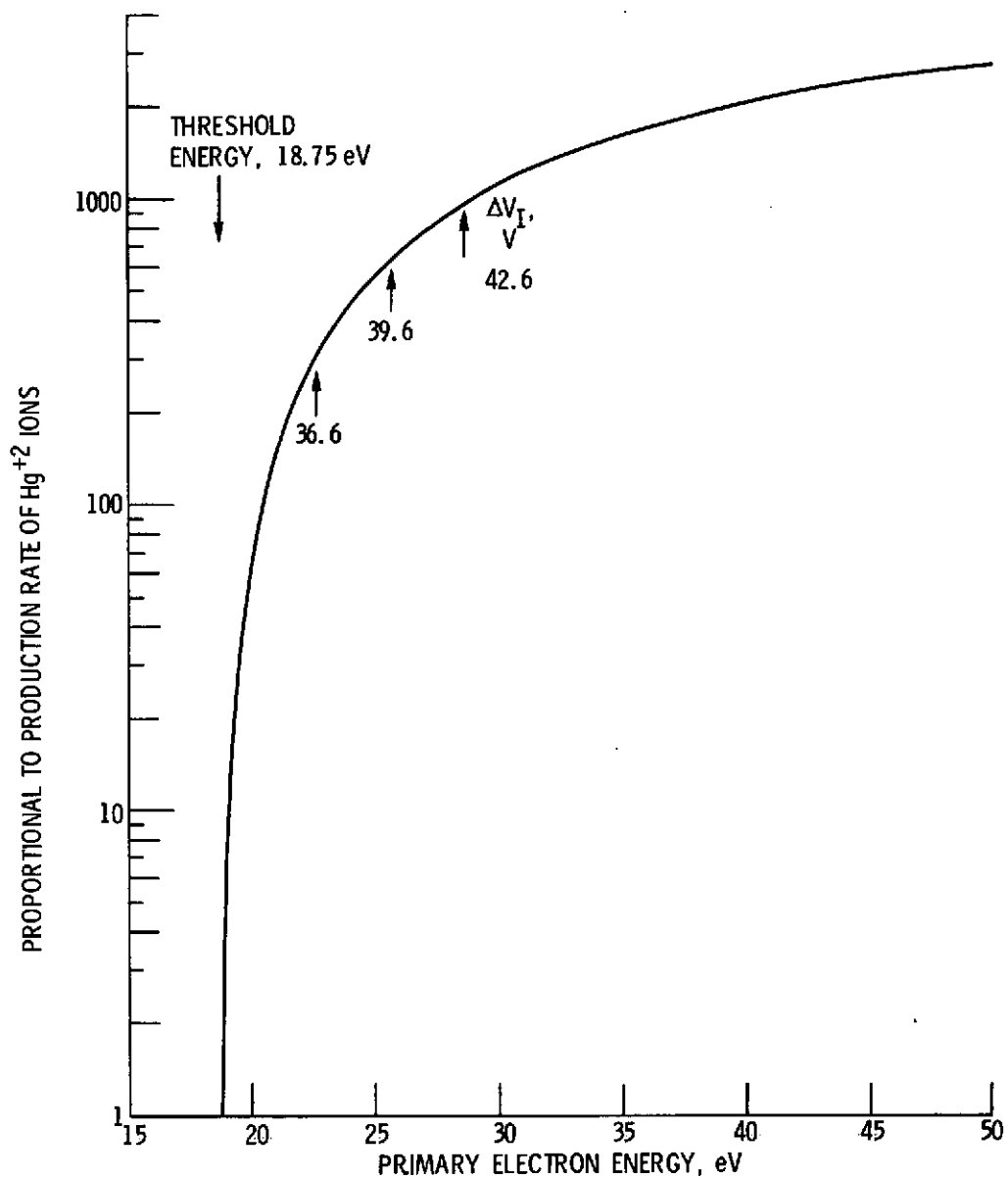


Figure 17. - Theoretical production rate of Hg^{+2} ions; dependence on primary electron energy. Production reaction, $\text{Hg}^+(\text{ground state}) + e^- \rightarrow \text{Hg}^{+2}(\text{ground state})$.

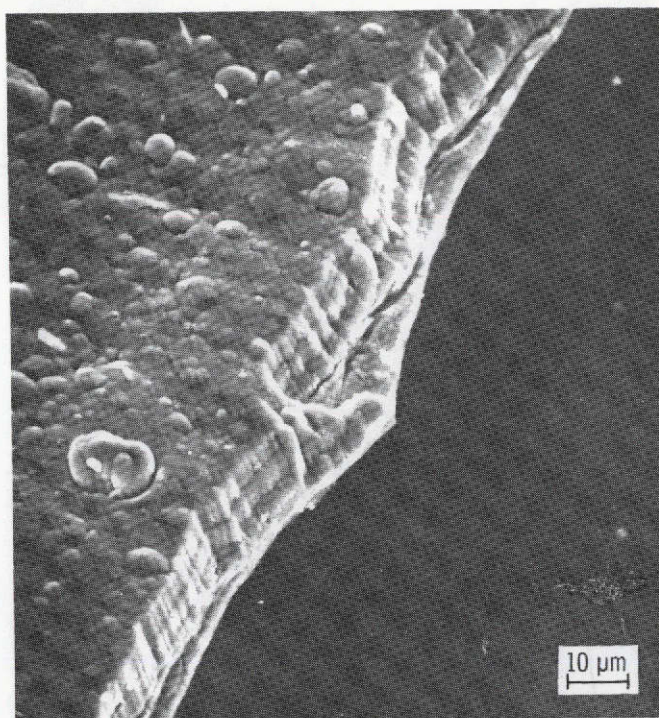


Figure 18. - Upstream anode coating flake from SIT-5 endurance test.

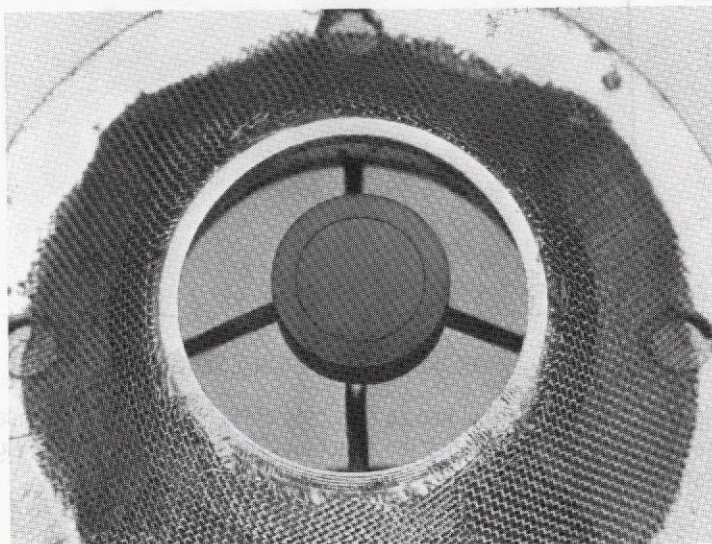


Figure 19. - Thick (2.8 mm) pyrolytic graphite baffle assembly mounted on cathode pole piece, before test.

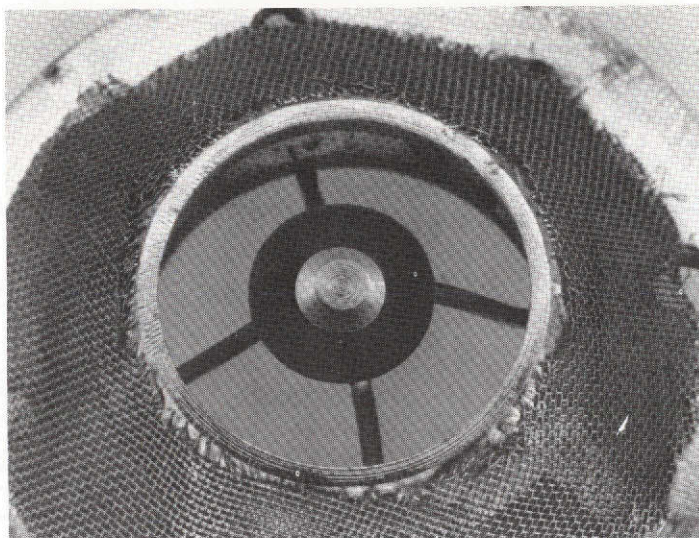


Figure 20. - Thin (0.63 mm) isotropic graphite baffle mounted on cathode pole piece with tantalum hold-down screw, before test.

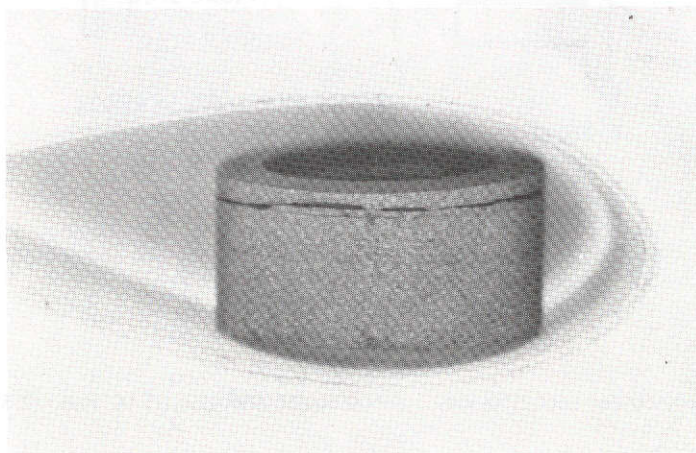
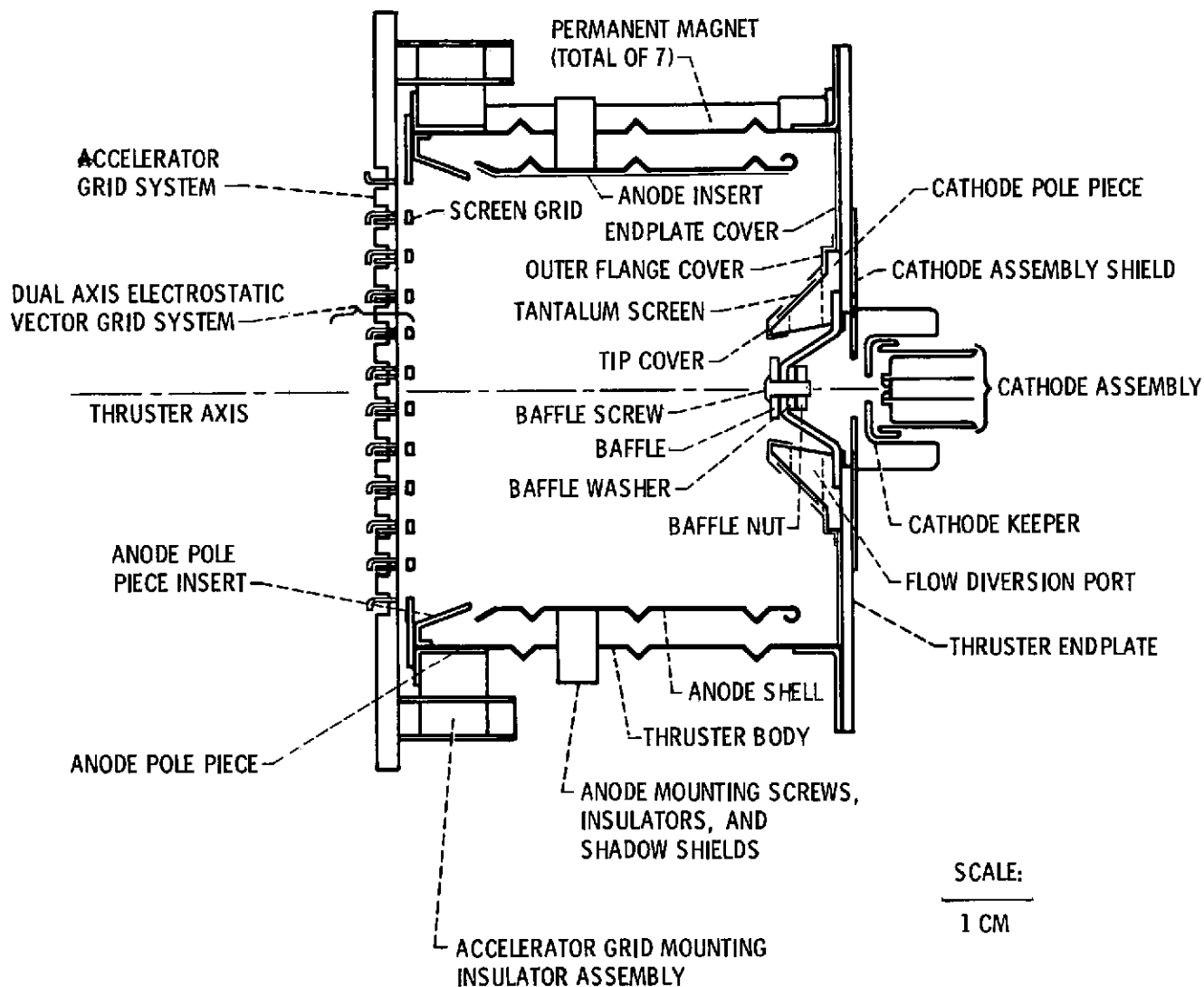


Figure 21. - Thick pyrolytic graphite baffle base following 400 hour test.



E-8113

Figure 22. - Modified 5-cm thruster sectional view. Neutralizer and ground screen not shown. (Fig. 1 of ref. 30.)

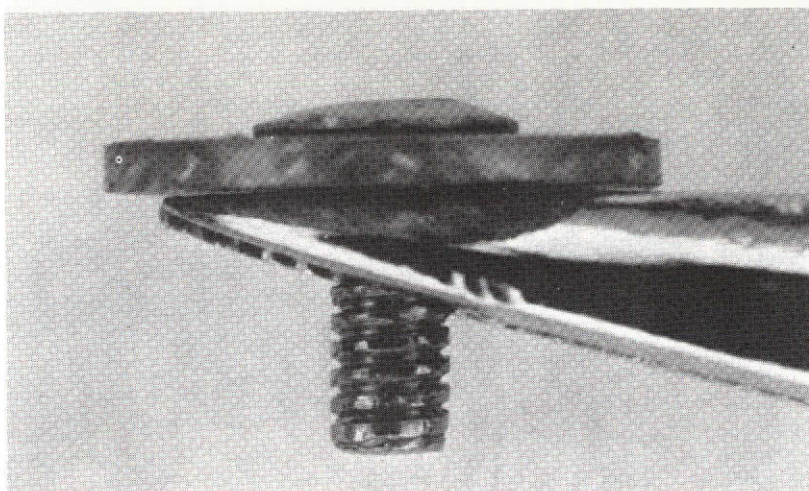


Figure 23. - Tantalum baffle and baffle screw, before test.

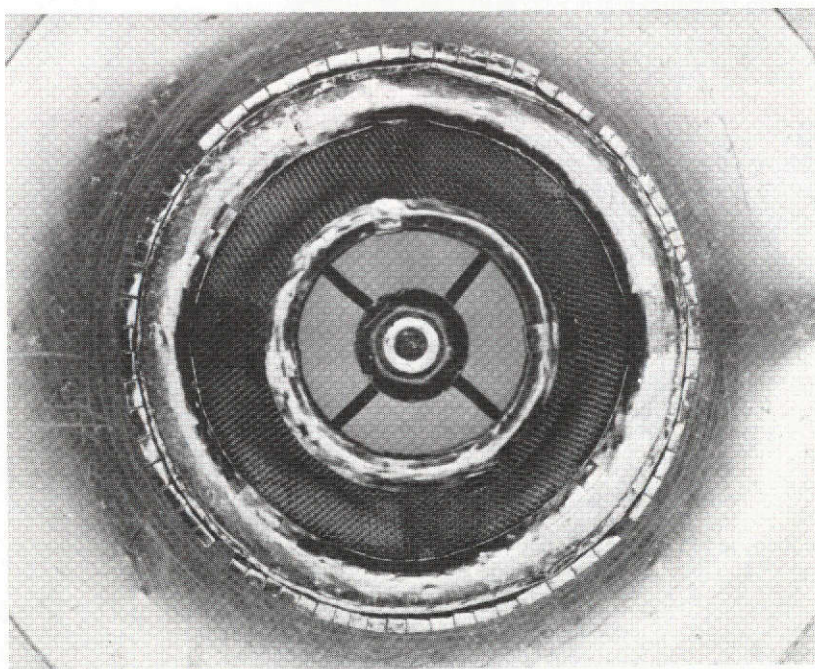


Figure 24. - Cathode pole piece-baffle assembly with tantalum foil covers, before test.

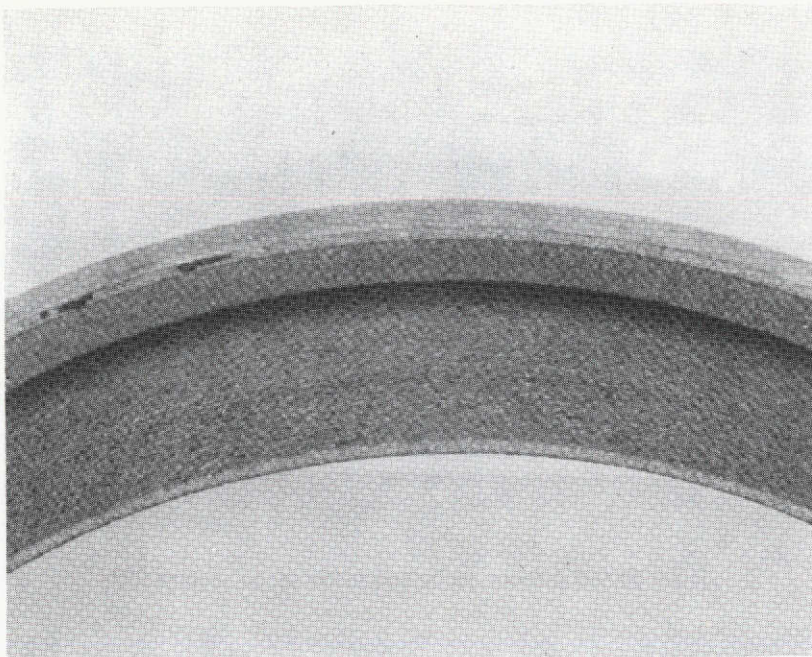


Figure 25. - Upstream side of anode pole piece insert, before test, showing tantalum plasma-sprayed interior surfaces.

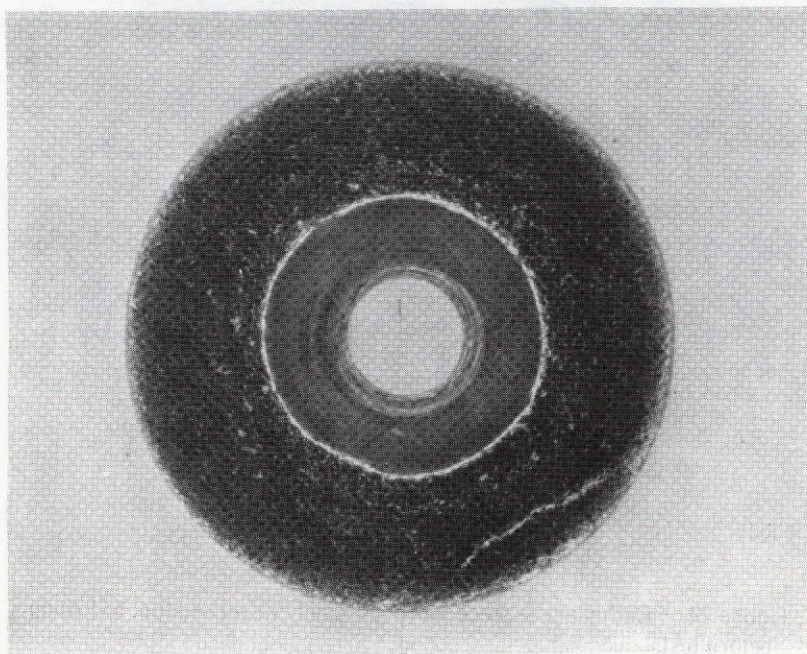


Figure 26. - Downstream surface of baffle, after test. Central area covered by baffle screw head.

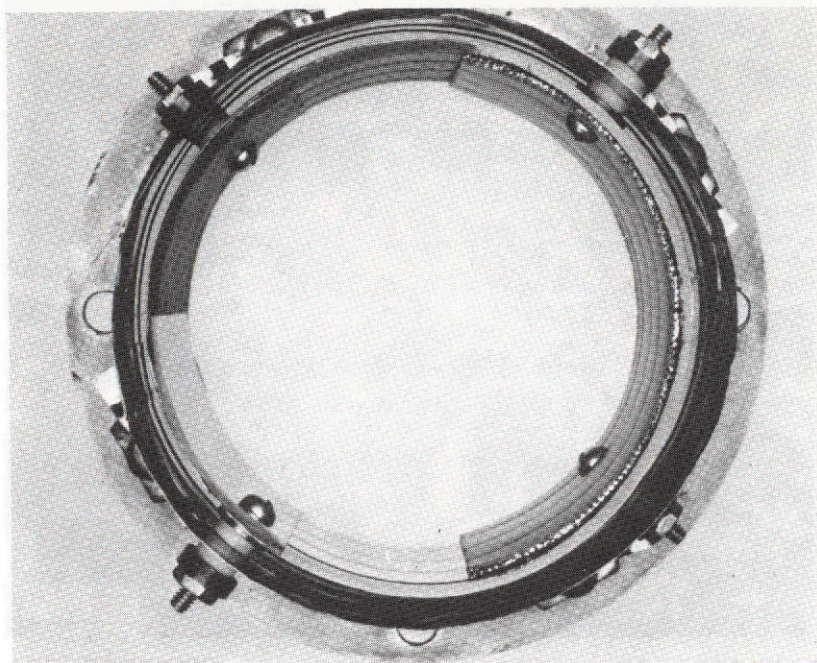


Figure 27. - Composite anode-thruster body assembly before test. Tantalum foil insert on left; stainless steel wire cloth insert on right.

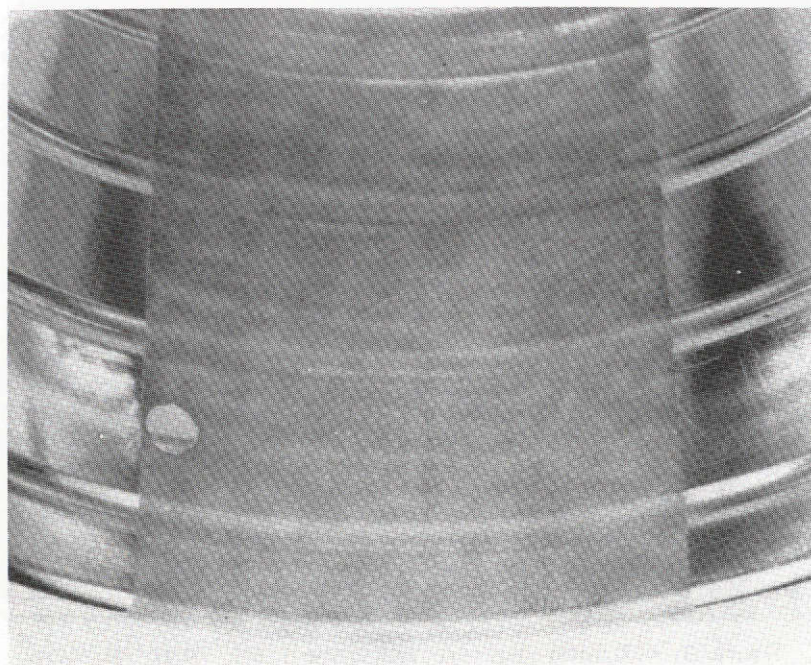


Figure 28. - Grit-blasted interior anode surface, before test.

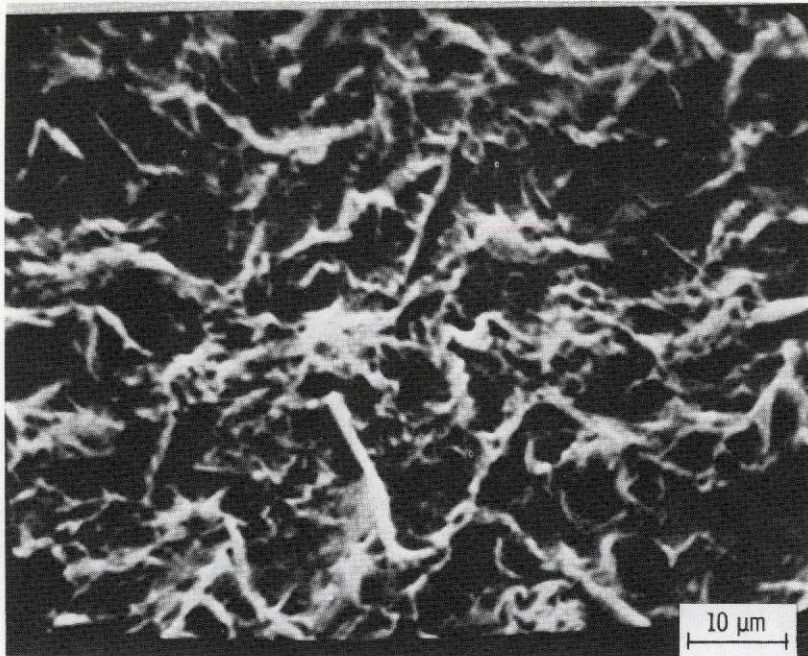


Figure 29. - Electron micrograph of grit-blasted interior anode surface, before test.

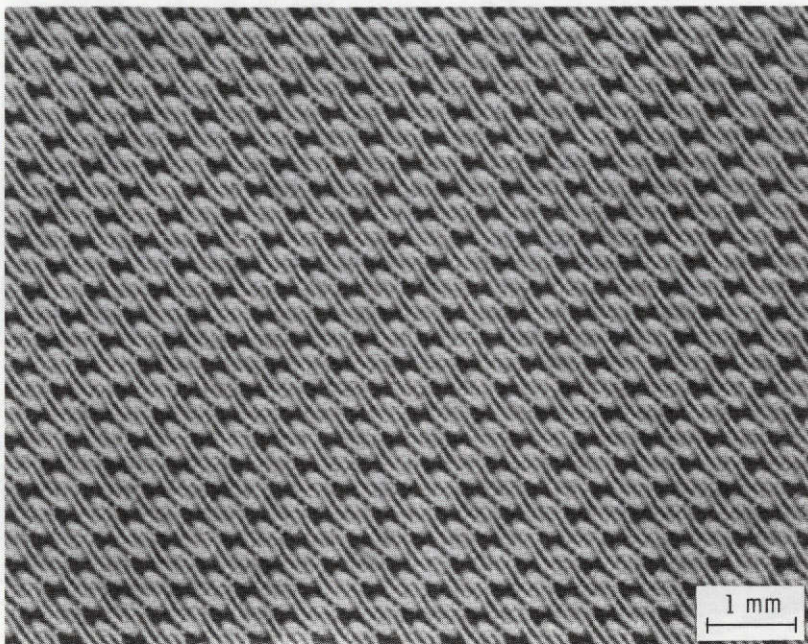


Figure 30. - Stainless steel wire cloth anode insert, before test; magnified view.

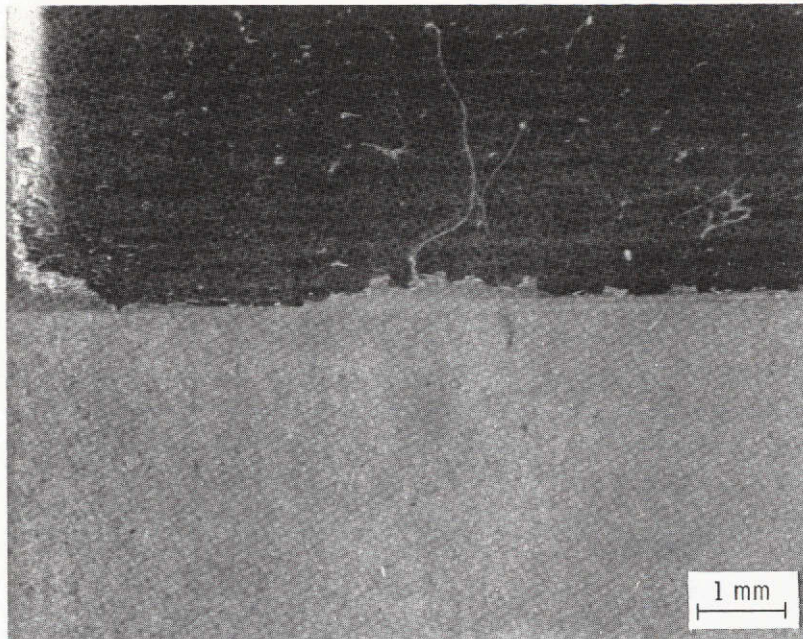


Figure 31. - Portion of tantalum foil anode insert, after test, showing coated grit-blasted surface, at bottom, and smooth surface with coating spalled off, at top. View magnified.

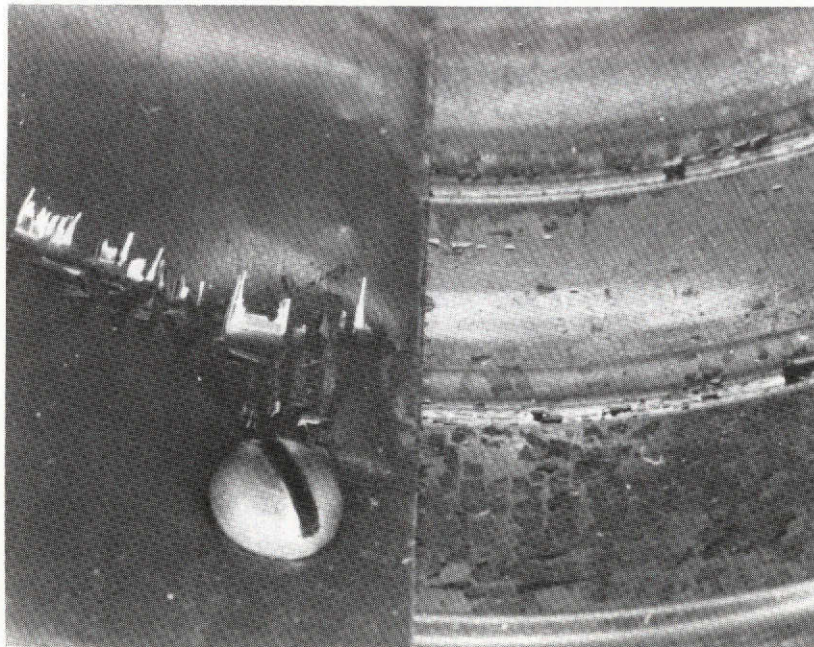


Figure 32. - Interior view of anode surface, after test. Smooth tantalum foil insert surface on left; smooth stainless steel anode surface on right.



Figure 33. - Portion of loose flakes and material collected from thruster discharge chamber after test. Smallest divisions on ruler each 0.254 mm (0.01 in.).

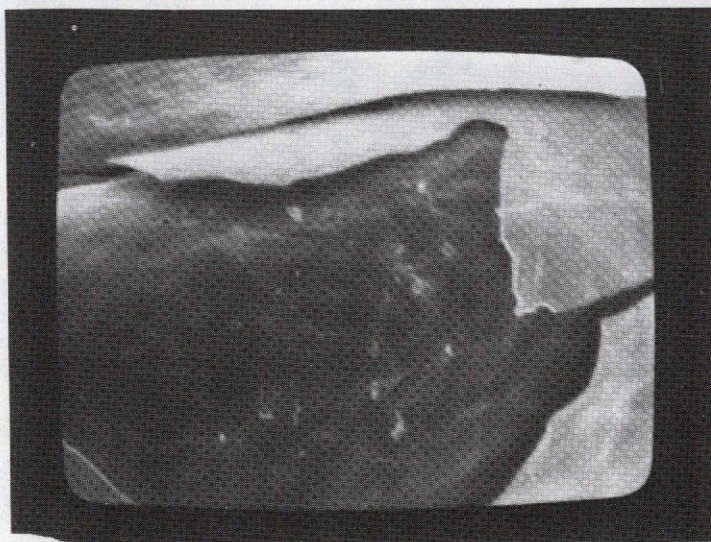


Figure 34. - Electron micrograph of spalled coating on wire cloth anode insert.

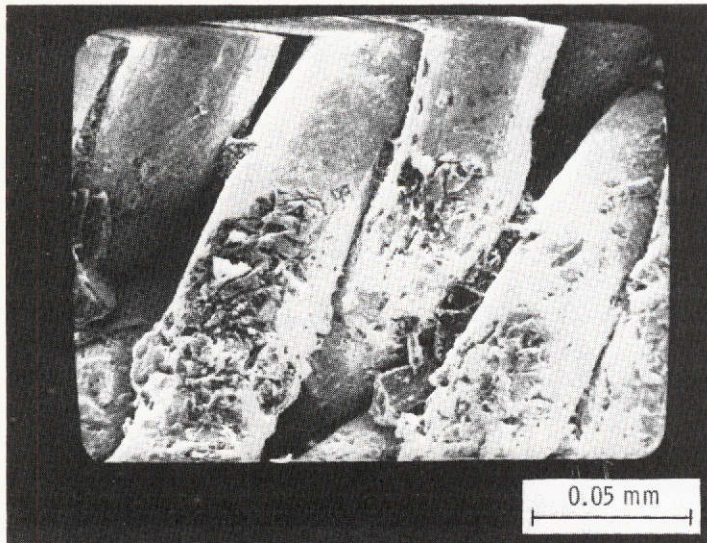


Figure 35. - Electron micrograph of fine mesh stainless steel screen for use as anode surface. Lower portion coarsely grit-blasted.

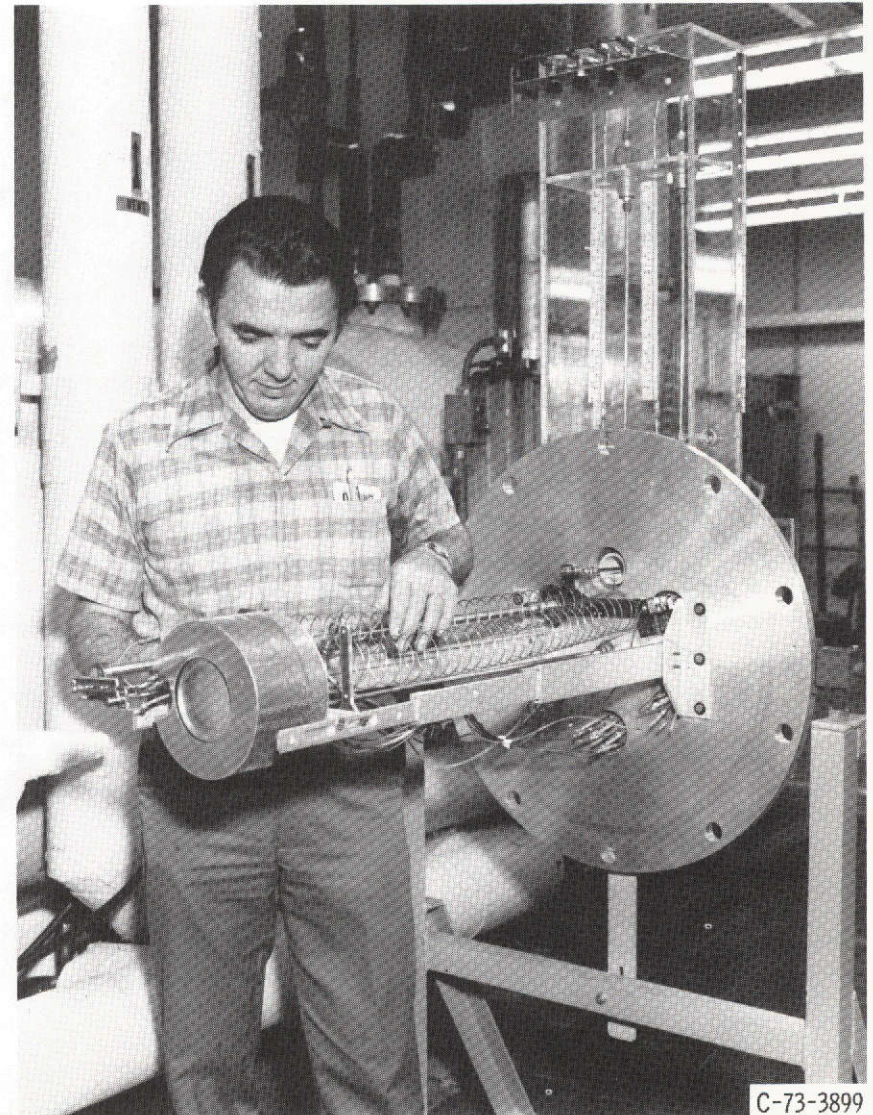
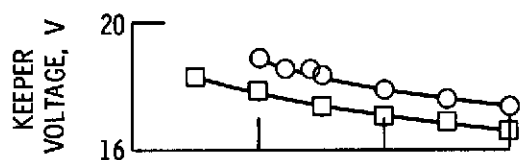
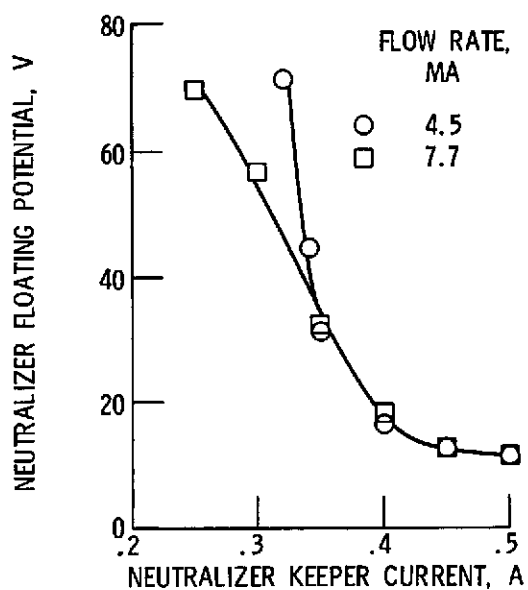


Figure 36. - Movable thruster and neutralizer mounted on cover flange.



(a) NEUTRALIZER KEEPER VOLTAGE.



(b) NEUTRALIZER FLOATING POTENTIAL.

Figure 37A. - Effects of varying neutralizer keeper current. Keeper hole, 0.159 cm; keeper gap, 0.108 cm; axial distance, 5.0 cm; radial distance, 2.75 cm.

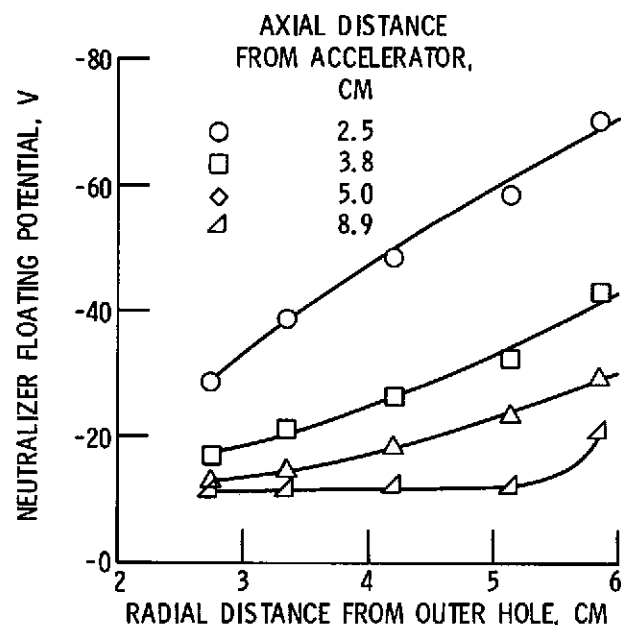


Figure 37B. - Effects of neutralizer position on floating potential. Keeper hole, 0.159 cm; keeper gap, 0.108 cm; flow rate, 7.7 MA; keeper current, 0.45 A.

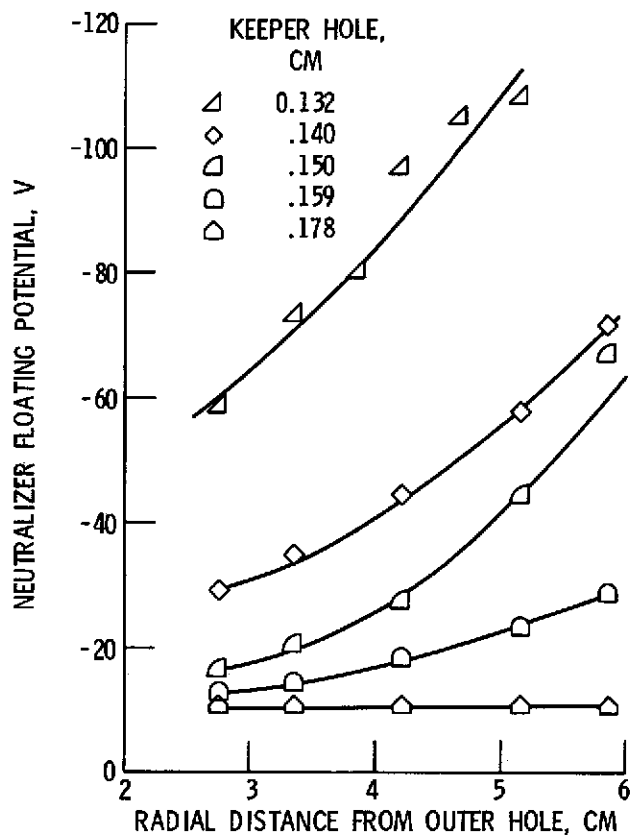


Figure 38. - Effects of neutralizer position and keeper hole size on floating potential. Axial position, 5 cm; flow rate, 7 MA; keeper current, 0.45 A; keeper gap, 0.108 cm.

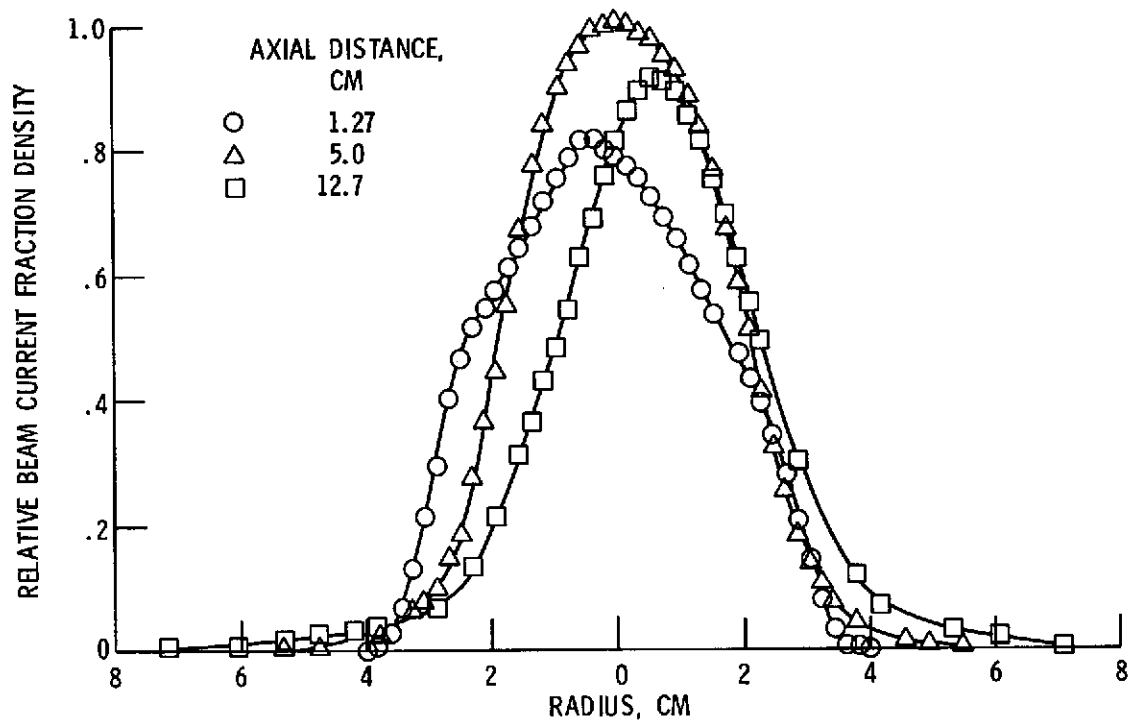


Figure 39. - Beam current density profile obtained with planar probe.

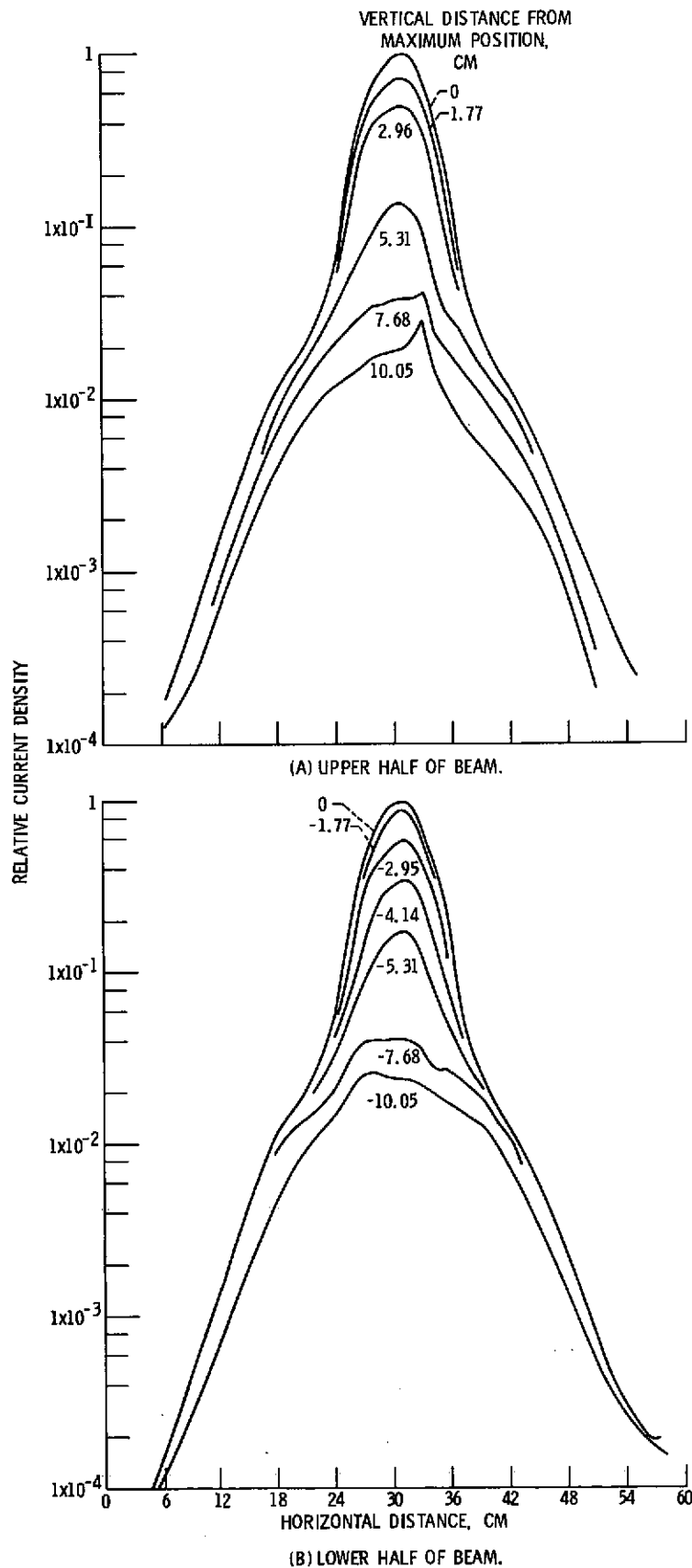


Figure 40. - Ion beam profile taken with Faraday cup rake.

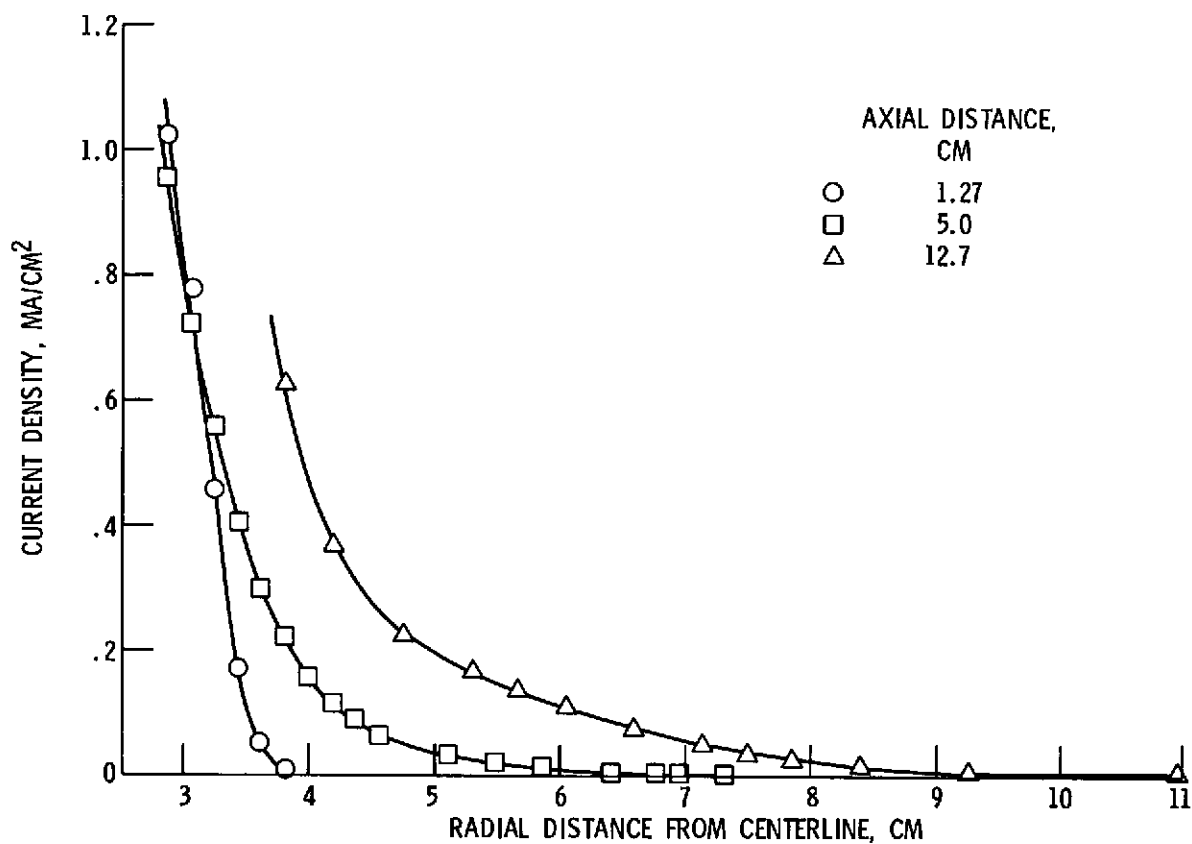


Figure 41. - Ion beam current density along beam boundary as measured with planar probe.

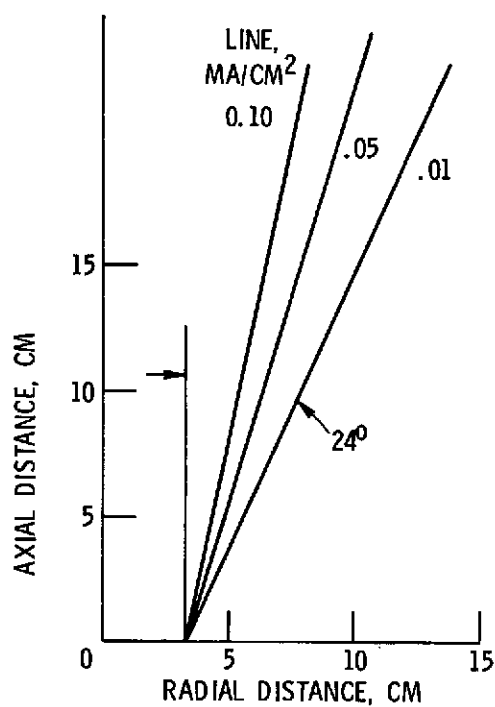


Figure 42. - Ion beam current density envelopes.

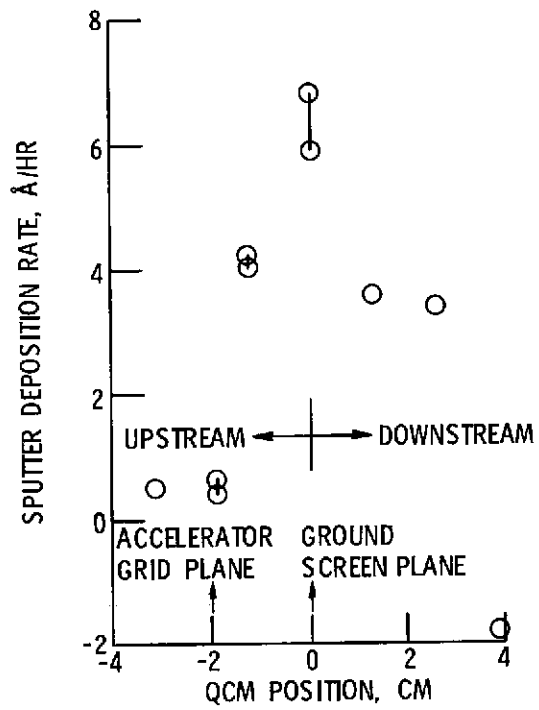


Figure 43. - Sputter deposition rate versus QCM position for 8 cm cyclic endurance test.

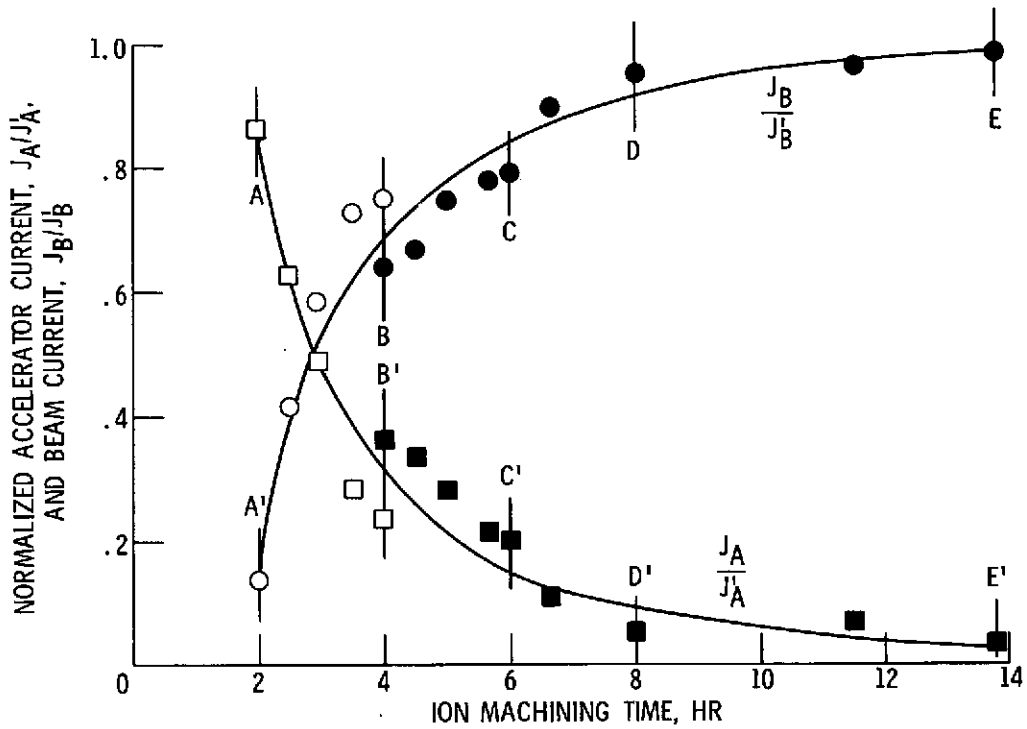


Figure 45. - Normalized accelerator and ion beam current as a function of time.

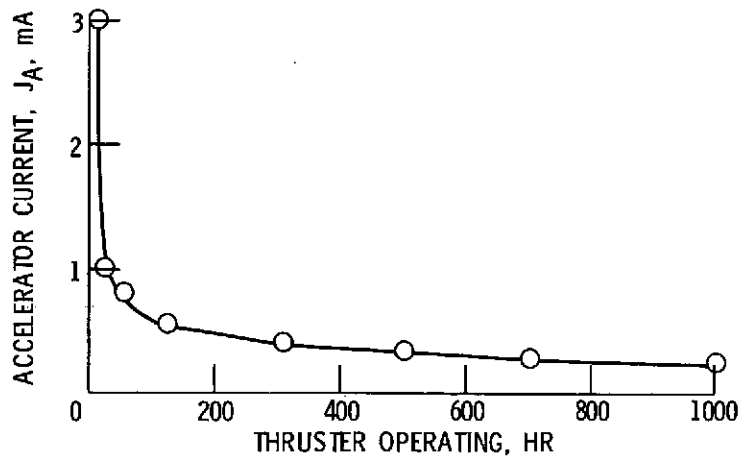
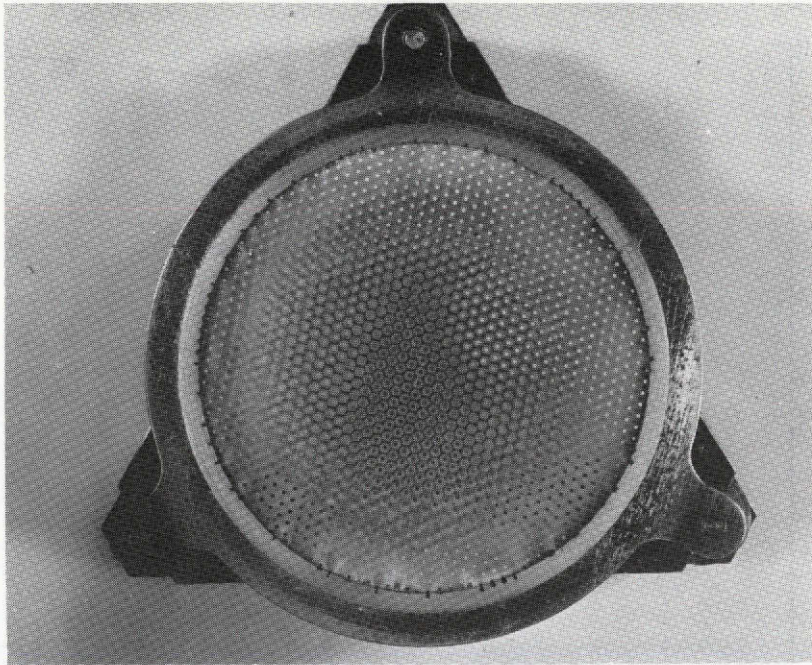
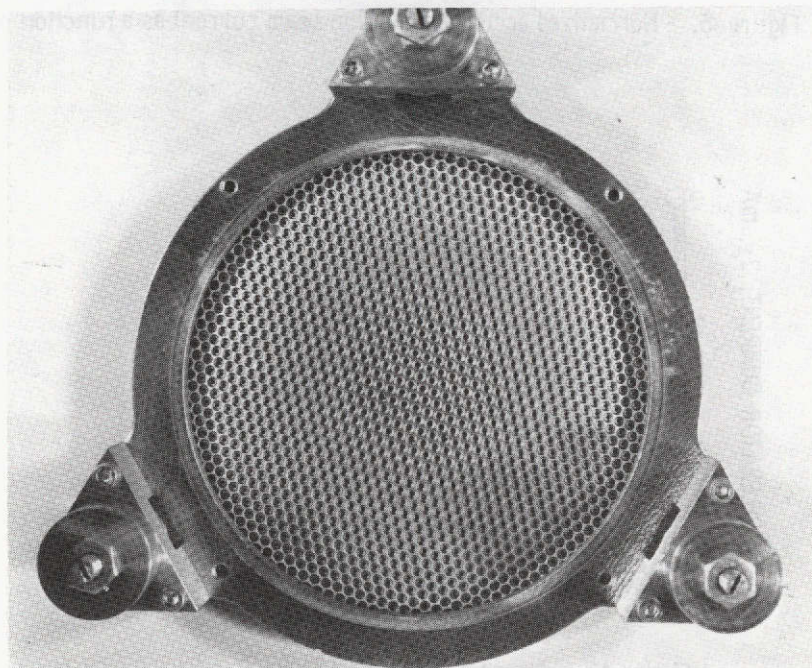


Figure 46. - Plot showing variation of accelerator current with thruster operating hours.



(a) DOWNSTREAM SURFACES.



(b) UPSTREAM SURFACES.

Figure 47. - Ion machined accelerator grid system after 1006 hours operation.

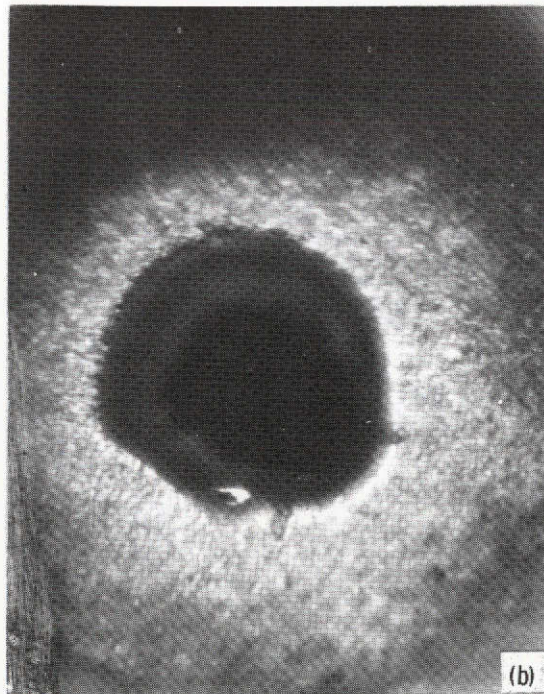
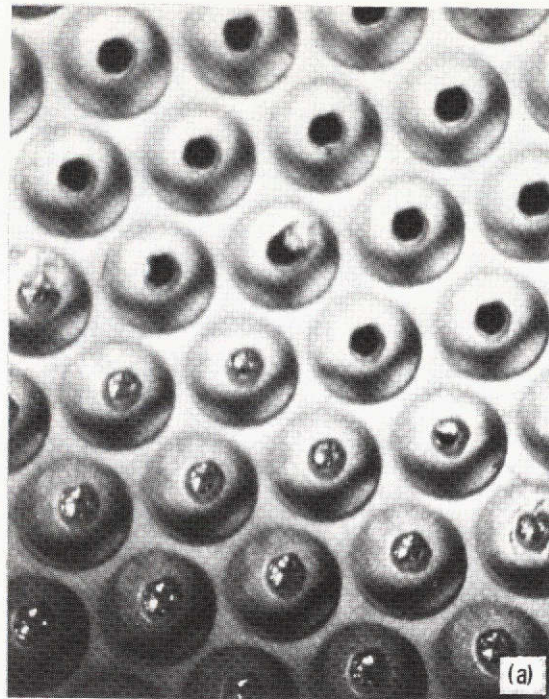
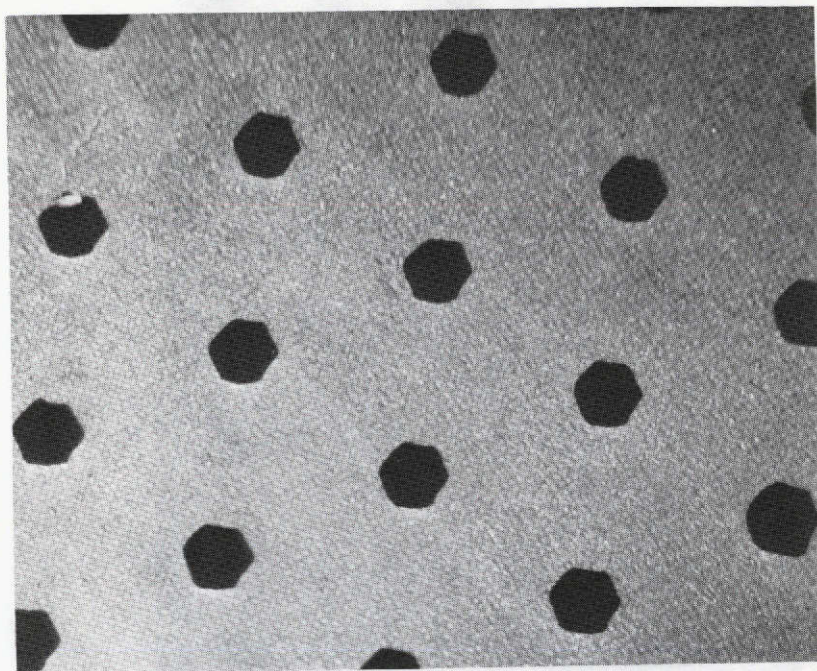
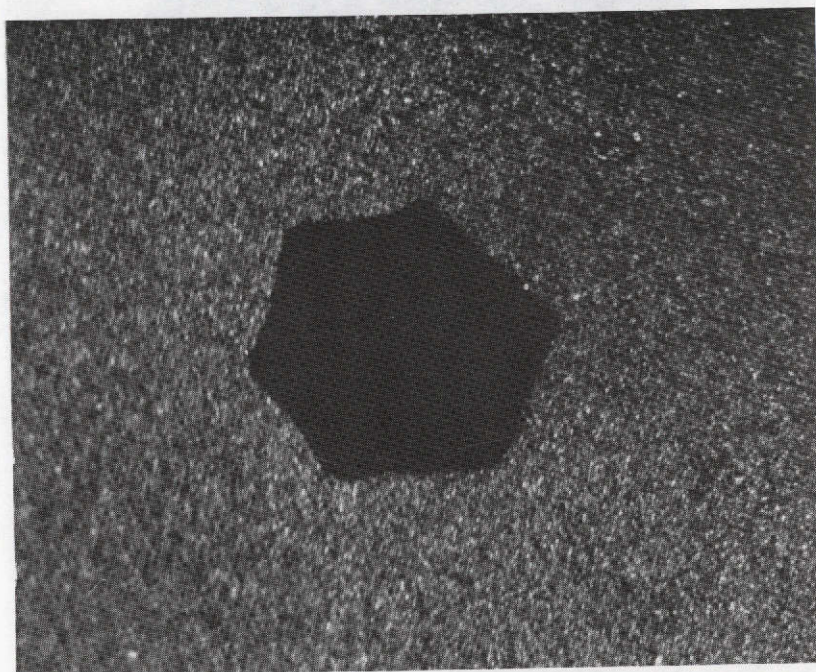


Figure 48. - Upstream views of the partially sputtered through region of the accelerator grid. (a) Low magnification view of some, partially sputtered through hole. (b) High magnification view of one particular accelerator hole.



(a) ORIENTATION OF HEXAGONAL GRID APERTURES.



(b) HIGH MAGNIFICATION VIEW OF ONE APERTURE.

Figure 49. - Photomicrographs of hexagon accelerator hole geometry on downstream side of accelerator grid taken after 462 hours.

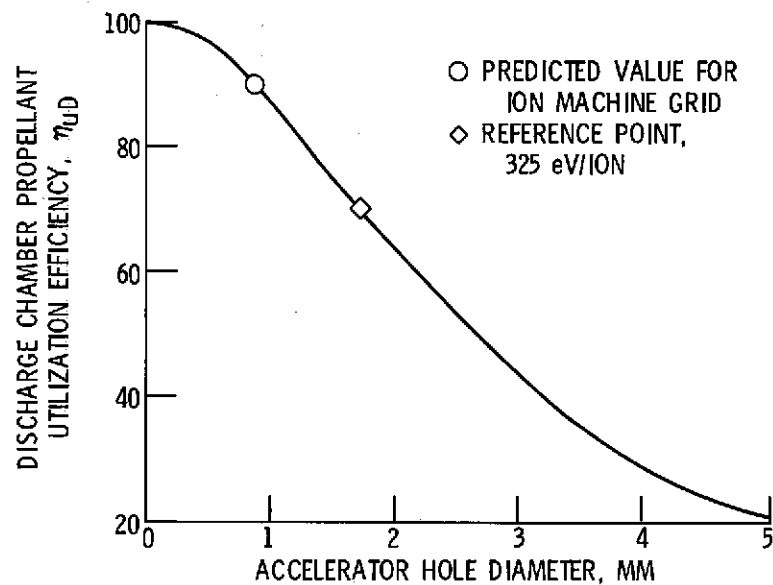


Figure 50. - Propellant utilization efficiency as a function of accelerator hole diameter as predicted by equation (3), $\eta_{UD} = 1/(1 + 0.149 D^2)$. The reference point corresponds to $\eta_U = 70\%$ at 325 eV/ion.

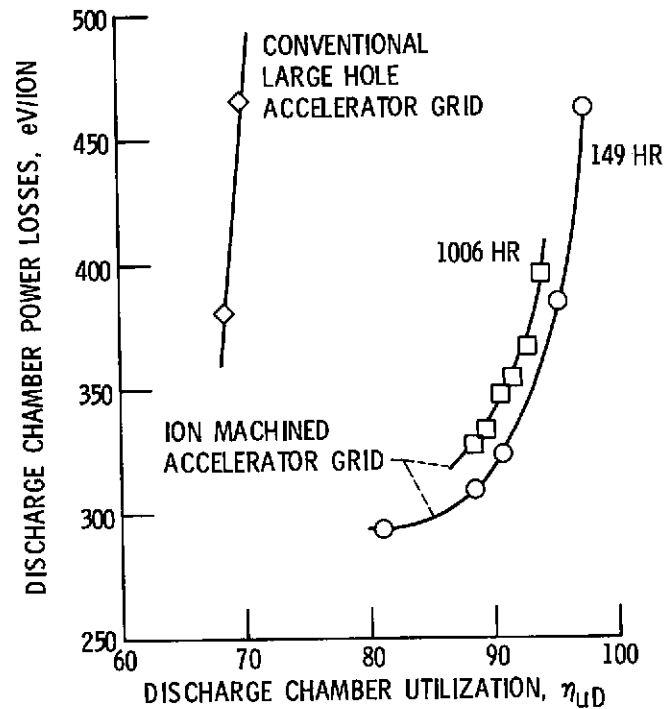


Figure 51. - Discharge chamber losses as a function of discharge chamber utilization for thruster with ion machined accelerator grid. Data was taken at constant mercury flow. V_I , 1220 volts; V_A , -300 volts.

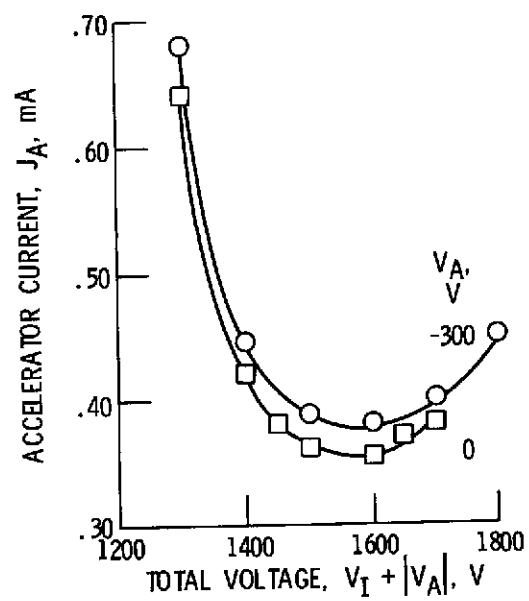


Figure 52. - Accelerator current dependence on total voltage at J_B , 72 mA; η_{up} , 88.5%. Data taken after 149 hours of operation.

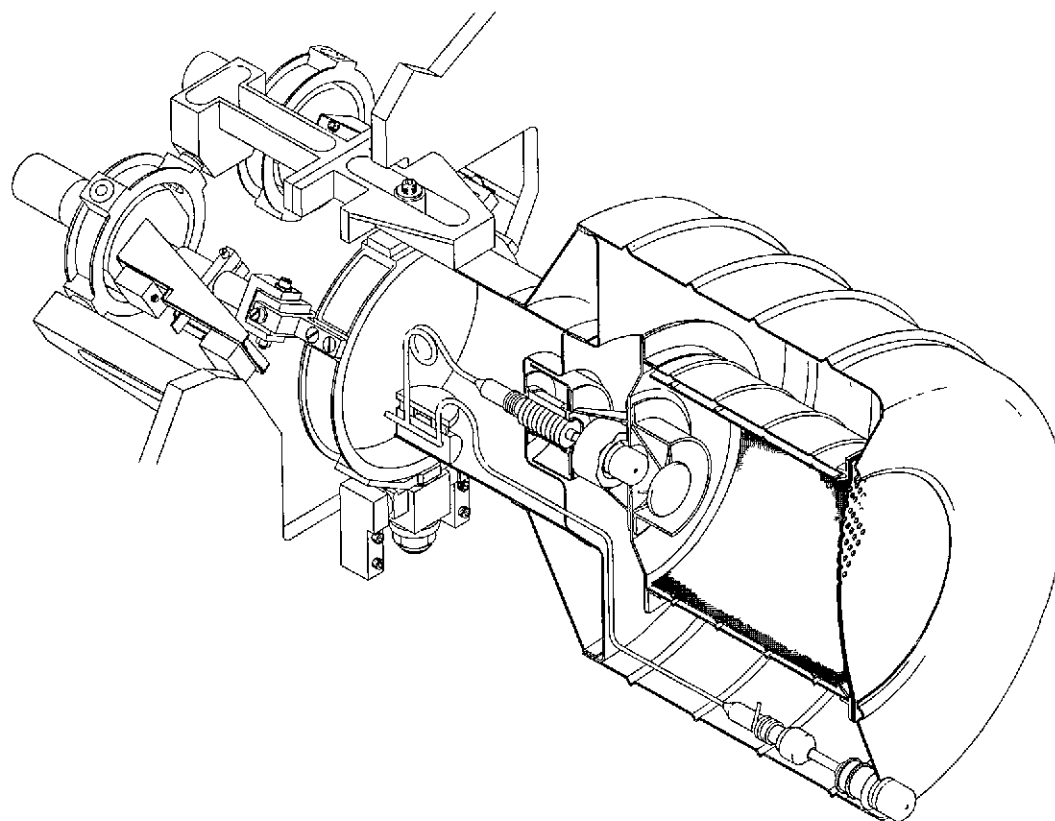
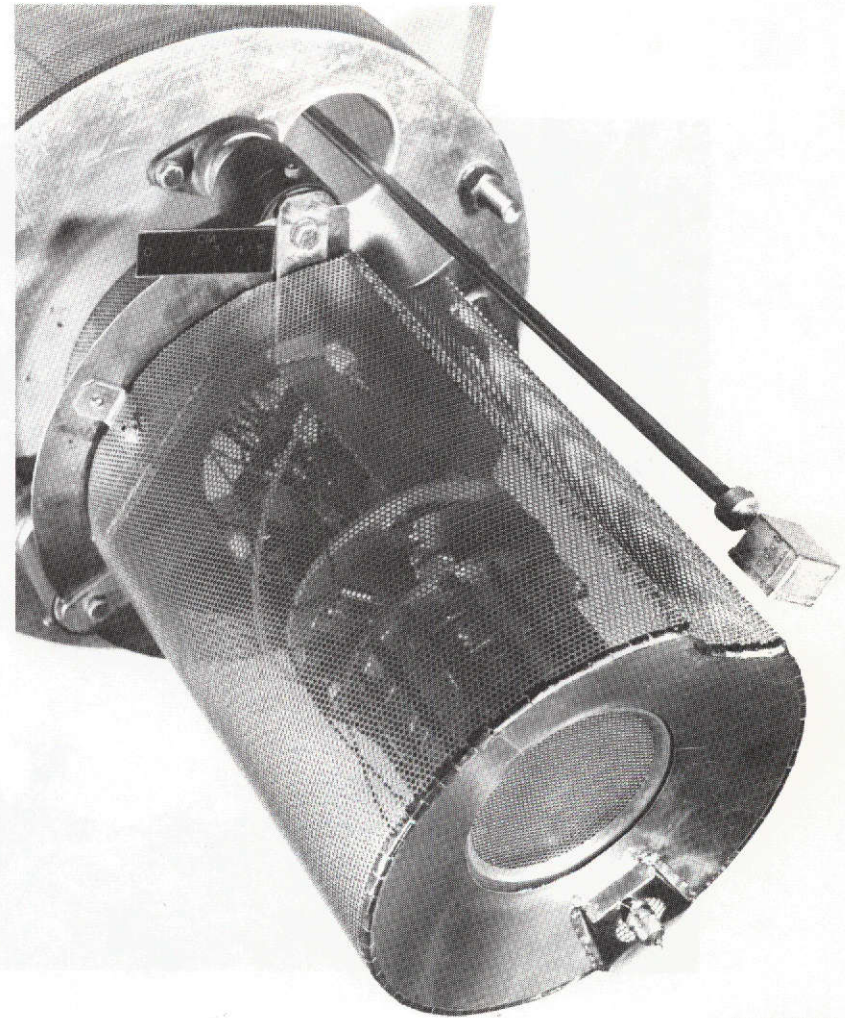


Figure 53. - Engineering model SIT-8 thruster



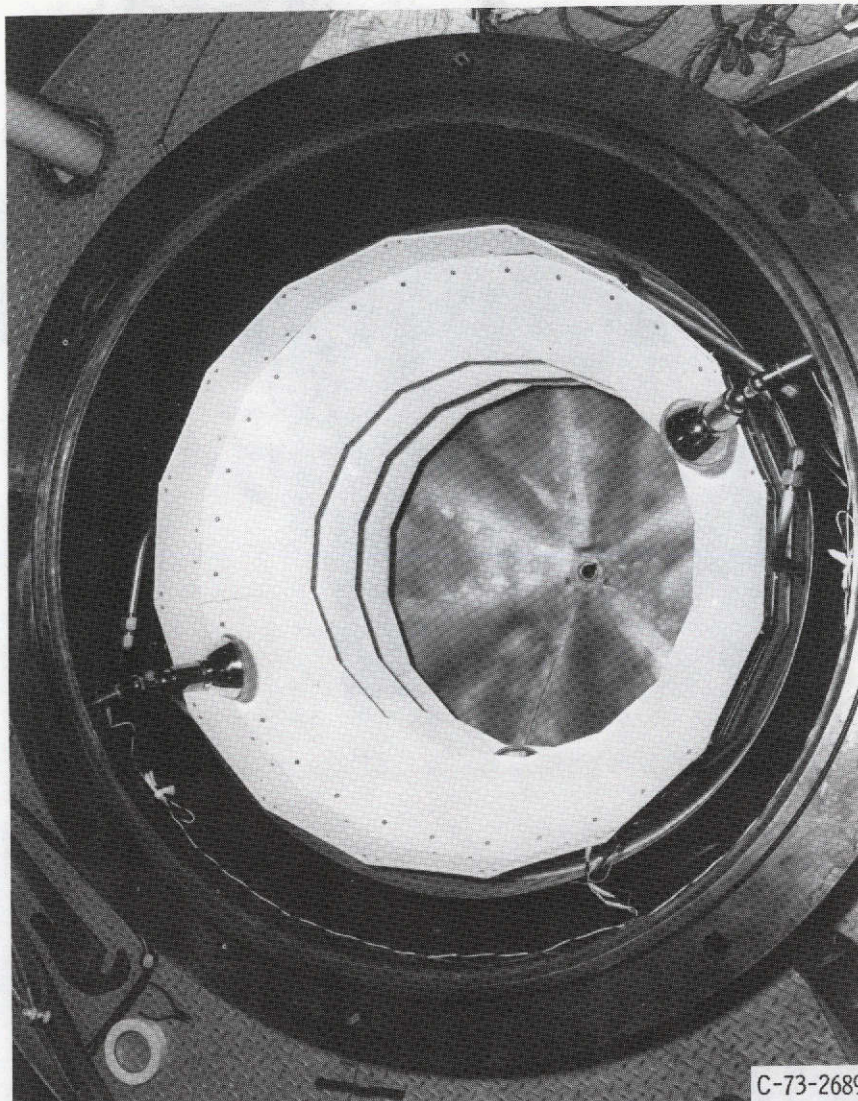
C-74-1308

Figure 54. - SIT-8 thruster.



C-73-2691

Figure 55. - 8 cm Diameter ion thruster mounted for cyclic-endurance testing.



C-73-2689

Figure 56. - Interior of vacuum test facility prior to test.

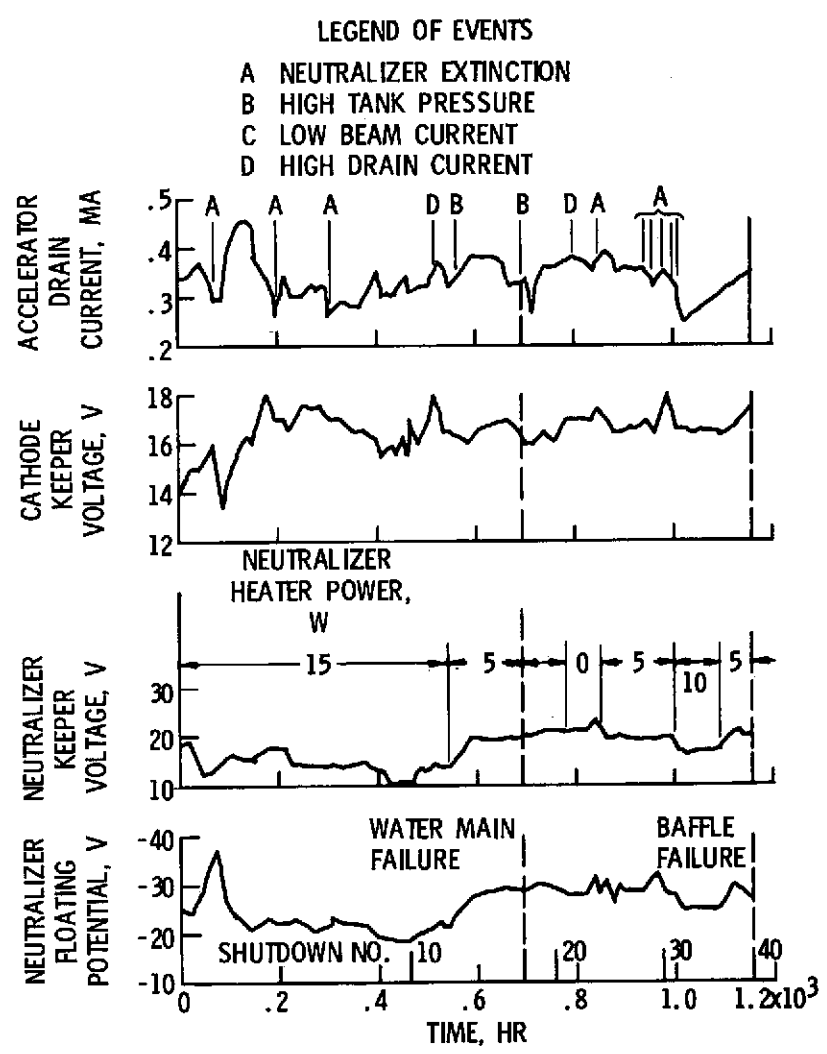


Figure 57. - History of cyclic-endurance test.

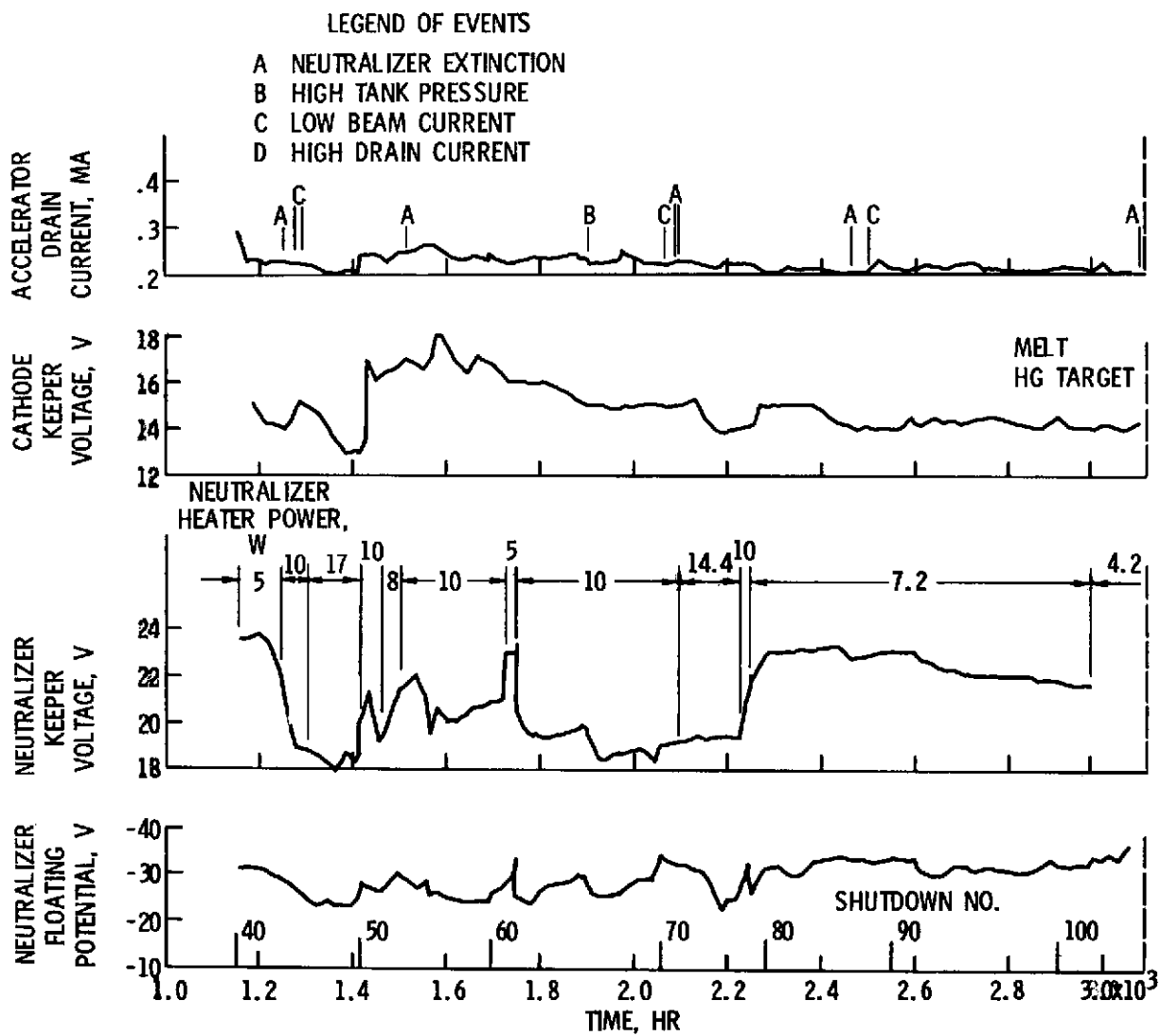


Figure 57. - Continued.

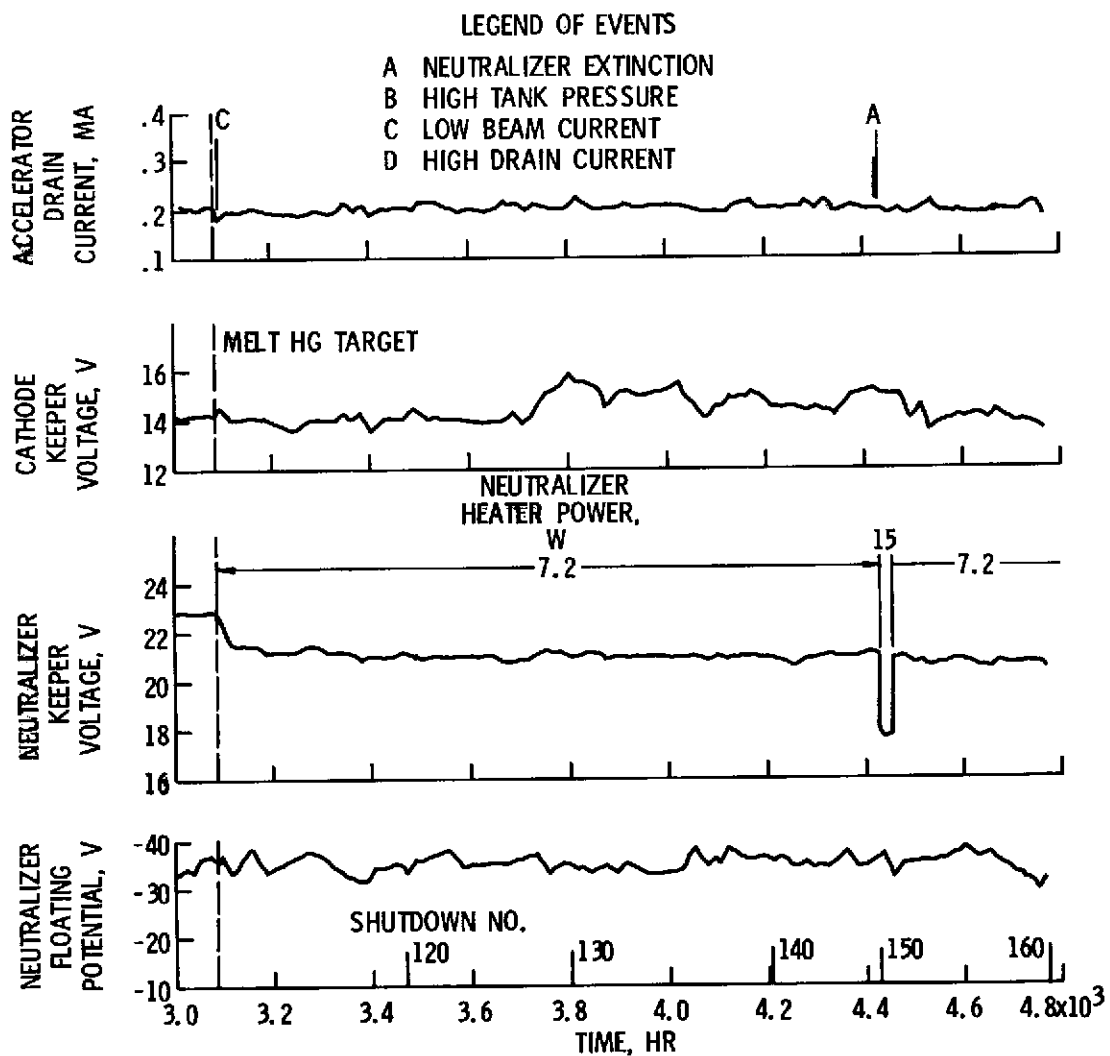


Figure 57. - Continued.

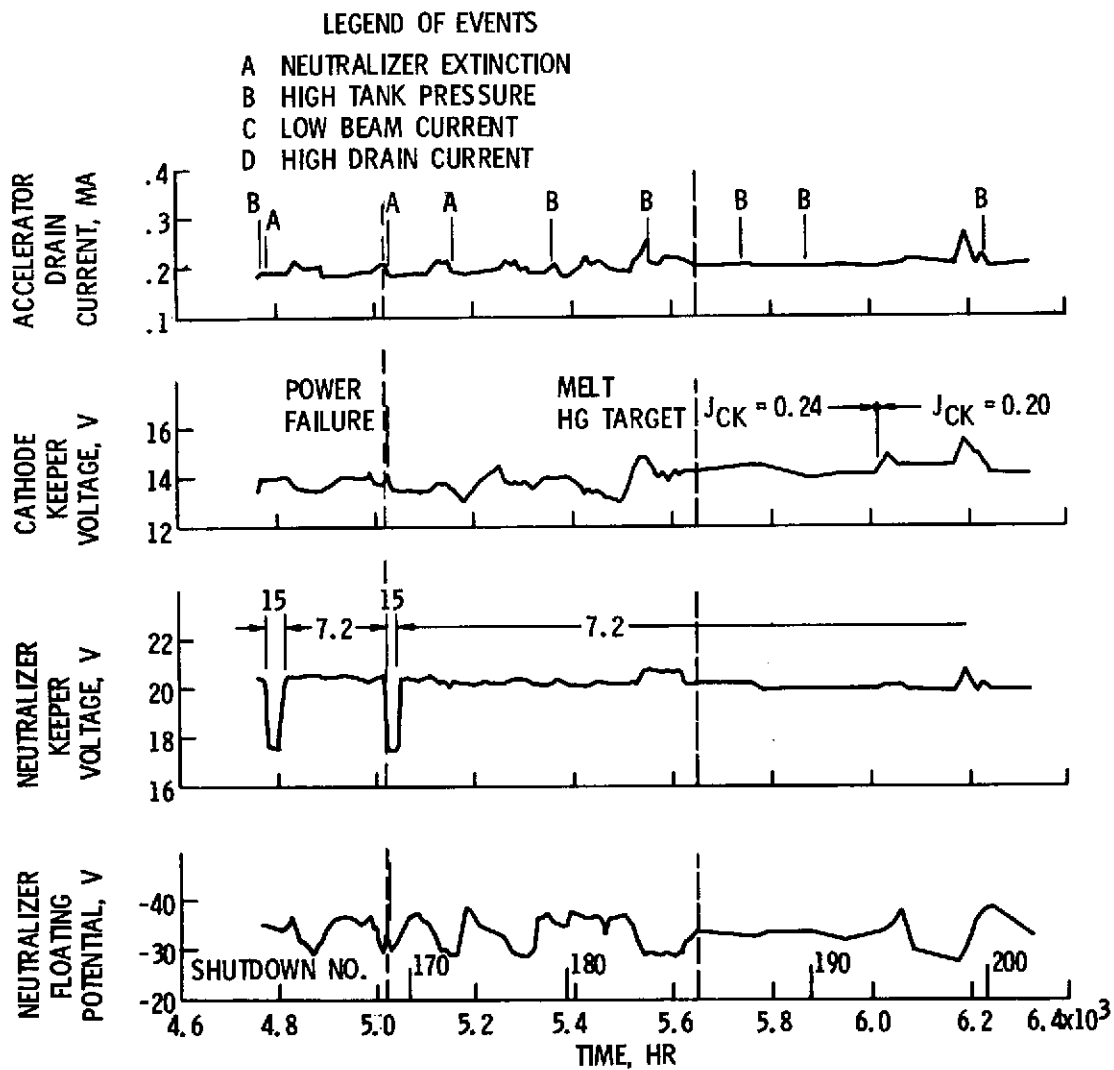
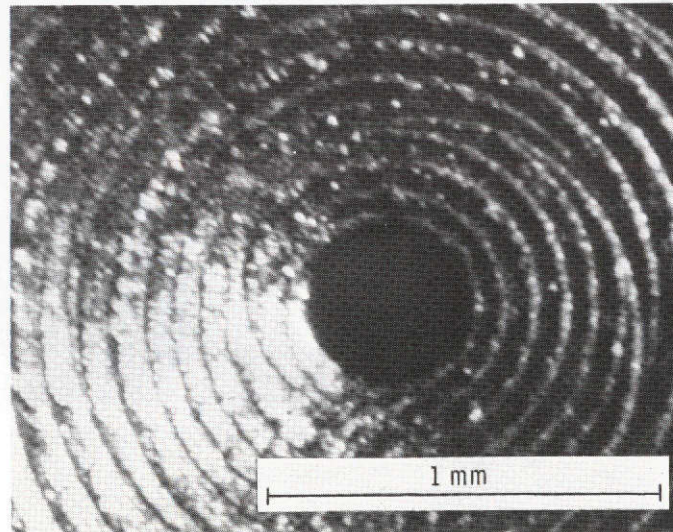
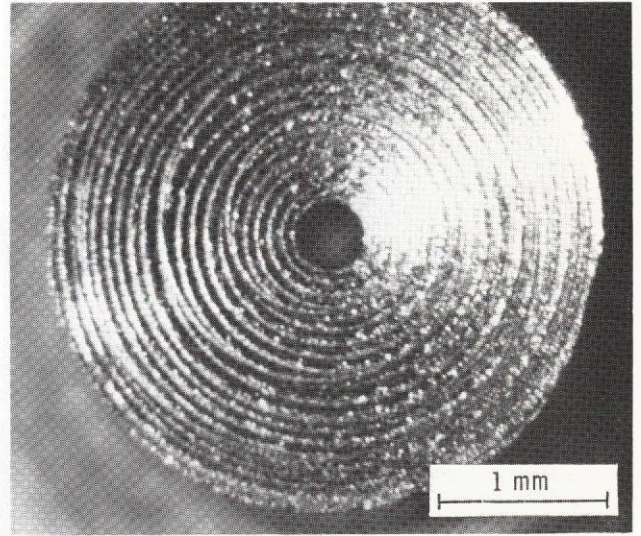
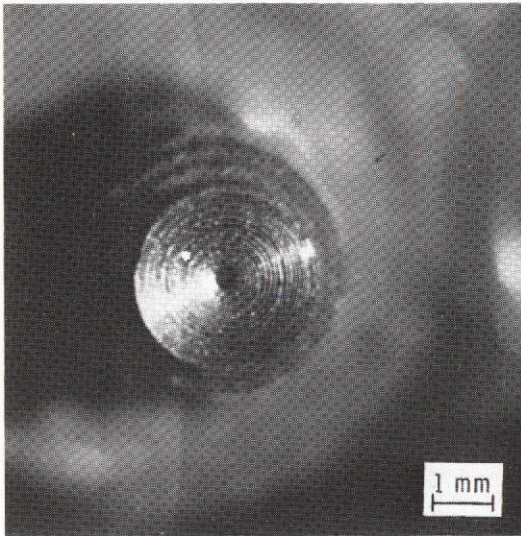


Figure 57. - Concluded.



<0.34 mm ORIFICE, DIAMETER, <0.37 mm

Figure 58. - Microphotographs of neutralizer tip after 1156 hours of operation.

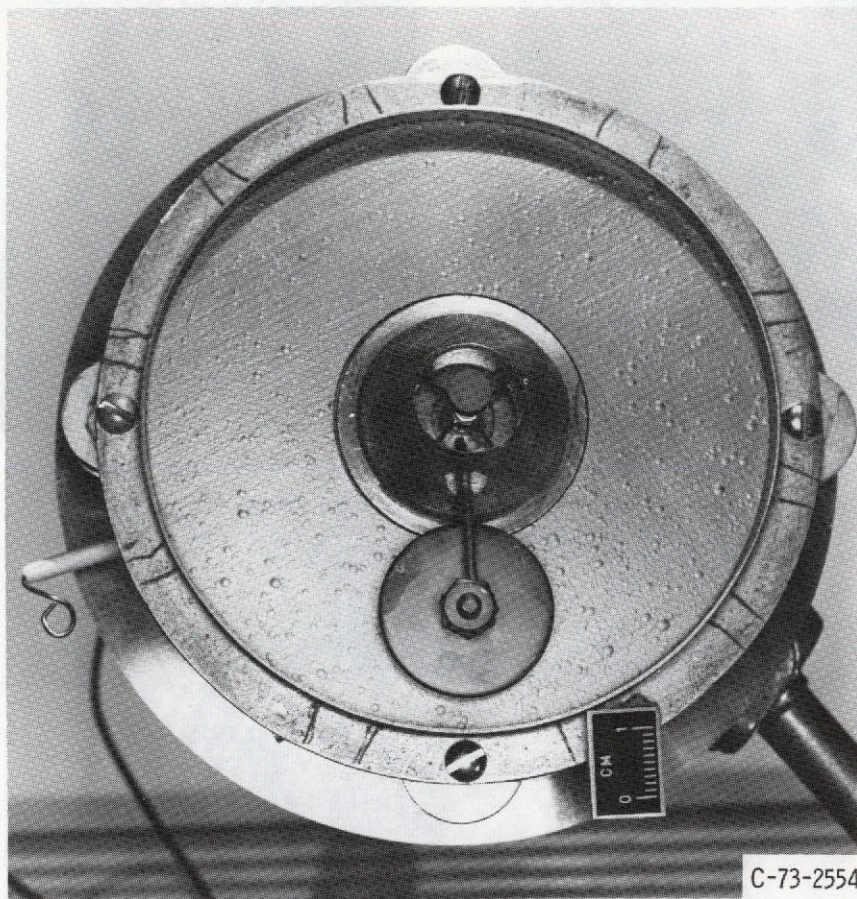


Figure 59. - Thruster back plate assembly before test.

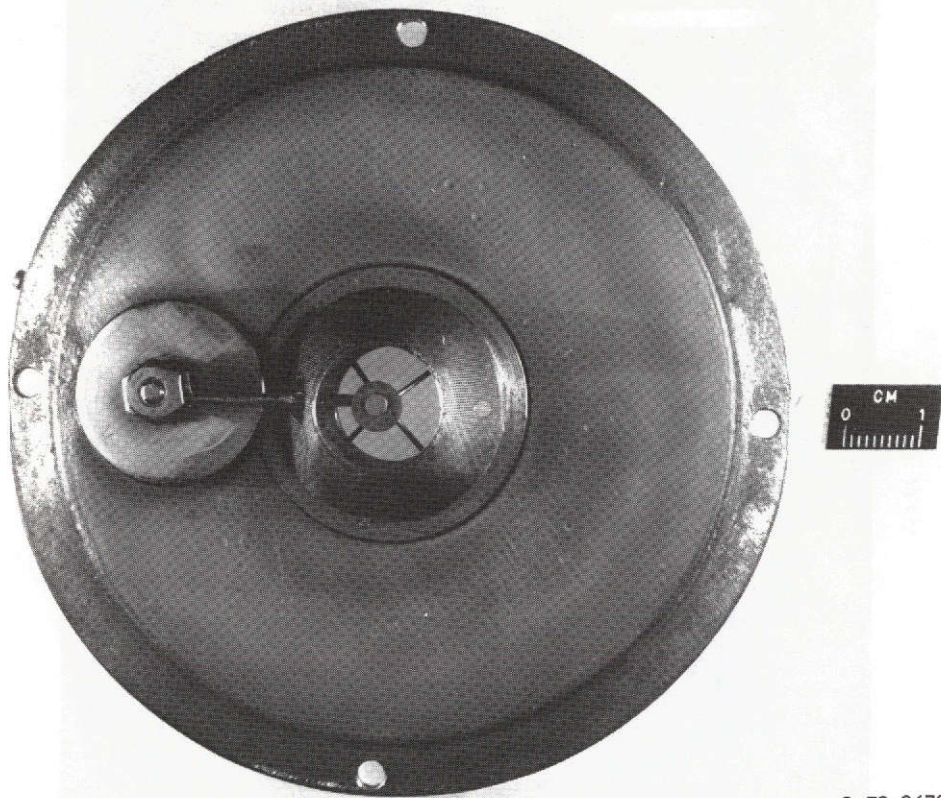


Figure 60. - Thruster back plate assembly after 1156 hours operation.

C-73-3678

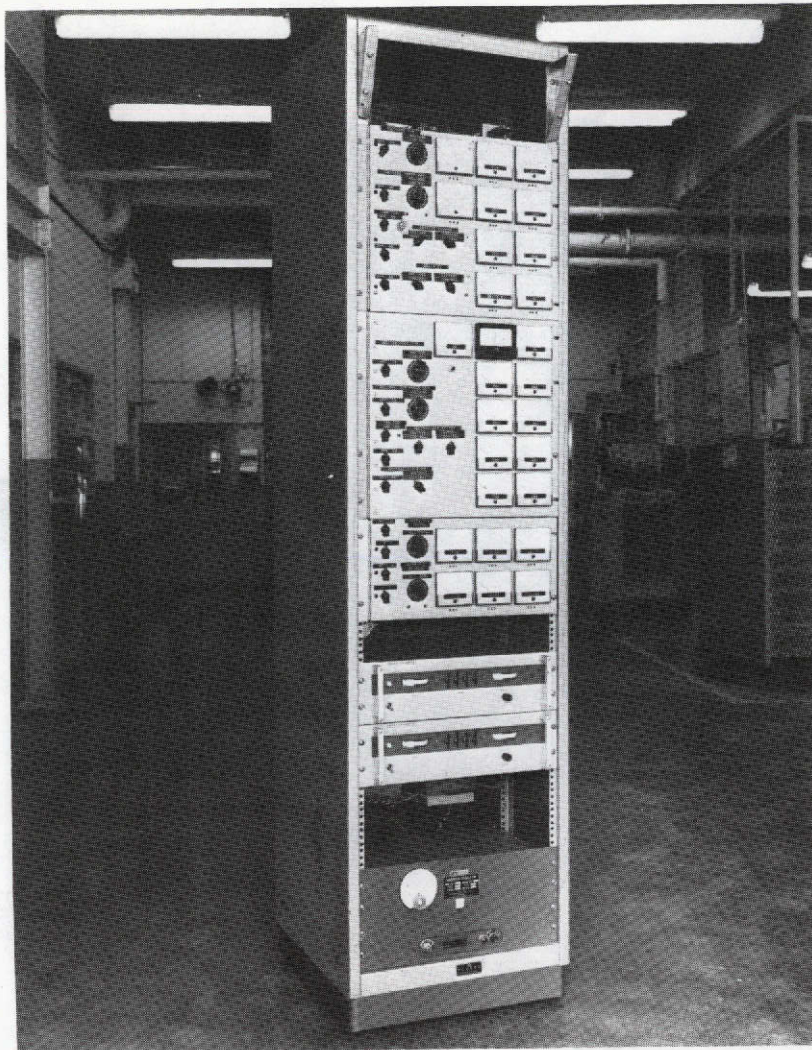


Figure 61. - Laboratory thruster test console.

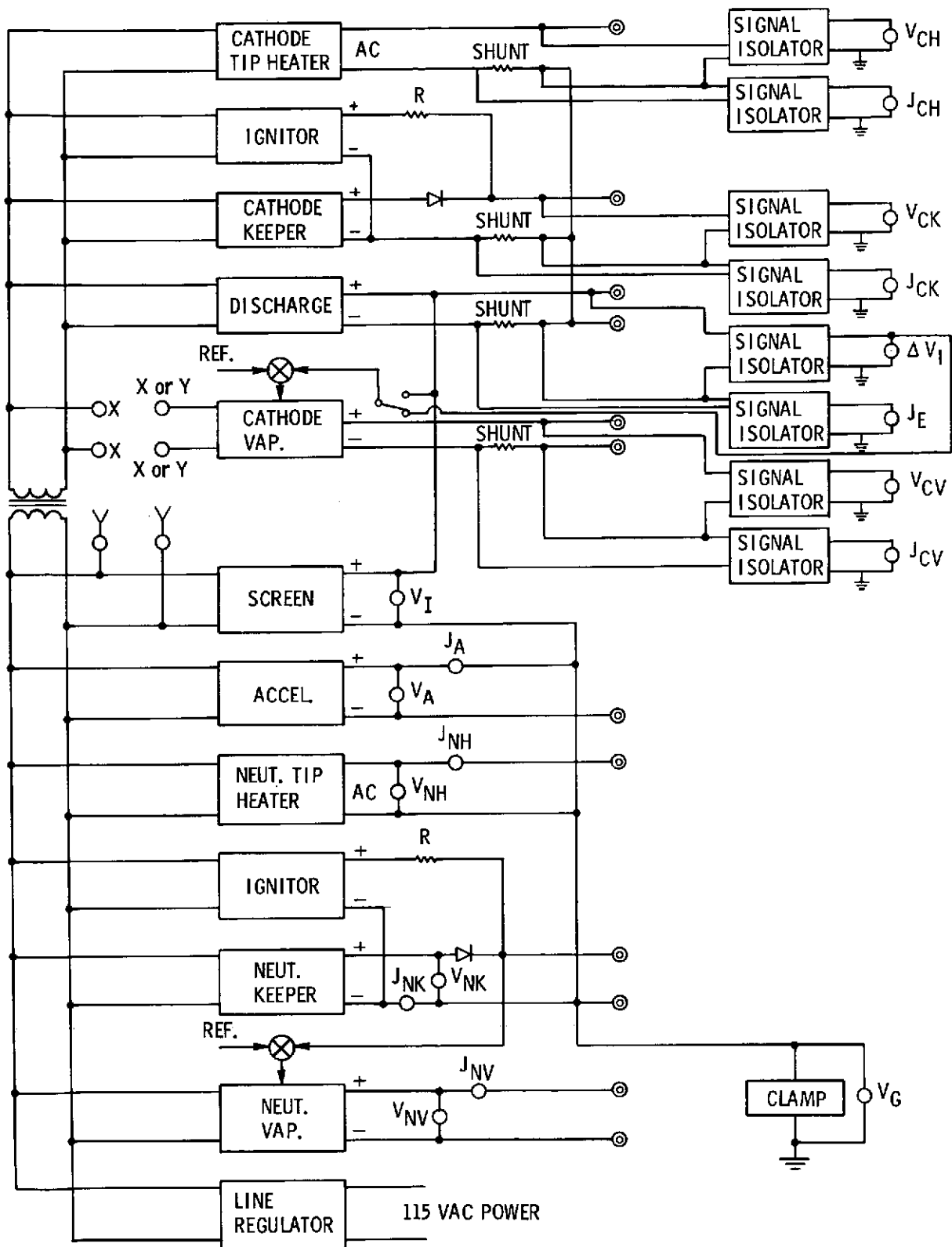


Fig. 62. - Block diagram of laboratory thruster test console.

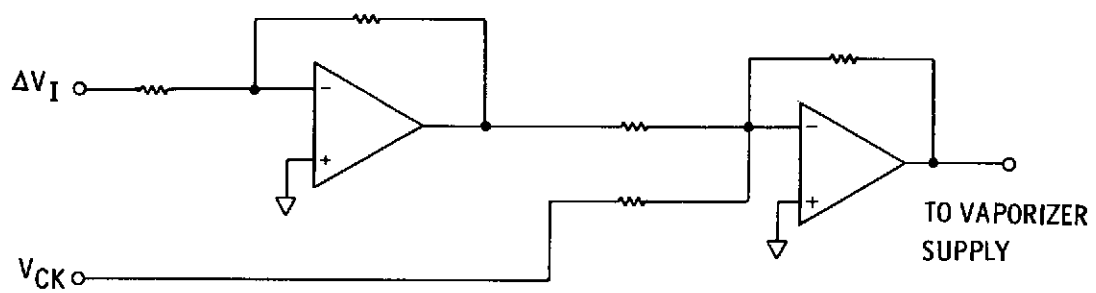


Figure 63.- $\Delta V_I - V_{CK}$ feedback control circuit.

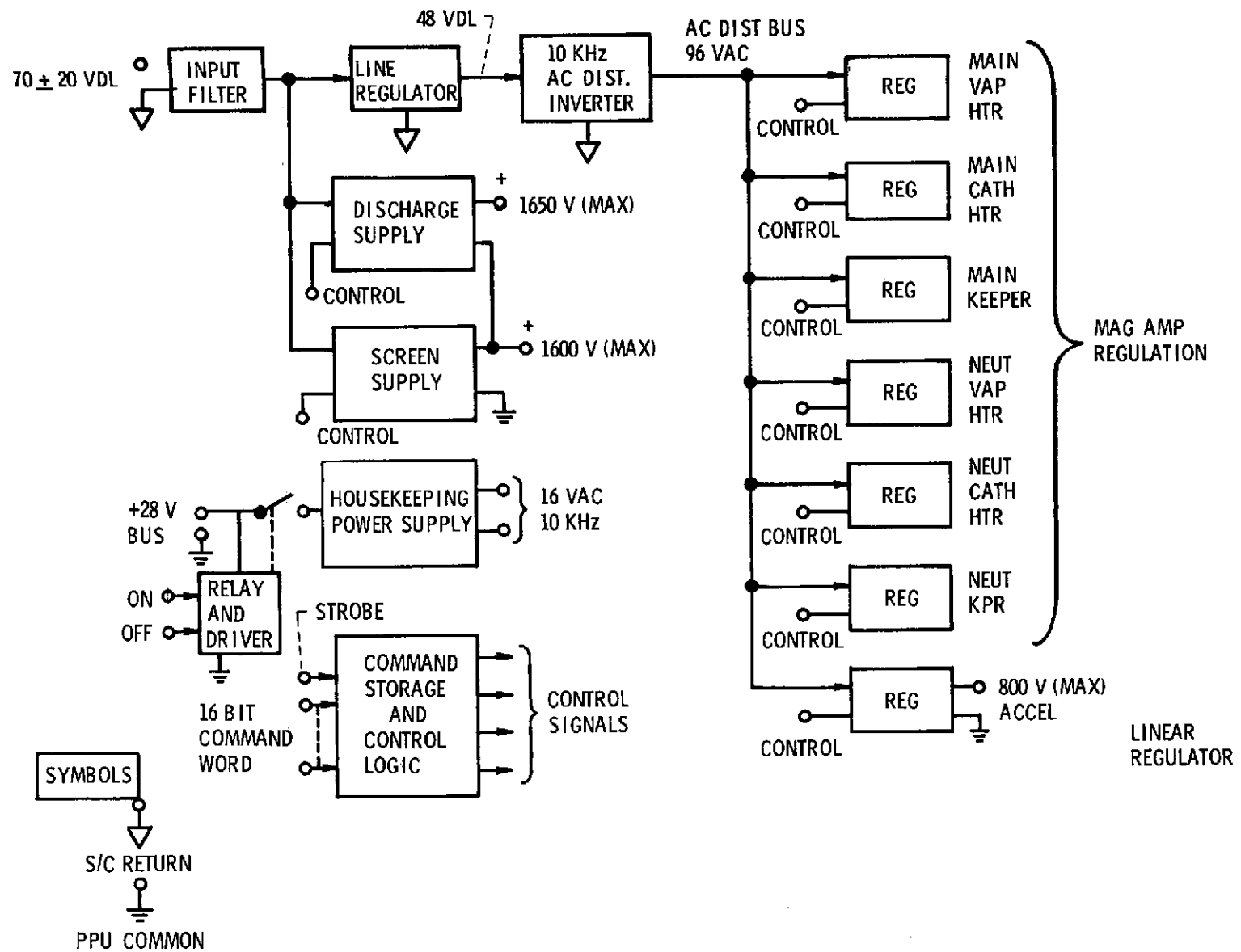


Fig. 64. - Power processor block diagram.

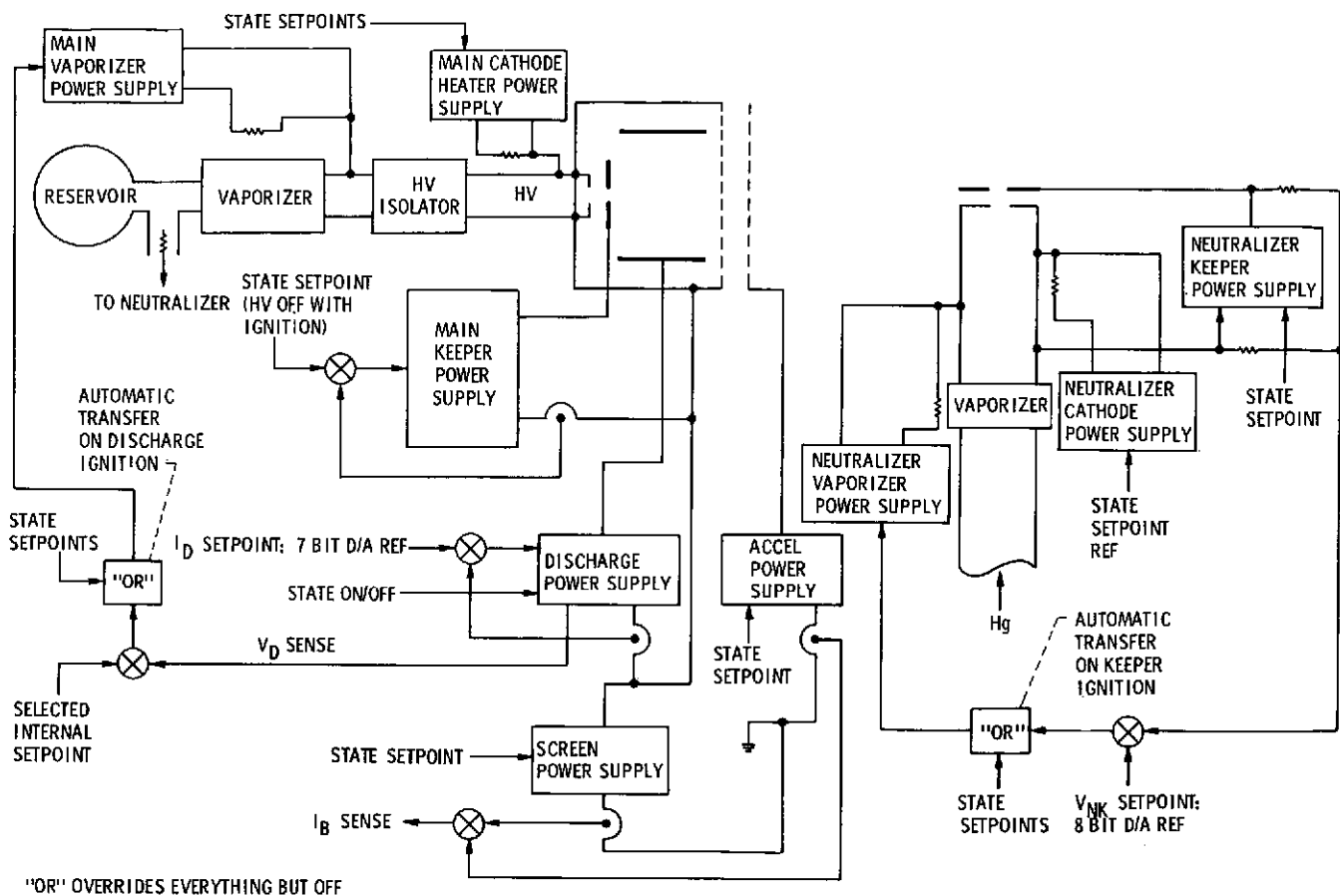


Figure 65. - Block diagram of power processor supplies interconnections for 8-cm thruster operations.

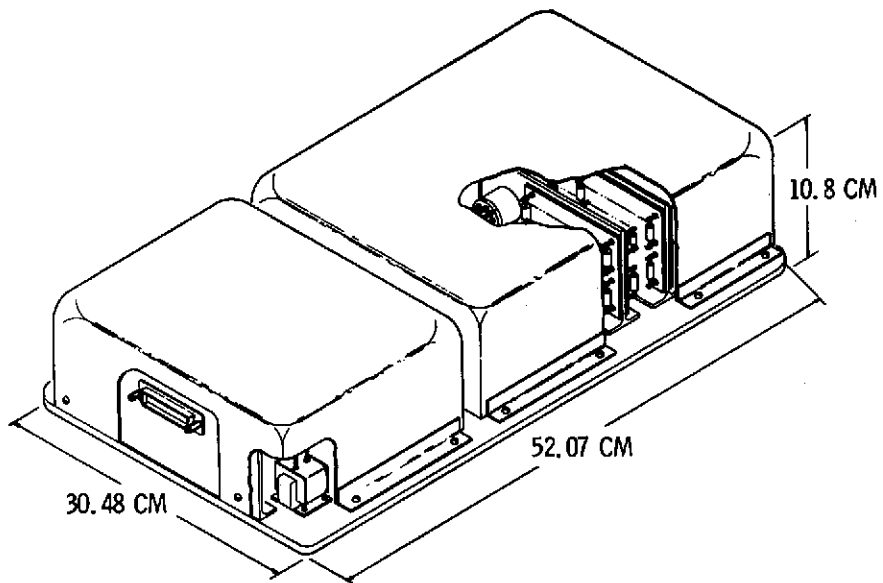


Figure 66. - Preliminary power processor physical layout.

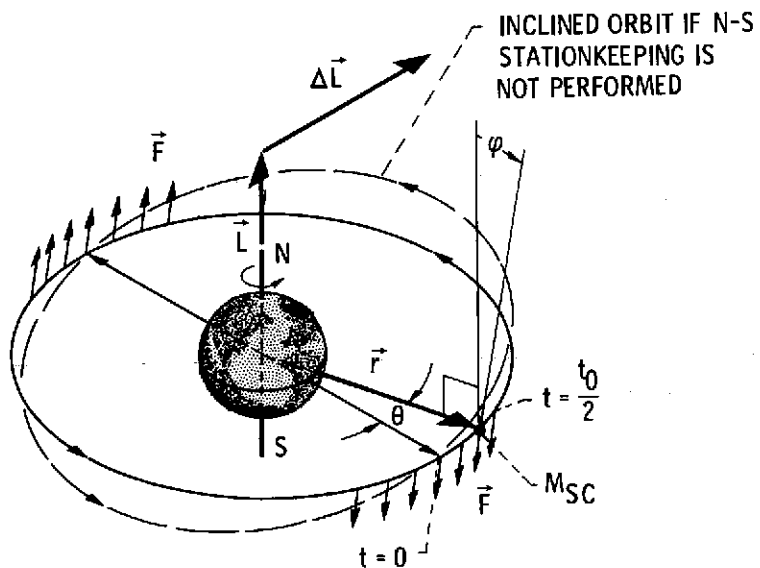


Figure 67. - N-S stationkeeping parameters.

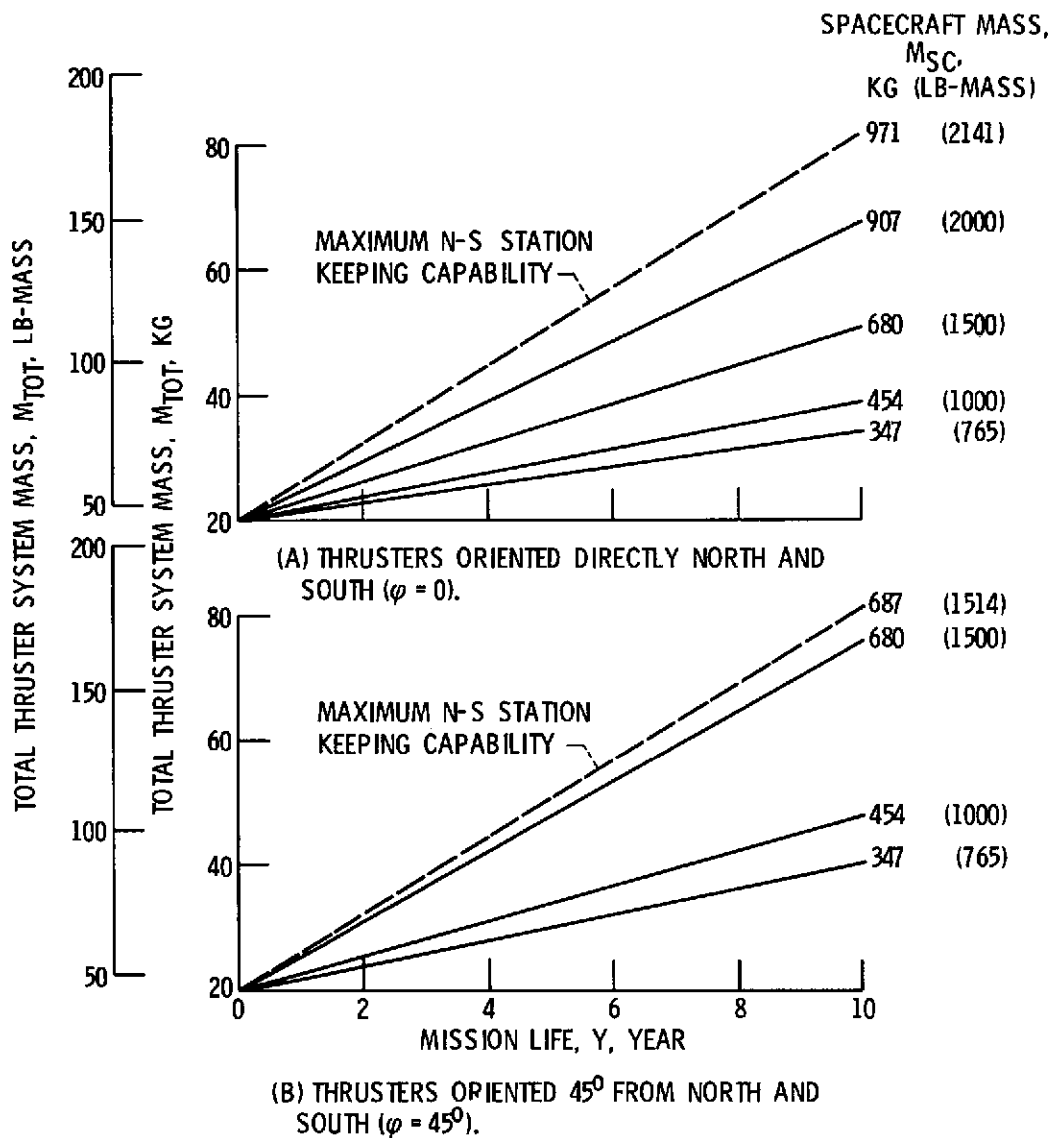
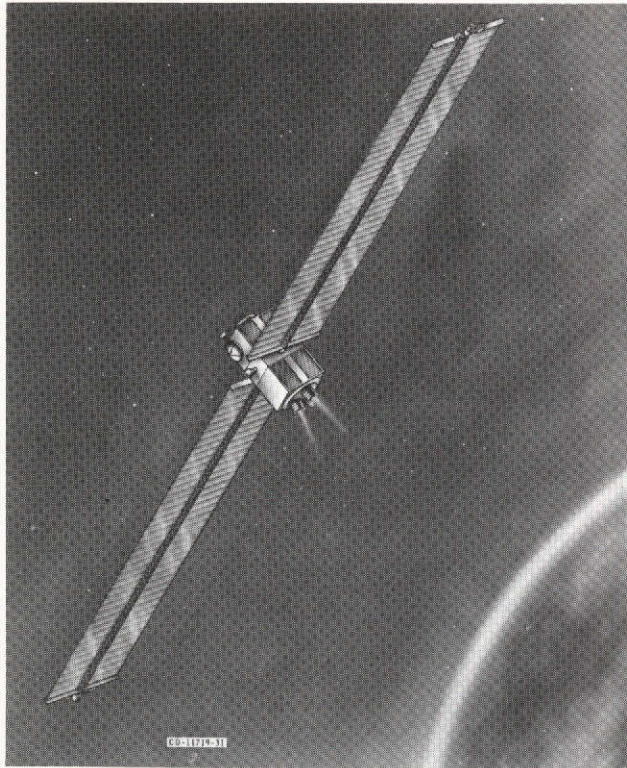
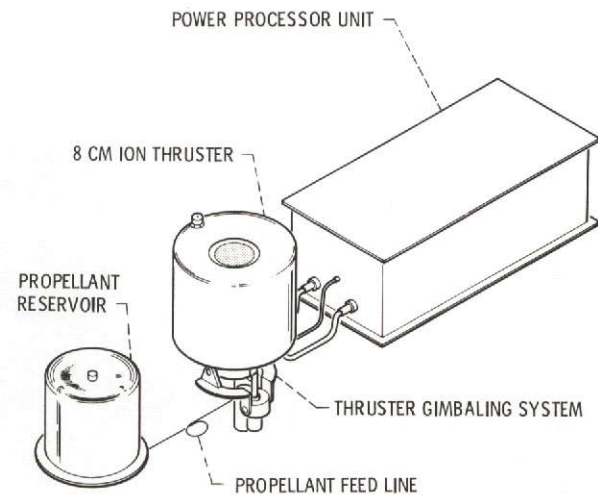


Figure 68. - Total thruster system mass for two thruster systems (one is redundant) as a function of mission length.



(a) VIEW OF ENTIRE SPACECRAFT.



(b) SIT-8 THRUSTER SYSTEM AS CONFIGURED AT THE END OF THE SOLAR ARRAY.

Figure 69. - Spacecraft with ion thrusters at ends of the solar array.